NASA CR-1030

STUDIES OF SPECIFIC NUCLEAR LIGHT BULB AND OPEN-CYCLE VORTEX-STABILIZED GASEOUS NUCLEAR ROCKET ENGINES

by G. H. McLafferty and H. E. Bauer

Prepared by
UNITED AIRCRAFT CORPORATION
East Hartford, Conn.
for

NATIONAL AERONAUTICS AND SPACE ADMINISTRATION • WASHINGTON, D. C. • APRIL 1968

NASA CR-1030

STUDIES OF SPECIFIC NUCLEAR LIGHT BULB AND OPEN-CYCLE

VORTEX-STABILIZED GASEOUS NUCLEAR ROCKET ENGINES

By G. H. McLafferty and H. E. Bauer

Issued by Originator as Report No. F-910093-37

Prepared under
UNITED AIRCRAFT CORP. NASw-847 by
East Hartford, Conn.

for

NATIONAL AERONAUTICS AND SPACE ADMINISTRATION

Studies of Specific Nuclear Light Bulb and

Open-Cycle Vortex-Stabilized Gaseous Nuclear Rocket Engines

Studies of Specific Nuclear Light Bulb and

Open-Cycle Vortex-Stabilized Gaseous Nuclear Rocket Engines

SUMMARY

Analytical studies were conducted to determine the characteristics of two specific vortex-stabilized gaseous nuclear rocket engines: a nuclear light bulb engine and an open-cycle engine. Both engines are based on the transfer of energy by thermal radiation from gaseous nuclear fuel suspended in a vortex to seeded hydrogen propellant. The two engines differ in that the nuclear light bulb engine employs an internally-cooled transparent wall to separate the fuel-containing vortex region from the propellant region, while the open-cycle engine relies entirely on fluid mechanics containment for preferential retention of the nuclear fuel. The majority of the work has been directed toward the nuclear light bulb engine, since recent fluid mechanics results indicate that the fuel retention characteristics of an open-cycle vortex-stabilized engine are insufficient to provide economic fuel containment. The nuclear light bulb engine offers the possibility of providing essentially perfect containment of the nuclear fuel.

One specific nuclear light bulb engine and one specific open-cycle engine have been selected for study. Both engines have a cavity volume of 170 cu ft. The open-cycle engine employs a single cavity having both a diameter and a length of 6 ft; the nuclear light bulb engine employs seven separate cavities, each having a length of 6 ft. The studies indicate approximate values of the thrust, weight, and specific impulse of both configurations. The studies have been made only in sufficient detail to provide information necessary for guidance of the research efforts which are being conducted to determine the feasibility of the engines.

The appendixes to the report describe: an analysis by the United Technology Center, a division of United Aircraft Corporation, of the weight of a filament-wound pressure vessel for a nuclear light bulb engine, and an analysis of the radiant energy emitted from the propellant stream of a nuclear light bulb engine.

RESULTS

1. A typical vortex-stabilized nuclear light bulb rocket engine might have the following characteristics:

    a. Cavity configuration -- seven separate cavities having a total overall volume of 170 ft^3 and each having a length of 6 ft.

    b. Cavity pressure -- 500 atm.

    c. Specific impulse -- 1870 sec.

    d. Total propellant flow (including seed and nozzle transpiration coolant flow) -- 49.3 lb/sec.

    e. Thrust, 92,000 lb.

    f. Engine power -- 4600 megw.

    g. Engine weight -- 70,000 lb.

    h. Ratio of average density in fuel-containment region to neon density at edge of fuel -- 0.7.

    i. Equivalent axial flow Reynolds number in neon vortex -- 5000.

2. A typical open-cycle vortex-stabilized engine might have the following characteristics (note that fluid mechanics tests have indicated that such an engine would not provide economic fuel containment):

    a. Cavity configuration -- single cylindrical engine cavity having both length and diameter of 6 ft and volume of 170 ft^3.

    b. Cavity pressure -- 1000 atm.

    c. Specific impulse -- 2190 sec.

    d. Propellant flow -- 660 lb/sec.

    e. Thrust -- 1.45×10^6 lb.

    f. Engine power -- 90,000 megw.

g. Engine weight -- 140,000 lb.

h. Ratio of average density in fuel-containment region to propellant density at edge of fuel -- 10.0.

i. Equivalent axial flow Reynolds number in vortex -- 480,000.

3. The use of a variable-throat-area nozzle in a nuclear light bulb engine rather than a fixed-throat-area nozzle will result in a major decrease in required cavity pressure during the startup process.

INTRODUCTION

One of the most interesting propulsion concepts for future space travel is the gaseous nuclear rocket engine in which heat is transferred from a gaseous fissioning fuel by thermal radiation to seeded hydrogen propellant. Because of the high temperatures obtainable in the gaseous nuclear fuel, such an engine can theoretically provide a value of specific impulse on the order of 1500 to 3000 sec and a thrust-to-weight ratio greater than unity. Successful development of a gaseous nuclear rocket engine having these characteristics would result in orders-of-magnitude decreases in the cost of many space missions.

Investigations of various phases of gaseous nuclear rocket technology are being conducted at the United Aircraft Corporation Research Laboratories under Contract NASw-847 with the Space Nuclear Propulsion Office. These investigations are designed to obtain information applicable to determining the feasibility of three different gaseous nuclear rocket concepts: the coaxial-flow reactor (Ref. 1); the vortex-stabilized nuclear light bulb reactor; and the open-cycle vortex-stabilized reactor. The most recent work conducted under this contract is described in Refs. 2 through 16. The present report along with Refs. 12 through 16 describe the progress in certain of the technical areas made through September 16, 1967.

The majority of the work under Contract NASw-847 up to 1967 has been directed toward determining the fluid mechanics characteristics of two-component gas vortexes. The information determined from these investigations is essential in determining the feasibility of the open-cycle vortex-stabilized engine, since the open-cycle engine relies on fluid mechanics phenomena for preferential containment of the nuclear fuel. This fluid mechanics information is also important in the nuclear light bulb engine because the characteristics of vortex flow appear to be ideally suited for providing separation between the gaseous nuclear fuel and the transparent wall. Results of fluid mechanics tests conducted at Reynolds numbers approximately equal to those in a full-scale open-cycle engine (Refs. 2 and 3) indicate that the fuel-retention characteristics of a vortex at high density ratios and high Reynolds numbers are insufficient to provide economic containment of fuel in a full-scale open-cycle engine. As a result, the program has been redirected so that the vortex fluid mechanics and other related programs will provide information applicable to the nuclear light bulb vortex-stabilized engine.

The work described in the following sections is part of a continuing program to provide information which can be used in interpreting the results of the research programs in terms of the characteristics of a full-scale engine (see Refs. 9, 10, 11, 14, and 17). The majority of the work described in the following sections is applicable to a nuclear light bulb engine. However, the analyses which were directed toward the open-cycle engine and which were employed in Ref. 2 in evaluating the fuel-retention characteristics of this engine are included because of their possible application to other concepts.

VORTEX-STABILIZED NUCLEAR LIGHT BULB ENGINE

Principle of Operation

Sketches illustrating the principle of operation of the nuclear light bulb engine are given in Fig. 1. Energy is transferred by thermal radiation from gaseous nuclear fuel suspended in a neon vortex to seeded hydrogen propellant. The vortex and propellant regions are separated by an internally-cooled transparent wall. A seven-cavity configuration is shown in Fig. 1 rather than a single-cavity configuration in order to increase the total surface radiating area at the edge of the fuel. The total radiating surface area for the seven-unit configuration is approximately 2.2 times that for a single-unit cavity configuration having the same total cavity volume.

Neon is injected to drive the vortex, passes axially toward the end walls, and is removed through a port at the center of one or both end walls. The resulting aerodynamic configuration is referred to as a "radial inflow" vortex (see Refs. 2 through 5). The neon discharging from the cavity, along with any entrained fuel and fission products, is cooled by being mixed with low-temperature neon, thus causing condensation of the nuclear fuel into liquid form. The liquid fuel is centrifugally separated from the neon and pumped back into the vortex region. The neon is then further cooled and pumped back to drive the vortex.

Reference Configuration at Design Point

A reference engine design has been chosen for use in evaluating the results of various component studies in terms of the characteristics of a full-scale nuclear light bulb rocket engine. The general configuration of the reference design is based on seven decisions which, although somewhat arbitrary in nature, appear logical on the basis of engine studies made using the component information available to date. These seven decisions are:

(1) Overall configuration: seven separate unit cavities with moderator-reflector material located between each cavity and surrounding the assembly of cavities.

(2) Size: length of individual cavity equal to 6.0 ft and volume of all seven cavities equal to 169.8 ft^3 (equal to the volume of a single cavity having a diameter of 6 ft and a length of 6 ft).

(3) Vortex volume for seven cavities: equal to half of the total cavity volume or 84.9 ft^3. The corresponding volume within the transparent wall of each of the seven unit cavities is 12.1 ft^3.

(4) Cavity pressure: a value of cavity pressure of 500 atm is chosen on the basis of criticality and fuel density ratio considerations (see following section).

(5) Fuel-containment region: the radius of the fuel-containment region is assumed to be 85 percent of the radius of the transparent wall.

(6) Fuel radiating temperature: assumed to be equal to 15,000 R.

(7) Propellant exit temperature: assumed to be equal to 80 percent of the fuel radiating temperature, or 12,000 R.

Sketches showing the dimensions and conditions in a unit cavity of the reference nuclear light bulb engine are given in Figs. 2 and 3. A side view drawing of the complete reference engine configuration is given in Fig. 4 and cross-sectional views showing details of the engine are given in Figs. 5, 6, and 7.

Engine Power

The black-body heat flux at the outside edge of the fuel-containment region for the assumed black-body radiating temperature of 15,000 R is 24,300 Btu/sec-ft^2. The "surface area" at the edge of the cylindrical fuel-containment region of all seven unit cavities is 179.8 ft^2. Therefore, the total energy radiated outward from the fuel is the product of these two quantities or 4.37 x 10^6 Btu/sec (4600 megw).

Surface reflection at the transparent walls will result in approximately 15 percent of the incident energy being reflected back toward the fuel-containment region. Thus, the net heat transfer by radiation through the transparent wall to the propellant region will be 85 percent of that indicated in the preceding paragraph. However, the energy lost from the fuel-containment region by thermal radiation represents only approximately 85 percent of the total energy created in the fission process. The remaining 15 percent of the energy created in the fission process is convected away from the fuel-containment region by neon flow (see following sections) or is deposited in the moderator walls by neutrons and gamma rays. Therefore, it has been assumed that the total energy created in the engine is equal to that corresponding to black-body radiation at 15,000 R (i.e., a total power of 4.37 x 10^6 Btu/sec or 4600 megw). The engine size and radiating temperature chosen provide an engine power which is approximately equal to that considered for advanced solid core nuclear rockets. Therefore, many of the facilities that are to be developed for the Rover program and that are sized by engine power level should be applicable to the reference nuclear light bulb configuration.

Hydrogen Propellant Stream Properties

At the assumed hydrogen exit temperature of 12,000 R, the enthalpy according

to Ref. 9 is 1.033 x 10^5 Btu/lb. If the total engine power is divided by this value of hydrogen enthalpy, a resulting hydrogen flow rate of 42.3 lb/sec is indicated for all seven units, which yields a value of 6.04 lb/sec for each unit cavity.

Since the hydrogen propellant must absorb approximately 15 percent of the total energy created in the process of removing heat from the engine walls and the neon recycle system, the hydrogen inlet enthalpy must be 15 percent of the hydrogen exit enthalpy, or 15,500 Btu/lb (see Fig. 3). The corresponding hydrogen inlet temperature according to Ref. 9 is 4050 R. This temperature is approximately the same as that considered for the hydrogen exit temperature in solid-core nuclear rockets.

The hydrogen flow cross-sectional area in the propellant region has been assumed to be proportional to the local average hydrogen enthalpy. Thus, the cross-sectional area at the inlet is 15 percent of the cross-sectional area at the exit. The corresponding values of hydrogen velocity at the inlet and exit are 35.5 and 23.7 ft/sec respectively (Fig. 3). It might be desirable to increase the inlet area and decrease the exit area in order to provide a uniform hydrogen velocity of approximately 30 ft/sec in the propellant region. However, insufficient information is available at present to properly design the geometry of the propellant region.

The calculated dynamic pressure of the hydrogen at the inlet to the propellant region is less than 0.05 psi (see Fig. 3). Note that this dynamic pressure is much less than that usually considered in solid-core nuclear rockets. The dynamic pressure at the exit of the propellant region is less than that at the entrance of the propellant region because of the change of hydrogen density.

Propellant Seed Characteristics

It is assumed in the following discussion that the required normal optical depth of the seeds at the propellant inlet station is 3.0. If all of the light emitted from the fuel-containment region passed only in a direction normal to the propellant region, the energy transmitted through the propellant region would be $1/e^3$, or 5 percent of the incident energy. However, many of the light rays emitted from the fuel-containment region pass in an oblique direction through the propellant region. According to Fig. 3 of Ref. 19, the percentage of light which is emitted from a black body and which would pass through a region having an optical depth of 3.0 is approximately 2 percent of the incident energy. It is also expected that a large portion of the energy which passes through the seeded propellant region and impinges on the outer wall will be reflected back into the propellant stream (see Appendix B).

It is also assumed in the following discussion that the hydrogen seed is composed of tungsten particles having a diameter of 0.05 micron. Information on

7

the absorption characteristics of such tungsten particles is given in Fig. 19 of Ref. 6. Integration of the spectral absorption parameters in this figure yields an average absorption parameter weighted by the black-body spectrum at 15,000 R of approximately 5000 cm^2/g or 2440 ft^2/lb. The distance across the propellant stream at the duct inlet is 0.0931 ft or 2.84 cm (see Fig. 2). Thus, the absorption coefficient required to provide an optical depth of 3.0 must be 1.06 cm^{-1} or 32.2 ft^{-1}. The required seed density, obtained by dividing the required absorption coefficient by the absorption parameter, is 1.32×10^{-2} lb/ft^3. This seed density is equal to 3.9 percent of the inlet propellant density.

As noted in Ref. 6, it is expected that the opacity obtainable by using thin plates will be greater than that obtainable by using spherical particles. However, the data on spherical particles rather than flat plates has been used in the preceding analysis because no information is available on the absorption character- istics of these thin flat plates, whereas data on absorption of light in streams containing spherical tungsten particles is available in Refs. 20, 21, and 22.

Neon Characteristics

The reason for injecting neon coolant between the nuclear fuel and the transparent wall is to prevent diffusion of the nuclear fuel toward the wall, thereby preventing fuel plating on the wall and preventing fission fragments from impinging on the wall. If the neon coolant is to serve this purpose, the thickness of the diffusion layer at the outside edge of the fuel-containment region must be less than the distance between the edge of the fuel-containment region and the transparent wall. This diffusion layer thickness is related to the thickness of the viscous layer in this region. In the following calculations it is assumed that the thickness of the viscous layer evaluated on the basis of the conditions at the edge of the fuel-containment region is 0.05 ft. The actual thickness of the viscous layer would be considerably less than 0.05 ft because of the decrease in temperature (and the corresponding decrease in diffusivity) with increasing radius in this region. In addition, the thickness of the diffusion layer will be less than the thickness of the viscous boundary layer because the Schmidt number is greater than unity for low fuel concentrations (see Ref. 23).

The thickness of the viscous boundary layer at the outside edge of the fuel-containment region is a function of the axial velocity in this region and the turbulence level of the flow. It is assumed in the following discussion that the flow in this region is laminar because of the stabilizing effect of radial temper- ature gradients. It was determined on the basis of the calculations procedures in Ref. 24 that a viscous boundary layer thickness at the edge of the fuel region of 0.05 ft would require an axial velocity in this region of 1.95 ft/sec near the end walls. (The axial velocity increases linearly from zero at the midplane to a specified value near the end wall according to the analysis of Ref. 24.) It was also assumed in the analysis of Ref. 24 that the axial dynamic pressure is constant in the region between the outside edge of the fuel-containment region and the

peripheral wall (neglecting boundary layer effects at both boundaries of this region). Since density increases by a factor of 7.5 between the outside edge of the fuel-containment region and the peripheral wall, the velocity must decrease by a factor of $(7.5)^{0.5} = 2.74$ in order to provide a constant axial dynamic pressure. The corresponding axial velocity of the neon next to the peripheral wall is 0.71 ft/sec.

Insufficient information is available at present to determine the variation of temperature with radius in the neon region (this temperature distribution can be controlled by proper selection of seeds in the neon). However, sample calculations were carried out assuming a linear variation of temperature with radius between the values of 15,000 deg R at the edge of the fuel and 2000 deg R at the wall. This assumed variation of temperature permitted calculation of a variation of density with radius and, from the assumption of constant axial dynamic pressure, a variation of axial velocity with radius. The total flow passing towards both end walls, obtained by integrating the resulting mass flow distribution, is equal to 2.96 lb/sec per cavity. The total energy carried away by this fluid was determined by integrating the product of density, axial velocity, specific heat, and the neon temperature rise as a function of radius. The total energy carried away from each unit by the propellant flow passing towards both end walls was determined to be 4120 Btu/sec (a constant neon specific heat of 0.253 was assumed in this analysis). The total energy carried away by the neon in all seven units is equal to 28,900 Btu/sec. This energy removal rate is approximately 0.7 percent of the total energy created in the engine.

An axial-flow Reynolds number of 5500 was calculated on the basis of the axial neon velocity of 1.95 ft/sec, the radius of the inside edge of the transparent wall, and the density and viscosity of neon at the edge of the fuel-containment region. Note that the radius of the fuel-containment region is assumed to be equal to 85 percent of the transparent wall radius according to Fig. 2. In studies of the characteristics of an open-cycle vortex-stabilized engine (Ref. 17), the edge of the fuel-containment region has been assumed to be equal to 75 percent of the radius of the vortex tube. If the neon flow of 2.96 lb/sec were passed through this increased-area annular region, the equivalent axial-flow Reynolds number would be 3500.

It will probably be necessary to provide a tangential velocity within the transparent wall of the nuclear light bulb engine which is somewhat greater than the axial neon velocity in order to provide the stabilizing effect necessary to create laminar flow at the edge of the fuel-containment region. It has been arbitrarily assumed in the following calculations that this tangential velocity is 10 ft/sec, or approximately 5 times the maximum axial velocity. The corresponding dynamic pressure of the neon at the inside edge of the transparent wall is approximately 0.075 lb/in.^{2}.

The centrifugal acceleration corresponding to the tangential velocity at the

inside edge of the transparent wall is 3.9 g's. Insufficient information is available at present to determine whether this centrifugal acceleration is sufficient to prevent problems resulting from axial vehicle accelerations. If such problems should arise, it will be necessary to increase the tangential velocity at the outer periphery of the vortex tube. However, the dynamic pressures at injection are sufficiently low in the present reference design that relatively large increases in velocity can be tolerated without encountering intolerably high dynamic pressures due to this tangential velocity.

Fuel Region Characteristics

Corporate-sponsored studies have indicated a critical mass requirement for the reference engine of approximately 25 lb. (More detailed studies described in Ref. 14 indicate that this mass may be somewhat low, but it has been used in the calculation described in the present report.) This critical mass is less than that for the open-cycle engine because of the moderating effect of the material located between adjacent cavities (the open-cycle engine is assumed to have a single cavity rather than seven separate cavities). The average fuel density based on the volume inside the edge of the fuel-containment region of the seven cavities in the reference engine is 0.409 lb/ft^3. Thus, the average density of the fuel is only 44 percent of the density of the neon at the outside edge of the fuel-containment region. The gases in the fuel-containment region are considerably hotter than the gases at the outside edge of the fuel-containment region. On the basis of the studies of Ref. 8, the average temperature in the fuel-containment region is approximately 42,000 R. The resulting average neon density in the fuel-containment region is approximately 0.24 lb/ft^3 (accounting for the fuel partial pressure but neglecting neon ionization). Thus, the average total density (the sum of average fuel density and average neon density) in the fuel-containment region is approximately 0.65 lb/ft^3. This total density is only 70 percent of the density of the neon at the outside edge of the fuel-containment region. On the basis of results obtained under the fluid mechanics portion of the work under Contract NASw-847 (see Refs. 2, 3, 4, 5, 15 and 16), it is believed that this low value of the ratio of average density in the fuel-containment region to edge-of-fuel density will result in greater stability in the flow in a nuclear light bulb engine than in an open-cycle engine, where the corresponding required density ratio is approximately 10.

The volume flow of neon passing through the cavity obtained by dividing the neon mass flow of 2.96 lb/sec by the neon density at the outside edge of the fuel-containment region of 0.924 lb/ft^3 is 3.2 ft^3/sec. The resulting average neon dwell time obtained by dividing the vortex volume of 12.1 ft^3 by the neon volume flow rate is 3.8 sec. If the average fuel dwell time is equal to 5 times the average neon dwell time (see Refs. 2, 3, 4, 5, 15 and 16), the average fuel dwell time would be approximately 19 sec. Since the nuclear fuel mass per unit is approximately 3.6 lb, this fuel retention time would correspond to a fuel flow rate of approximately 0.19 lb/sec per unit cavity.

An estimate of the energy carried away by the fuel passing through the cavity can be obtained by multiplying the fuel flow rate by the average fuel exit enthalpy. This average fuel exit enthalpy can be estimated by multiplying the average fuel temperature of 42,000 R by a specific heat of 0.1 Btu/lb-deg R. The corresponding energy removal rate is approximately 800 Btu/sec per unit, or 5600 Btu/sec for the seven unit cavities. This energy removal rate is approximately 0.13 percent of the total energy creation rate in the engine.

Specific Impulse and Thrust

The exhaust velocity which would be created by converting all of the hydrogen enthalpy of 1.033×10^5 Btu/lb to kinetic energy would be 71,900 ft/sec. This exhaust velocity would correspond to a specific impulse of 2230 sec. This ideal specific impulse has been reduced to account for the following factors:

(1) The specific impulse has been reduced by 8 percent to allow for incomplete expansion due to an area ratio of 545 rather than infinity (corresponding pressure ratio equals 1000, see Ref. 9).

(2) The specific impulse has been reduced by 6 percent to account for the requirement for approximately 12 percent transpiration coolant flow for the nozzle (see Ref. 25).

(3) The specific impulse has been reduced by 1.95 percent to allow for the 3.9 percent mass fraction of tungsten seeds.

(4) The specific impulse has been reduced by 1 percent to allow for friction and recombination losses in the nozzle.

The final specific impulse on the basis of these four corrections is 84 percent of the ideal specific impulse, or 1870 sec.

The total flow passing through the nozzle exit (including an allowance for 3.9 percent seed and 12 percent transpiration cooling for the nozzle) is 49.3 lb/sec. The thrust produced by this flow at a specific impulse of 1870 sec would be 92,000 lb.

According to Ref. 9, the hydrogen flow per unit area at the throat for a stagnation temperature of 12,000 R and a stagnation pressure of 500 atm is 1062 lb/sec-ft^2. If the flow area occupied by the seed flow is neglected, and half of the transpiration coolant flow is assumed to be injected upstream of the throat, the corresponding throat flow area would be 0.0422 ft^2. If a single nozzle were employed, the throat diameter would be 0.232 ft. For the nozzle area ratio of 545 assumed in calculating a loss in specific impulse due to a finite area ratio, the nozzle exit area would be 23.0 ft^2. The corresponding diameter of the exit of a single nozzle is 5.40 ft, which is substantially less than the overall engine

diameter. For the seven-nozzle configuration shown in Figs. 2 through 7, the throat and exit diameters would be 0.0875 ft (1.05 in.) and 2.04 ft, respectively.

Moderator Cooling Circuits

Heat Deposition Rates

Heat is deposited in various portions of the engine by a number of different mechanisms: neutron and gamma ray heating; convection and thermal radiation from the hot gases; convective cooling of the fuel recycle system; and conduction from one portion of the structure to another. The results of a preliminary analysis to determine the magnitude of the net energy deposited in each portion of the reference engine design is given in Table I. In some regions, more complete analysis of the specific configuration shown in Figs. 4 through 7 has led to different heat deposition rates than those shown in Table I. In other regions, insufficient information is available to permit a more accurate estimate of heat deposition rates. However, the heat deposition rates shown in Table I are believed to be sufficiently accurate for the purposes of this report, which is to provide only a preliminary indication of a possible engine configuration. More complete information on the energy deposited by thermal radiation in the transparent walls is given in Ref. 26, and on the energy deposited by thermal radiation in the reflecting walls is given in Appendix B.

General Configuration of Cooling Circuits

The moderator is cooled by two hydrogen circuits, the primary hydrogen propellant circuit and the secondary closed hydrogen circuit. A schematic flow diagram is shown in Fig. 8. The primary hydrogen circuit enters the pressure vessel and is pumped to a pressure of approximately 708 atm. It then passes through a series of heat exchangers and then through a turbine which provides the power for the primary hydrogen, secondary hydrogen, neon and fuel recycle pumps. After exiting from the turbine, the primary hydrogen flow cools the solid moderator regions (beryllium oxide and graphite) and then is injected between the cavity liner and the transparent structure. The temperature and pressure levels in this circuit are shown in Table II.

The hydrogen in the secondary circuit has a minimum temperature of approximately 300 R at the exit of the secondary circuit pump. This hydrogen is first used to cool the pressure vessel, the solid moderator flow divider, the tie rods and the cavity liner tubes. After cooling the cavity liner tubes the secondary hydrogen circuit passes through a hydrogen-neon heat exchanger where it extracts the heat generated in the fuel recycle system and then passes through the transparent structure. The heat absorbed by the secondary circuit is rejected to the primary hydrogen circuit in a series of heat exchangers. After exiting from the hydrogen-hydrogen heat exchanger, the secondary hydrogen circuit passes through

the secondary circuit pump and then repeats the same circuit. The temperature and pressure levels in the secondary closed circuit are shown in Table III. The vent at the exit of the transparent structure region (Station 13 on Fig. 8) connects the secondary hydrogen circuit at that point with the primary hydrogen circuit at its point of injection into the cavity (Station 6 on Fig. 8). The pressure at these two stations is equal during design-point operation and the vent is provided to reduce the possibility of overpressure in the transparent structure during start up or in the event of other flow or pressure variations.

Transparent Structure

It is assumed in the present study that the entire transparent structure is made from high-quality fused silica. This transparent structure is divided into three segments within each unit cavity, with each segment occupying 120 deg of the total circumference of each cavity, as shown in Fig. 7. Each segment of the transparent structure is divided into two regions: a hydrogen-cooled region and a neon-cooled region. The hydrogen-cooled region consists of a feeder pipe and a collector pipe which are connected by a series of transparent tubes. Each of· the transparent tubes passes radially inward through one strut, passes in a circumferential direction between the vortex region and the propellant region, and then passes radially outward through a second strut. Table IV lists the specifications and operating conditions of the hydrogen-cooled portion of the transparent structure.

The neon-cooled portion of the transparent structure consists of a feeder pipe and a series of neon injection tubes. The neon injection tubes pass radially inward from the feeder pipe through a strut into the vortex region. These tubes are used to inject neon tangentially along the inner surface of the hydrogen-cooled portion of the structure. The neon passes through the vortex and exits from the vortex chamber through the forward end plug.

Cavity Liner

The cavity liner is constructed from a series of beryllium tubes which are internally cooled by the secondary hydrogen circuit. The tubes are coated on the outside with a thin layer of aluminum to provide a high reflectivity for incident thermal radiation (see Appendix B). The maximum surface temperature of the cavity liner tubes is approximately 1360 R which is considerably lower than the melting point of aluminum (1670 R). If necessary, the temperature of the cavity liner could be further reduced by cooling the cavity liner before the tie rod and the divider between the beryllium oxide and graphite. Although the use of an aluminum wall rather than a wall made from a higher temperature material will increase the convective heat transfer to the wall, the resulting change in convective heat transfer is small because the change in wall temperature is small relative to the difference between stream temperature and wall temperature. The specifications of

the cavity liner and its components are listed in Table V, and a section of the liner region is shown in Fig. 7.

Solid Moderator Region

The solid moderator region consists of a beryllium oxide region surrounding each cavity and a graphite region surrounding the seven-cavity array (see Figs. 5 and 6). In addition to the cylindrical moderator regions surrounding the cavities, there are end plugs of graphite moderator on both ends of each cavity. The cylindrical beryllium oxide and graphite regions are separated by an annulus formed by two insulated beryllium walls. These walls serve as a flow divider for the solid moderator regions and as a container for the graphite and beryllium oxide.

The solid moderator region is cooled by passing hydrogen through a series of axial coolant passages. The coolant enters the beryllium oxide at the forward end of the reactor, passes through the beryllium oxide, and returns to the forward end through the graphite. The number and spacing of coolant holes in the solid moderator regions is determined by the internal heat generation rates, desired coolant-to-wall temperature difference and the cooling hole orientation. The characteristics at the selected design point are shown in Table VI.

Structural Support

The structural components which support the moderator and separate it from other portions of the engine are: a grid at both ends of the reactor; a series of 24 tie rods connecting the grids; an annular flow divider between the beryllium oxide and graphite; and a tungsten liner surrounding the graphite region. The grid on the aft end of the reactor is attached to the pressure vessel by a series of ribs as shown in Fig. 4. The design criteria which was used to determine the size of the grids and tie rods was an acceleration load of 10 g's with the reactor at ambient temperatures ($\sim$ 530 R) and 1 g at operating temperature (1700 to 2700 R depending upon location).

The forward grid may be constructed of inconel or some similar alloy since the temperature in the forward region is approximately 1800 R and the grid is external to the moderator so that the neutron absorption characteristics are not critical. Those portions of the rear grid which support the moderator end plugs must be insulated since they are exposed to the propellant stream at the exit.

The tie rods are constructed from beryllium insulated with pyrolytic graphite and internally cooled by the secondary hydrogen circuit. The tie rods were sized for a 10 g acceleration load at ambient temperature and their specifications and operating conditions are listed in Table VII.

The solid moderator flow divider is an irregular shaped structure following

14

the outer contours of the beryllium oxide region. The structure is formed by two beryllium walls with pyrolytic graphite insulation on the outside and hydrogen coolant passing between the beryllium walls. The specifications and operating conditions are shown in Table VIII.

The external graphite container is a thin-walled tungsten liner which serves primarily as a flow divider between the graphite and the pressure vessel. It also provides support to the graphite pieces in the external moderator.

Heat Exchangers and Piping

The secondary hydrogen circuit transfers the energy absorbed in cooling the pressure vessel, support structure, beryllium oxide-graphite flow divider, cavity liner, transparent walls and fuel recycle system to the primary hydrogen circuit via a series of hydrogen-to-hydrogen heat exchangers. The specifications for these heat exchangers are shown in Table IX. Seven heat exchangers were used since this allows the flow from each cavity to be piped directly to a heat exchanger without additional manifolding; also, the size of the heat exchangers is such that they may be installed in the space between the pumps and the pressure vessel. The high pressure portion of the primary hydrogen circuit ($P \sim 700$ atm) is on the tube side of the heat exchangers and the secondary hydrogen circuit ($P \sim 500$ atm) is on the shell side in order to minimize shell thickness.

The present coolant flow scheme requires an extremely complex piping and manifolding system as indicated in Figs. 4 and 5. At present the pressure losses and insulation requirements for the piping have been estimated. The insulation thickness has been estimated based on a 1775 R operating temperature in the forward region and pyrolytic graphite insulation. The approximate thickness of insulation required is 0.025 inches of insulation per inch of pipe radius, and this approximation was used to estimate the insulation weight required.

The secondary hydrogen circuit piping may be beryllium from the pump to the fuel recycle heat exchanger entrance, since the coolant temperature is low (< 1100 R). The manifolding from the graphite outlet to the propellant inlet region must be tungsten since the coolant temperature is above 4000 R. The intermediate-temperature piping, the fuel recycle heat exchanger and the hydrogen-to-hydrogen heat exchanger (1600 R to 2000 R temperature range) may be constructed from stainless steel alloys.

Engine Weight

Results of a study to determine the weight of a nuclear light bulb engine are given in Table X. The weight of most of the components in Table X were made on the basis of configurations discussed in preceding sections. The turbopump weight was determined from the turbopump weight given in Ref. 11 with an allowance for differences in engine pressure and hydrogen flow. The miscellaneous weight noted in

15

Table X includes an allowance for exhaust nozzles, fuel recycle systems, and the equipment necessary to provide a magnetic field within the cavity to prevent impingement of beta particles on the cavity walls (see Ref. 27).

Particular attention was devoted in this study to determining the weight of the pressure vessel because of the uncertainty in pressure vessel weight noted in Ref. 11. The present study was based on an analysis which is described in Appendix A and which was made by the United Technology Center, a division of United Aircraft Corporation. Of four pressure shell configurations which are considered in Appendix A, the configuration of greatest interest is the one which has a contour approximately similar to the contour shown in Fig. 4 and which contains seven separate holes in the aft end for passage of separate nozzles from each of the seven unit cavities. The actual volume enclosed by the pressure shell considered in Appendix A is less than that in Fig. 4. The pressure shell from Appendix A was estimated to weigh 19,400 lb for an internal pressure of 500 atm and a total enclosed volume of 559 ft^3. The shell weight parameter, Z (see Ref. 11), is therefore

$$Z_s = \frac{\text{Weight}}{(P)(\text{Volume})} = \frac{19,400}{(500)(559)} = 0.0695 \frac{\text{lb}}{\text{atm-ft}^3} \tag{1}$$

This value of Z_s is approximately 40 percent less than the value of Z_s of 0.116 for a cylindrical maraging steel pressure vessel from Ref. 11.

One of the problems noted in Appendix A is the high axial load per unit circumferential length in the joint separating the two halves of the pressure shell. This load per unit length could be reduced by employing more than two separate pressure shells (again, with a control system to set the pressure between adjacent shells so as to equalize the stresses in each shell). The use of more than two shells would also reduce shell weight. For instance, use of four shells rather than two shells would reduce the weight associated with the joints by a factor of 2 from 2350 lb to 1175 lb. This represents a reduction in overall shell weight of approximately 6 percent. In addition, the resulting ratio of wall thickness to shell diameter would be reduced, with a resulting decrease in the factor associated with the finite shell thickness (see Appendix A). A reduction by a factor of two in the shell thickness would result in a reduction in shell weight by approximately 9 percent. Thus, the overall reduction in weight resulting from the use of four rather than two shells would be approximately 15 percent.

It is also noted in Appendix A that no allowance has been made for radiation damage to the shell material or for fatigue due to many pressure cycles within the shell. Therefore, it has been arbitrarily decided to employ the 15 percent factor of safety which would result from using four rather than two pressure shells as an allowance for radiation damage and pressure cycling effects.

The pressure shell shown in Fig. 4 also has a larger internal volume than the

pressure shell considered in Appendix A by a factor of approximately 1.57. Therefore, on the basis of Eq. (1), the pressure vessel weight should be increased by a factor of 1.57 to approximately 30,500 lb. This pressure vessel weight is shown in Table X.

Reference Configuration During Startup

Two analyses have been made to determine the startup characteristics of the reference engine discussed in preceding sections. The first analysis is based on the use of a fixed nozzle throat area of 0.0398 ft^2 (excluding the allowance for half of the transpiration coolant flow -- see preceding section). The second analysis is based on the use of a variable-throat-area nozzle which will maintain a fixed neon density at the outside edge of the fuel-containment region. Results of these two analyses are described in the following two subsections.

Engine Startup with Fixed Nozzle Throat Area

The mass flow passing through the throat area of the reference engine discussed in the preceding section is a function of the total pressure and total temperature of the hydrogen propellant upstream of the throat. Results of calculations of this weight flow made using the parameters tabulated in Ref. 9 are given in Fig. 9. The engine power obtained by multiplying the nozzle flow in Fig. 9 by the enthalpy determined from Ref. 9 is shown in Fig. 10.

The power created in the engine is proportional to the fourth power of the fuel radiating temperature if the ratio of radiated energy to total energy is independent of engine power. Fuel radiating temperatures calculated on this basis using the total engine powers given in Fig. 10 are shown in Fig. 11. The combinations of conditions in Fig. 11 which lead to a propellant exit temperature equal to 80 percent of the fuel radiating temperature are also indicated on Figs. 9 and 10.

The density of the neon at the edge of the fuel is proportional to engine pressure and inversely proportional to fuel radiating temperature. Values of neon density at the edge of the fuel determined from the temperatures and pressures in Fig. 11 are given in Fig. 12. As noted on this figure and in preceding figures, the design value of edge-of-fuel density is 0.924 lb/ft^3. The conditions which lead to this edge-of-fuel density are also noted on the curves in Figs. 9 through 11.

The fuel density required for criticality will probably not be significantly different during startup than it is during operation at the engine design point. Since the ratio of average fuel density to edge-of-fuel density during design-point operation will probably be close to the maximum value allowable from fluid mechanics stability considerations, it will probably not be possible to operate with a reduced edge-of-fuel density during engine startup. It can be seen from Fig. 12 that operating with a propellant exit temperature equal to 80 percent of the edge-of-fuel temperature results in very low edge-of-fuel densities during

17

startup. If the density at the edge of fuel is fixed at 0.924 lb/ft^2 during startup, the engine pressures and weight flows become extremely high. This can be partially avoided by the use of a variable-throat-area nozzle as discussed in the following subsection.

Engine Startup with Variable Nozzle Throat Area

With a variable nozzle throat area, it is possible to adjust the density at the edge of the fuel-containment region to any arbitrarily specified value independent of the characteristics of the propellant stream. The engine pressure required to maintain an edge-of-fuel density of 0.924 lb/ft^3 is shown in Fig. 13 as a function of fuel radiating temperature (pressure is inversely proportional to fuel radiating temperature in this example). The energy created in the reactor is also shown in Fig. 13 and is proportional to the fourth power of fuel radiating temperature (see preceding section). The hydrogen propellant flow rate passing through the reactor is a function of the total power and the ratio of propellant exit temperature to fuel radiating temperature, T_e/T^*. The effect of fuel radiating temperature on this weight flow is shown in Fig. 14 for values of T_e/T^* of 0.5 and 0.8. These weight flows were determined by dividing the total power by the enthalpy corresponding to the propellant exit temperature.

The exhaust nozzle throat area required to pass the propellant flow indicated in Fig. 14 is also shown in this same figure. This nozzle area was determined on the basis of the information tabulated in Ref. 9. It can be seen from Fig. 14 that a reduction in radiating temperature by a factor of 2 (with a corresponding reduction in engine power by a factor of 16) will result in a required reduction in nozzle throat area by a factor of approximately 3. The mechanism required to vary the throat area must withstand a high pressure differential; however, since the absolute areas involved are small, this mechanism should not be extremely heavy. It might be desirable to employ two different throats: a fixed-geometry transpiration-cooled throat for use at high temperatures and a variable-geometry throat located downstream of the fixed-geometry throat for use at lower temperatures.

Values of specific impulse corresponding to the temperatures and pressures shown in Figs. 13 and 14 are given in Fig. 15. Values of engine thrust determined by multiplying weight flow by specific impulse are also shown in Fig. 15. These values of thrust were corrected to allow for the thrust of the transpiration coolant flow in the same manner as described in a preceding section.

VORTEX-STABILIZED OPEN-CYCLE ENGINE

Principle of Operation

The principle of operation of an open-cycle vortex-stabilized engine (Refs. 2, 11 and 24) is the same as that for a vortex-stabilized nuclear light bulb engine except that the open-cycle engine does not employ a physical transparent wall between the fuel-containment and propellant regions. The open-cycle engine relies entirely on fluid mechanics phenomena to provide preferential retention of the nuclear fuel. Because of this, the primary problems in such an engine are fluid mechanic in nature. As a result, the investigation of the characteristics of an open-cycle vortex-stabilized engine which was initiated at the UAC Research Laboratories in 1959 have concentrated on the fluid mechanics characteristics of vortex flow. Extensive investigations of the characteristics of vortex flow have indicated that the fuel retention characteristics of this engine are lower than are required from economic considerations. Summaries of these fluid mechanics investigations are given in Refs. 2, 3, 4 and 5. Although this engine does not appear to be feasible at the present time, the results of studies of the characteristics of the engine are described in the following sections because of the possible application of this information to other engine concepts.

Specific Configuration at Design Point

The results of studies of the characteristics of a specific configuration of an open-cycle vortex-stabilized engine are given in Refs. 10 and 11. A sketch of the configuration chosen is given in Fig. 16. The diameter of the cavity in this engine is 6 ft and the average cavity length is 6 ft. The conditions in the cavity of the reference engine design are given in Table XI. This engine was determined to have a specific impulse of 2190 sec and a thrust of 1.45×10^6 lb according to Ref. 11. The fuel density ratio in Ref. 11 was based on a critical fuel mass of 18.1 lb. However, early results of more recent studies (Ref. 14) have indicated that the actual critical fuel mass is approximately twice this value, or 36.2 lb. Therefore, the corresponding fuel density ratio is 10.0 rather than the value of 5.0 noted in Ref. 10.

Moderator Configuration

Three modifications to the moderator configuration of the specific gaseous nuclear rocket engine configuration presented in Ref. 11 were investigated to determine their effects on overall design and performance. These modifications were (1) replacement of the tungsten liner tubes with pyrolytic-graphite-coated beryllium tubes, (2) elimination of the heavy water moderator, and (3) substitution of hydrogen for helium in the moderator coolant circuit. The specific combinations of these modifications which were investigated are listed in Table XII. Configuration A represents the original design of Ref. 11, Configuration B incorporates

modification (1) above; Configuration C incorporates modifications (1) and (2), Configuration D incorporates modifications (1) and (3); and Configuration E incorporates all three of the modifications. The effects on the moderator configuration, operating conditions, and engine weight, exclusive of pressure vessel, are discussed.

Beryllium Liner Tubes

The use of beryllium liner tubes reduces the amount of tungsten in the inner liner region and eliminates the bimetallic tungsten-beryllium joints where the tubes join the beryllium liner. The basic configuration of the liner tubes is similar to the original design and is shown in Fig. 8 of Ref. 11.

Because of the high cavity wall temperatures (~ 5000 R) and the high radiant and convective heat flux (~ 2360 Btu/sec-ft^2), the beryllium tubes must be surrounded by an insulator such as pyrolytic graphite. The pyrolytic graphite is coated with niobium carbide to protect it from the hot hydrogen in the cavity. It is assumed that the pyrolytic graphite is deposited on the beryllium tubes in such a manner that the thermal conductivity is low in the radial direction ($\sim 1.8 \times 10^{-4}$ Btu/sec-ft-deg R) and is high in the circumferential direction ($\sim 1.7 \times 10^{-2}$ Btu/sec-ft-deg R). The ratio of pyrolytic graphite thickness to half circumference is on the order of 0.3, and a comparison of the quotient of the thermal conductivity and distance predicts a relatively uniform circumferential temperature distribution. The entire surface area of the liner tube was used as a heat transfer area in the calculation of the film temperature drop and the required tube diameter.

A comparison of the design characteristics of the liner tubes for the various configurations is shown in Table XIII. The operating conditions for the beryllium tube configurations are based on a maximum beryllium temperature of 1500 R.

Referring to Configuration B, where helium is used as a moderator coolant and the heavy water moderator is present, the calculations predict an extremely high pressure loss in the tubes. The heat generated in the heavy water moderator increases the minimum inlet temperature to the tubes to 900 R and allows only 600 R for a film temperature drop in the tubes. The required film temperature drop can be achieved only by a small tube diameter (~ 0.031 in.) with a high dynamic pressure (~ 8 atm) or a change in tube length which would modify the inner liner configuration. If the heavy water is removed, the inlet temperature is reduced to 564 R and the resulting configuration is shown as Configuration C.

If hydrogen is used as a coolant, the total pressure loss in the tubes decreases by a factor of 10, and the beryllium tubes could be used with the heavy water present (Configuration D) or with the heavy water removed (Configuration E).

Elimination of Heavy Water Moderator

The heat generated in the heavy water region of the moderator is approximately 9.0×10^5 Btu/sec and, since the heavy water must be maintained at a temperature below 1000 R, it represents a relatively low-temperature heat source. The heavy water must be cooled by the moderator coolant before it enters the liner tubes, and the combined heat from the pressure vessel and the D_2O raises the coolant inlet temperature to 903 R. Elimination of the D_2O lowers the tube inlet temperature to 564 R, eliminates the D_2O heat exchangers and circulation system, and eliminates the outer containment shell of the D_2O region. The thickness of the beryllium oxide and graphite regions is increased in order to maintain the 4500 R outlet temperature.

The characteristics of the moderator region with the heavy water removed (Configurations C and E) are compared with the design of Ref. 11 in Table XIV. In addition to the weight saving in the solid moderator which is shown in the table, there is a decrease of 4.3 in. in the inside radius of the pressure vessel which would reduce the pressure vessel weight.

Substitution of Hydrogen as a Moderator Coolant

The use of hydrogen as a moderator coolant permits a reduction by a factor of 3.2 in the moderator coolant flow rates if the temperature levels are maintained at the same levels as specified in the preliminary design. This reduction in flow rate is more than enough to offset the decreases in fluid density, and the dynamic pressure is reduced by a factor of 5 to 10 depending on the fluid temperature. If all of the cooling hole and piping dimensions are held constant, the total coolant pressure drop would be reduced from 35 to 7 atm and the pumping power requirements reduced. Another alternative is to reduce the piping and heat exchanger dimensions in order to reduce the engine weight. A comparison of piping sizes and weights is shown in Table XV. A redesign of the high-temperature heat exchanger showed a 40 percent reduction in the weight was possible with a hydrogen moderator coolant.

The use of hydrogen as a moderator coolant makes it necessary to coat the graphite moderator with niobium carbide in order to protect it from attack by the hot hydrogen. The quantity of niobium carbide necessary as a function of pressure drop in the graphite region is shown in Fig. 17. This plot is based on the graphite thickness used in engine Configuration D (8.7 in.) and a 0.002 in. niobium carbide coating on the cooling hole surfaces. In addition to the niobium carbide on the cooling passages, approximately 15 lb are required to coat the graphite in the region of the propellant and coolant inlets.

Engine Weight

A comparison of total engine weight exclusive of pressure shell for the configurations investigated is shown in Table XVI. In addition to total weights,

21

the absorbing area of the tungsten-184 and niobium carbide are listed to show the relative amounts of neutron absorbing materials present in the various configurations.

The largest uncertainty in the estimate of the weight of the overall configuration in Ref. 11 was due to uncertainty in the weight of the pressure vessel. As noted in Table XIV of Ref. 11, the estimates of pressure vessel weight varied from 30,000 to 125,000 lb. The studies conducted at the United Technology Center Division of United Aircraft Corporation (see Appendix A) permit a more accurate estimate to be made of the pressure vessel weight. These estimates of pressure vessel weight were made on the basis of a value of the parameter Z_s of 0.0695 lb/ft^3-atm (see Eq. (1)). The volumes within the pressure shell required in the estimation of pressure vessel weight are given in the upper row of Table XVII for each of the engine configurations noted in Table XII. The corresponding weights of the pressure vessel are shown in the second row. The third row contains weights of components other than the pressure vessel from Table XVI. The fourth and last row indicates the total weight of the overall configuration.

<center>Interpretation of Fuel Loss Rate Parameters</center>

Criteria for Acceptable Fuel Loss Rate

In the following discussion, it is assumed that economics will govern the minimum acceptable loss rate of nuclear fuel from a gaseous nuclear rocket engine. In determining this acceptable fuel loss rate, it is necessary to specify a mission for the engine. In the following discussion, the mission considered will be that of Ref. 17 in which the gaseous-nuclear-rocket-powered vehicle is boosted by a Saturn I-C launch vehicle, after which the gaseous nuclear rocket engine is employed to accelerate the vehicle into orbit and thence to a velocity 50,000 ft/sec greater than orbital velocity. It is assumed that there is one gaseous nuclear rocket engine stage and two tankage stages. The engine considered in the analyses is assumed to have the characteristics discussed in the preceding section (see Table XI). According to Fig. 76 of Ref. 17, this engine could be used to accelerate a payload of 285,000 lb through the velocity increment considered. If there were no loss of nuclear fuel, the total propellant consumed by the gaseous nuclear rocket would be approximately 875,000 lb, and the cost would be $225 per lb of payload on the basis of the information in Fig. 100 of Ref. 17.

The permissible fuel loss rate must be judged on the basis of the difference in mission costs calculated using gaseous nuclear rockets and solid-core nuclear rockets. According to Table V of Ref. 17, the cost of using four stages of solid-core nuclear rockets in a suborbit-start mode would be $2,426 per lb of payload for the same mission considered for the gaseous nuclear rocket. Thus the potential savings that could be accrued by using a gaseous-core nuclear rocket providing perfect containment rather than solid-core nuclear rockets is $2,426 minus $225 or

$2,201 per lb of payload. Since the payload for the gaseous nuclear rocket is 285,000 lb, the absolute savings per flight would be $6.28 x 10^8.

The first reference point for fuel loss rate in a gaseous nuclear rocket is calculated on the basis that the total cost per pound of payload would be the same for the gaseous nuclear rocket as for the solid-core nuclear rocket. If the fuel cost is assumed to be $7,000 per lb (as in Ref. 17), this break-even criteria would permit loss of 89,700 lb of nuclear fuel. Therefore, the ratio of the total propellant employed to total fuel loss would be 875,000/89,700 or 9.76. The actual ratio of propellant flow to fuel flow would have to be considerably greater than this value in order to justify the development of a gaseous nuclear rocket.

Next, assume that the costs associated with the flight of a gaseous nuclear rocket must be one-third of those for a solid-core nuclear rocket in order to justify engine development. Thus the cost per pound of payload would be 2426/3 or $808 per lb of payload. The allowable cost of the fuel would be $808 minus $225 or $583 per lb of payload, or $1.66 x 10^8. Proceeding as before, the total fuel loss would be (1.66 x 10^8)/(7000) or 23,700 lb, and the ratio of the total propellant used to fuel loss would be 875,000/23,700 or 36.9.

Interpretation of Acceptable Fuel Loss Rates in Terms of Time Constant Parameters

A number of different fuel loss rate parameters have been employed in the fluid mechanics tests described in Refs. 2, 3, 4 and 16. One of these is the fuel time constant parameter, t_F, which is defined as the fuel stored (36.2 lb for the conditions of Table XI) divided by the fuel flow rate. Fuel or heavy-gas time constants measured in the fluid mechanics tests of Refs. 2, 3, 4 and 16 have been made dimensionless by dividing by the parameter $(\rho/\mu)r_1^2$. In interpreting these dimensionless fuel time constants in terms of the characteristics of a full-scale engine, it is necessary to select the value of ρ/μ which has the greatest influence on the fuel loss rate in the full-scale engine. The studies of Ref. 17 employed a value of ρ/μ determined on the basis of the propellant characteristics at the centerline temperature and the fuel cavity pressure. As noted in Table XI, the resulting definition of $(\rho/\mu)r_1^2$ provides a value of fuel time constant parameter of 1195 sec. It is also possible to define the fuel time constant parameter on the basis of ρ/μ at the outside edge of the fuel-containment region (Station 6). This second choice of ρ/μ provides a value of $(\rho/\mu)r_1^2$ of 2820 sec as noted in Table XI.

Some of the data in Refs. 2, 3, 4 and 16 has also been plotted in terms of the ratio of fuel time constant to a minimum time constant determined on the basis of complete mixing of the fuel and propellant at injection. In converting values of $t_F/t_{F_{MIN}}$ from model tests to full-scale engines, it is also necessary to make a choice as to the density employed in calculating volume flow. In Table XI, this volume flow, Y_6, was determined by dividing the cavity propellant flow by the density at Station 6. As noted by the last item in Table XI, the resulting minimum

time constant determined by dividing the cavity volume by the volume flow is equal to 0.01546 sec.

The interrelation between various parameters which are a measure of fuel loss rate or containment time and various criteria for containment is given in Table XVIII. In addition to the economics criteria determined in the preceding subsection, all parameters are calculated on the basis of three additional criteria: fully-mixed flow, a value of τ_{F1-8} of 0.01, and a ratio of propellant flow to fuel flow of 10^3. The parameters $t_{F_{MIN}}$, $(\rho/\mu)_6 r_1^2$, $(\rho/\mu)_8 r_1^2$, w_F and W_T used in evaluating Columns ② through ⑥ of Table XVIII were obtained from Table XI. The constant employed in evaluating Column ⑦ was obtained by multiplying the cost per pound of fuel ($7,000 per lb) by the propellant consumed (875,000 lb) and dividing by the payload (285,000 lb). The reduction in hydrogen propellant weight resulting from the weight of the fuel required (i.e., the change in specific impulse due to the change in molecular weight) is neglected. The constant of 225 used in evaluating Column ⑧ represents the costs exclusive of the fuel costs. The economic criteria which states that the costs must be one-third of those associated with a solid-core nuclear rocket lead to values of $t_F/t_{F_{MIN}}$ of 150 or a value of τ_{F1-8} of 0.001942 at an axial-flow Reynolds number of 480,000.

An analysis similar to that described in the preceding paragraphs for the suborbit-start mission profile was also carried out for an orbit-start mission profile. If there was no loss of fuel from the gaseous nuclear rocket, the cost per pound of payload with orbit start would be $578 per lb of payload on the basis of using the same engine, the same payload, and the same required velocity increment beyond orbit as for the suborbit-start profile. According to Table V of Ref. 17, the costs with orbit start using solid-core nuclear rockets would be $2,703 per lb of payload. The required ratio of fuel time constant to minimum fuel time constant to provide overall mission costs equal to those for a solid-core nuclear rocket and equal to one-third of those for a solid-core nuclear rocket would be 22.0 and 194, respectively (the corresponding numbers for suborbit start are 39.8 and 150, respectively, according to Table XVIII).

24

REFERENCES

1. Ragsdale, Robert G. and Frank E. Rom: Gas-Core Reactor Work at NASA/Lewis. AIAA Paper No. 67-499 presented at the AIAA 3rd Propulsion Joint Specialist Conference, Washington, D. C., July 17-21, 1967.

2. Clark, J. W., J. S. Kendall, B. V. Johnson, A. E. Mensing, and A. Travers: Summary of Gaseous Nuclear Rocket Fluid Mechanics Research Conducted Under Contract NASw-847. UAC Research Laboratories Report F-910091-13 prepared under Contract NASw-847, May 1967. To be issued as NASA CR report.

3. Kendall, J. S., A. E. Mensing, and B. V. Johnson: Containment Experiments in Vortex Tubes with Radial Outflow and Large Superimposed Axial Flows. UAC Research Laboratories Report F-910091-12 prepared under Contract NASw-847, May 1967. To be issued as NASA CR report.

4. Johnson, B. V.: Exploratory Flow and Containment Experiments in a Directed-Wall-Jet Vortex Tube with Radial Outflow and Moderate Superimposed Axial Flows. UAC Research Laboratories Report F-910091-11 prepared under Contract NASw-847, May 1967. To be issued as NASA CR report.

5. Travers, A.: Experimental Investigation of Flow Patterns in Radial-Outflow Vortexes Using a Rotating-Peripheral-Wall Water Vortex Tube. UAC Research Laboratories Report F-910091-10 prepared under Contract NASw-847, May 1967. To be issued as NASA CR report.

6. Krascella, N. L.: Theoretical Investigation of the Absorptive Properties of Small Particles and Heavy-Atom Gases. UAC Research Laboratories Report E-910092-7 prepared under Contract NASw-847, September 1966. Also issued as NASA CR-693.

7. Kinney, R. B.: Theoretical Effect of Seed Opacity and Turbulence on Temperature Distributions in the Propellant Region of a Vortex-Stabilized Gaseous Nuclear Rocket. UAC Research Laboratories Report E-910092-8 prepared under Contract NASw-847, September 1966. Also issued as NASA CR-694.

8. Kesten, A. S. and N. L. Krascella: Theoretical Investigation of Radiant Heat Transfer in the Fuel Region of a Gaseous Nuclear Rocket Engine. UAC Research Laboratories Report E-910092-9 prepared under Contract NASw-847, September 1966. Also issued as NASA CR-695.

9. Roback, R.: Theoretical Performance of Rocket Engines Using Gaseous Hydrogen in the Ideal State at Stagnation Temperatures up to 200,000 R. UAC Research Laboratories Report E-910093-30 prepared under Contract NASw-847. Also issued as NASA CR-696.

10. Latham, T. S.: Nuclear Criticality Study of a Specific Vortex-Stabilized Gaseous Nuclear Rocket Engine. UAC Research Laboratories Report E-910375-1 prepared under Contract NASw-847, September 1966. Also issued as NASA CR-697.

11. McLafferty, G. H., H. E. Bauer, and D. E. Sheldon: Preliminary Conceptual Design Study of a Specific-Vortex-Stabilized Gaseous Nuclear Rocket Engine. UAC Research Laboratories Report E-910093-29 prepared under Contract NASw-847, September 1966. Also issued as NASA CR-698.

12. Douglas, F. C., R. Gagosz, and M. A. DeCrescente: Optical Absorption in Transparent Materials Following High-Temperature Reactor Irradiation. UAC Research Laboratories Report F-910485-2 prepared under Contract NASw-847, September 1967. To be issued as NASA CR report.

13. Gagosz, R., J. Waters, F. C. Douglas, and M. A. DeCrescente: Optical Absorption in Fused Silica During TRIGA Reactor Pulse Irradiations. UAC Research Laboratories Report F-910485-1 prepared under Contract NASw-847, September 1967. To be issued as NASA CR report.

14. Latham, T. S.: Nuclear Criticality Studies of Specific Nuclear Light Bulb and Open-Cycle Gaseous Nuclear Rocket Engines. UAC Research Laboratories Report F-910375-2 prepared under Contract NASw-847, September 1967. To be issued as NASA CR report.

15. Travers, A.: Experimental Investigation of Radial-Inflow Vortexes in Jet-Injection and Rotating-Peripheral-Wall Water Vortex Tubes. UAC Research Laboratories Report F-910091-14 prepared under Contract NASw-847, September 1967. To be issued as NASA CR report.

16. Kendall, J. S.: Experimental Investigation of Heavy-Gas Containment in Constant-Temperature Radial-Inflow Vortexes. UAC Research Laboratories Report F-910091-15 prepared under Contract NASw-847, September 1967. To be issued as NASA CR report.

17. McLafferty, G. H.: Analytical Study of the Performance Characteristics of Vortex-Stabilized Gaseous Nuclear Rocket Engines. UAC Research Laboratories Report D-910093-20 prepared under Contract NASw-847, September 1965. To be issued as NASA CR report.

18. McLafferty, G. H., H. H. Michels, T. S. Latham, and R. Roback: Analytical Study of Hydrogen Turbopump Cycles for Advanced Nuclear Rockets. UAC Research Laboratories Report D-910093-19 prepared under Contract NASw-847, September 1965. Also issued as NASA CR-68988.

REFERENCES (Cont'd)

19. Patch, R. W.: Methods for Calculating Radiant Heat Transfer in High-Temperature Hydrogen Gas. UAC Research Laboratories Report M-1492-1, November 1961.

20. Marteney, P. J.: Experimental Investigation of the Opacity of Small Particles. UAC Research Laboratories Report C-910092-2 prepared under Contract NASw-847, September 1964. Also issued as NASA CR-211.

21. Lanzo, C. D. and R. G. Ragsdale: Experimental Determination of Spectral and Total Transmissivities of Clouds of Small Particles. NASA Technical Note D-1405, September 1962.

22. Lanzo, C. D. and R. G. Ragsdale: Heat Transfer to a Seeded Flowing Gas From an Arc Enclosed by a Quartz Tube. NASA Technical Memorandum X-52005, June 1964.

23. Schneiderman, S. B.: Theoretical Viscosities and Diffusivities in High-Temperature Mixtures of Hydrogen and Uranium. UAC Research Laboratories Report C-910099-1 prepared under Contract NASw-847, September 1964. Also issued as NASA CR-213.

24. McLafferty, G. H.: Summary of Investigations of a Vortex-Stabilized Gaseous Nuclear Rocket Concept. Air Force Systems Command Report RTD-TDR-63-1097 prepared by UAC Research Laboratories, November 1963.

25. McLafferty, G. H.: Approximate Limitations on the Specific Impulse of Advanced Nuclear Rocket Engines Due to Nozzle Coolant Requirements. UAC Research Laboratories Report D-110224-1, April 1965.

26. McLafferty, George H.: Absorption of Thermal Radiation in the Transparent Wall of a Nuclear Light Bulb Rocket Engine. Journal of Spacecraft and Rockets, Vol. 4, No. 6, 1967.

27. McLafferty, G. H.: Analytical Study of Moderator Wall Cooling of Gaseous Nuclear Rocket Engines. UAC Research Laboratories Report C-910093-9 prepared under Contract NASw-847, September 1964. Also issued as NASA CR-214.

28. Darms, F. J., R. Molho, and B. E. Chester: Improved Filament-Wound Construction for Cylindrical Pressure Vessels. Aerojet-General Corporation, prepared under Contract No. AF 33(616)-8442. Technical Documentary Report No. ML-TDR-64-43, Vol. I, March 1964.

29. Soffer, Louis M. and Ralph Molho: Cryogenic Resins for Glass-Filament-Wound Composites. Aerojet General Corporation report prepared under NASA Contract No. NAS-3-6287 as NASA CR-72114, January 1967.

30. Brechna, H. and W. Haldemann: Physical Properties of Filament Wound Glass Epoxy Structure as Applied to Possible Use in Liquid Hydrogen Bubble Chambers. SLAC-PUB-121, July 1965.

31. Jaffe, L. D. and J. B. Rittenhouse: Behavior of Materials in Space Environments. Jet Propulsion Laboratory, California Institute of Technology, T. R. No. 32-150, November 1961.

32. Darms, F. J., R. Molho, and B. E. Chester: Improvied Filament-Wound Construction for Cylindrical Pressure Vessels. Aerojet-General Corporation, prepared under Contract No. AF 33(616)-8442. Technical Documentary Report No. ML-TDR-64-43, Vol. II, March 1964.

LIST OF SYMBOLS
(Includes Symbols Used in Appendix B, but not Appendix A)

A_T Nozzle throat area, ft^2

A_W Surface area of opaque walls surrounding propellant region, ft^2

A_6 Radiating area at edge of fuel-containment region, ft^2

D Diameter of engine cavity, $2r_1$, ft

F Engine thrust, lb

H Propellant or coolant enthalpy, Btu/lb

H_e Propellant exit enthalpy, Btu/lb

I_{sp} Specific impulse, sec

L Length of propellant duct or engine cavity, ft

P Engine pressure, atm

Q_F Energy deposited in propellant by radiation from the fuel-containment region, Btu/sec

Q_T Engine power, Btu/sec

Q_{W_R} Energy radiated from propellant region and absorbed in opaque surrounding walls, Btu/sec

r_1 Radius of vortex tube, ft or in.

$\bar{R}$ Average reflectivity of opaque walls surrounding propellant region

Re_Z Axial-flow Reynolds number in full-scale engine (see Ref. 17)

t_F Heavy-gas or fuel time constant, $\mathcal{W}_F/W_F$, sec

$t_{F_{6_{MIN}}}$ Minimum time constant based on ρ_6, sec

T Temperature, deg R

T_{BB} Black-body radiating temperature of incident energy spectrum, deg R

T_e Propellant exit temperature, deg R

T_m Median temperature, defined as temperature in propellant stream at axial location where $Y = Y_e/2$, deg R

T_6 Temperature at outside edge of fuel-containment region, deg R

T_8 Centerline temperature, deg R

$T*$ Effective black-body radiating temperature at edge of fuel-containment region, deg R

V	Volume of cavity tube, ft^3 or velocity, ft/sec
V_{Z_e}	Axial neon velocity at end of the tube, ft/sec
W_C	Cavity propellant flow, lb/sec
W_F	Fuel flow rate, lb/sec
W_P	Hydrogen propellant flow, lb/sec
W_T	Total propellant flow, lb/sec
$(W/A)_T$	Weight flow per unit area passing through nozzle throat (see Ref. 9), $lb/sec\text{-}ft^2$
w_F	Amount of fuel stored in engine cavity, lb
X	Cavity volume, ft^3
Y	Temperature integral parameter, see Eq. (3) in Appendix B
Y_e	Value of Y at propellant exit station
Y_6	Cavity volume flow based on ρ_6, ft^3/sec
Z	Distance from upstream end of propellant duct, ft
Z_s	Pressure shell weight parameter (see Eq. (1)), $lb/atm\text{-}ft^3$
ϵ_F	Effective fuel emissivity; ratio of radiant energy absorbed by propellant to that radiated by fuel
ϵ_P	Propellant emissivity; ratio of energy emitted by propellant stream to black-body radiation at propellant temperature
μ	Viscosity, $lb/sec\text{-}ft$
μ_6	Viscosity at outside edge of fuel-containment region, $lb/sec\text{-}ft$
μ_8	Viscosity of propellant at centerline conditions, $lb/sec\text{-}ft$
ρ	Density, lb/ft^3
$\bar{\rho}_{F_1}$	Volume-averaged fuel density, w_F/V, lb/ft^3
ρ_6	Neon or propellant density at edge of fuel-containment region, lb/ft^3
ρ_8	Density of propellant at centerline conditions, lb/ft^3
σ	Stefan-Boltzman constant, 0.48×10^{-12}, $Btu/sec\text{-}ft^2 - (\deg R)^4$

APPENDIX A

FILAMENT-WOUND PRESSURE VESSEL DESIGN STUDY
FOR NUCLEAR LIGHT BULB ENGINE

By: F. G. Siedow - Senior Design Engineer, Motor Case Design Group
             C. H. Martin - Group Head, Motor Case Design Group

Approved by: D. A. North - Section Chief, Mechanical Systems Design
             R. A. Jankowski - Program Manager

United Technology Center; Division of United Aircraft Corporation

Abstract

A design study was conducted to determine the optimum configuration for a
filament-wound glass pressure shell for a nuclear rocket engine. Also investigated
were the various problem areas associated with the design of components, materials,
fabrication methods, and structural degradation due to the anticipated environment.

Design Specifications (Furnished by UARL)

It is desirable to obtain preliminary estimates of the structural weight of
four different pressure shell designs which are shown in Fig. 18. Configurations
A and B are spherical and enclose a volume which is considerably larger than the
actual volume of the major engine components. Configurations C and D have a smaller
envelope which is slightly larger than the major components of a preliminary con-
figuration considered at UARL. All four configurations have a 0.5 ft-dia hole in
the forward end which will contain the duct through which the hydrogen is carried
into the engine. Configurations A and C have a 1 ft-dia hole in the aft end of the
pressure vessel to permit insertion of a single exhaust nozzle. Configurations B
and D have seven holes in the aft end of the pressure vessel, each hole having a
diameter of 0.4 ft, for insertion of seven separate nozzles for seven separate
unit cavities. Each of the configurations would require a flange of some kind near
the point of maximum diameter to permit access to the inside of the pressure vessel.
The design cavity pressure for all configurations is 500 atm (7350 psi).

The neutron and gamma flux approaching the pressure shell is approximately
100 Btu/sec-ft^2. If the density of the pressure vessel is taken as 120 lb/ft^3,
the attenuation coefficient is 1.8 ft^{-1}. Thus the energy deposition per unit volume

due to absorption of neutron and gamma energy near the inside surface of the pressure shell would be 180 Btu/sec-ft^3. This heat deposition rate would decrease by a factor of 1/e for every 0.55 ft of distance through the pressure shell.

It is necessary to conduct the heat deposited within the volume of the pressure shell to a coolant fluid located on one side or the other of the pressure shell. This conduction of heat requires that the temperature in the center of the shell thickness be greater than the temperature on either side. This temperature difference is a function of the thickness of the pressure shell. Preliminary calculations were made on the basis that the pressure shell was made from a series of individual shells, with the first shell having a thickness of 2.0 in. In a shell having a thickness of 2.0 in., the temperature at the center of the shell thickness would be approximately 100 R higher than the temperature at the edge for a thermal conductivity of 10^{-4} Btu/sec-ft-deg R. If the temperature at the edge is taken as 400 R, the centerline temperature would be 500 R. The allowable thickness of each succeeding shell for the same allowable temperature difference would be greater than in the first shell.

The major portion of the energy deposited in the shell would be removed by hydrogen propellant passing along the inside of the inner shell. The energy removed from the outer portion of the inner shell and from both sides of any succeeding shells would be deposited in hydrogen which would later be used for transpiration cooling of the nozzle. The pressure between each layer of pressure shell would be controlled so as to properly divide the bursting load on each layer. The outermost pressure shell would be cooled almost entirely from its inside surface. It is recommended that the initial design employ two pressure shells, although more are permissible.

The fast neutron flux incident on the inner shell is approximately 2 x 10^{14} neutrons/cm^2-sec. The burning time in a single flight is approximately 10^3 sec. Therefore, the total fast neutron dose to the inside surface of the pressure shell would be approximately 2 x 10^{17} neutron/cm^2.

Summary and Conclusions

An oblate-ovaloid shape, which generally follows the motor contour and employs a single centrally located nozzle opening, was employed in all studies unless otherwise specified. The design configuration selected is shown in Fig. 19 and was derived from the specifications given in Fig. 18c.

A weight and cost summary of the four configurations given in Fig. 18 is presented in Table XIX. The weight of the reference design selected for discussion in this Appendix is 18,965 lb. The estimated unit cost of the selected design, not including development cost, is approximately $300,000. (Note that the configuration discussed in the text is derived from Fig. 18d rather than 18c.)

The idealized glass stress level chosen is 400,000 psi, and the resulting design allowable stress levels are 251,000 psi for the helical fibers and 270,000 psi for the hoop fiber. The influence of glass strength on weight and cost is shown in Fig. 20. This data has been adapted from UTC experience gained in design and fabrication of filament-wound structures from 50 in. to 158 in. dia.

Table XIX illustrates that overall weight is not overly sensitive to the inclusion of multiple aft end openings. This is due to the fact that the opening sizes are small compared to the case diameter and wall thickness.

Figure 21 illustrates the influence of thermal environments on fiberglas laminate properties. At the temperatures anticipated, no strength reduction has been considered.

Design Assumptions and Limitations

The design specifications employed in this study were provided by United Aircraft Research Laboratories (UARL) (see preceding section). Since several aspects of the design study were not within current industry state-of-the-art, it became necessary to make certain assumptions and simplifications in order to complete the study. The specifications assumed in the study have been summarized below and are discussed in greater detail in subsequent paragraphs.

(1) A design ultimate pressure of 7350 psi.

(2) Hydrogen pressure can be controlled to 3675 psi between the two pressure shells.

(3) The optimum dome contours shown in Fig. 19 can be employed.

(4) The temperature at the wall surface will be maintained at 400 R and that a 100 R temperature rise will occur midway through the 2-in.-thick glass resin composite wall.

(5) Material properties have not been degraded for fatigue or radiation effects.

(6) Joint material properties assumed for the basic configuration are attainable in a case of this size.

(7) Fasteners are obtainable in the 300 KSI strength level with sufficient toughness to withstand loading at the lower temperature limits of the hydrogen coolant.

(8) Technical problems associated with fabrication could be solved given sufficient time for study.

(9) No transient conditions of pressure and temperature were assumed during
      startup or shutdown.

Design Considerations

The successful application of glass filament resin composite materials for
pressure vessels require special consideration be given the influence of case
geometry and total environment on the ultimate strength capability of the materials.
The extent to which these considerations influence the proposed design are dis-
cussed briefly in the following sections.

The strength of a strand (a bundle of continuous filaments gathered together
in the forming operation) is generally less than the pure filament strength by a
factor of 20 to 30 percent. The strength of a strand composite that is acting as
part of a filament-wound structure is generally 25 to 30 percent less than that
determined from a strand test. UTC design experience indicates that a pure strand
strength of 500,000 psi can be consistently obtained with S-901 glass. This
strength must be further reduced by various factors discussed in following sections.

Case Geometry

Filament-wound pressure vessels with small length-to-diameter ratios, equal
boss opening sizes, and small boss-to-case diameters are most efficient when using
a helical winding pattern employing a geodesic-ovaloid dome contour (see Ref. 28).
Accordingly, a helical winding pattern has been chosen and modified slightly to
account for the unequal end opening diameters and non-optimum winding angle
resulting from the unequal dome sizes.

Chamber wall thickness influences the realizable filament strength as a
result of the higher stresses developed at the inner surface than at the outer
surface due to the thick section and also by mandrel shrinkage during fabrication
which allows the inner windings to relax during winding under pretension. This
effect can be compensated for in either of two ways: (1) by application of Lame's
equations to determine the amount of winding tension required to produce equal
stress in each filament layer throughout the wall; or, (2) by application of a
strength reduction factor to the allowable strand strength to account for the
resulting degradation.

Past experience has indicated that there is some loss in strength with
increasing diameter. The loss in efficiency has been attributed to: (1) the
increased thickness if pressure remains constant; (2) the increased probability of
the presence of structural defects due to the added volume of material involved;
and (3) loads are transferred less efficiently between layers of fibers in very
thick laminates. Any stresses are manifested in the form of shear stress between
layers. This effect has been compensated for by appropriately reducing the design

allowable strand strength.

When a section or hole has been cut out of a dome, the membrane load must be transferred along another path surrounding the removed material. To provide this added load carrying capacity, reinforcing media, glass cloth, tape, etc. must be employed between filament layers during fabrication. As a result of the above, a strength reduction factor is generally applied to the design allowable strand strength to account for this effect.

To obtain a full-diameter opening in a filament-wound pressure vessel, the vessel must first be wound integrally and then sectioned. This requires that the joint area be reinforced to compensate for the redistribution of forces between the filaments and the joining medium, bolts, pins, etc. In addition, local discontinuities resulting from the different section sizes result in additional loads being imposed on adjacent filaments.

Environmental Factors

Elevated temperature affects filament-wound composites essentially as shown in Fig. 21. Since the temperature in the fiberglas wall in this application is estimated to be 500 R at the center and 400 R at the outside surface, no strength degradation has been assumed for this design. The above thermal gradients will result in a thermal stress of approximately 560 psi in the wall which is insignificant.

The exposure of filament-wound structures to low temperatures associated with liquid hydrogen during startup is not deemed to be a problem (see Ref. 29). Results of a test program conducted by Stanford Linear Accelerator Center, Stanford University, Stanford, California, on UTC-prepared specimens indicated that certain composites are entirely suitable for use at 50 R in pressure vessel applications. (see Ref. 30). Fatigue tests at 10^7 cycles and 9000 psi flexural and 300 psi shear stress showed that the filament-wound structure had not lost its original properties.

Gamma ray and particulate radiation, especially that above 1/2-1 MEV energy, are potentially dangerous to fiberglas laminates. The epoxy matrix, being an organic compound, can be attacked and degraded in several ways by both gamma rays and neutrons. No attempt has been made to estimate the influence of radiation on the design allowable glass strength.

Glass-fiber reinforced plastics are susceptible to degradation in a vacuum environment as a result of the weakening of long chain polymeric compounds. Degradation is a function of temperature and time, and is evidenced by a loss in weight and associated changes in mechanical properties. The results of Ref. 31 indicate that, at elevated temperature in a vacuum, a 5 to 10 percent reduction in strength per year can be expected. Accordingly, the mission duration, in addition

to actual operating duration, must be considered in considering glass-resin composite designs for space application.

Final burst pressure for any chamber is significantly affected by the number of prior pressurization cycles and their duration and the rate of pressurization; the faster rates providing higher burst values. Accordingly, to assure the maximum reliability with a minimum of structural degradation, it is UTC's practice to employ a minimum factor of safety of 1.25 times proof pressure and to proof test from 8 to 10 percent above the maximum expected operating pressure. This provides adequate margin for a 5 percent degradation during proof testing and assures successful operation at the subsequent operating pressure.

Description of Selected Design

The design employed in most of the studies is shown in Fig. 19. The oblate shape is terminated by modified geodesic isotensoid domes which are the most efficient design attainable. The single end openings were chosen for this study for manufacturing simplicity and weight savings. The weight increase for multiple openings would be only a few percent, but costs might be 8 to 10 percent higher. Multiple openings require the addition of special reinforcements surrounding each opening to transfer the loads around the opening, in addition to the extra fittings required.

Weights are presented in Table XIX for all four configurations shown in Fig. 18. There are several reasons for the weight increase for the spherical shell configuration. The first is that the glass and resin weight, and therefore weight performance, of a pure vessel of optimum isotensoid design is directly related to the enclosed volume. Since the volume of the sphere is greater than that for the oblate shape, the basic shell weights will also be greater. In addition, the oblate shape was chosen over the spherical shape because a true filament-wound sphere cannot be made because of manufacturing considerations. It is an approximation arrived at with a succession of windings, each at an angle and thickness corresponding to its stress at the highest point. Each winding, then, is under-stressed at all other points, and the vessel as a whole may be 20 to 30 percent heavier than an ovaloidal vessel.

A further disadvantage of the spherical case is the added weight of the full-diameter joint. The joint weight is increased over the primary design because of the greater radius, as the larger radius produces larger joint loads and the greater radius contains more volume of structural material in the joint. The cost of the spherical case is greater due to the added fabrication difficulties caused by the different winding patterns and therefore machine setups required during winding.

End Domes

The end domes are geodesic isotensoid shapes, modified slightly on the aft end to allow for the inclusion of joint buildups, and on the forward end to allow for

mismatches between the dome and conical case, non-optimum winding angle, and smaller forward polar opening. The aft domes will be wound at a nearly optimum angle (7°) and average contour to suit the shell and polar fitting diameters.

The forward domes are forced by case geometry to be wound at a much higher-than-optimum angle (10°), and will have modified contours to fit this condition, the transition from the conical case wall, and the small polar fitting.

Conical Section

The center section of the vessel is conical in shape, tapering from 60 in. inside radius on the aft end to 34.4 in. inside radius on the forward end with a 84 in. long conical section. The outer shell aft inside radius (65.6 in.) is sized to clear the inside shell joint buildup and tapers down to clear the inner shell at the forward end (37.4 in.). This produces a tapered gap between the shells as the outer shell has a higher cone angle than the inner shell.

The winding angle at the aft end matches the aft dome, increasing toward the forward end as the diameter decreases. The helical winding thickness increases toward the forward end, and the hoop winding thickness is tapered to compensate for these two effects to keep weight down. The total wall thickness is 2.108 in. aft and 2.016 in. fwd for the inner shell and 2.308 in. aft and 2.216 in. fwd for the outer shell.

The design allowable ultimate glass stress is 251,000 psi for the helical windings and 270,000 for the hoops. The maximum helical stress (theoretical) is near the joint and the hoop stress is uniform. The case is designed so that each shell withstands half the pressure load with the hydrogen coolant located between the shells at half the chamber pressure.

The resin content is 24 percent bw which gives a laminate density of 0.0705 lb/in.^{3}.

Joints

The joint design was dictated by the very high axial loads present (117,500 lb/in.). This load is near or above the load/diameter ratio at which fiberglas joints become difficult because of the low bearing-shear to tensile strength ratio. If small bolts are used, the bearing, shear, and bolt stresses are too high, and with large bolts the tensile and shear stress between the bolts is too high.

The double-row bolted flange concept allows enough bearing, shear, and inter-bolt tensile area with a moderately thick section, and still allows enough bolt tensile area by virtue of the double row of bolts. Bolts are spaced every 4.2 in.

average, which means every two bolts share 494,000 lb, or 247,000 lb per bolt. The bolts are 1.125-in.-dia studs made from a material having 287,000 psi min tensile yield strength.

The fiberglas stress values are: bearing - 54,200 psi, shear - 17,850 psi, interlaminar shear - about 3800 psi, and inter-bolt tensile - about 34,200 psi. These are all at the upper limit of UTC's present fiberglas joint technology, and some development would have to be done to verify and improve these values. The joint problems could be alleviated, if necessary, by the use of three or more separate shells rather than the two shells shown in Fig. 19. ·

Usually, a double-clevis joint is the most efficient because of the greater ratio of inter-pin to pin dia dimensions. This allows a greater number of pins, reducing the fiberglas bearing stress and the pin and link shear stresses. With very high loading, however, the sections become very thick which is evident in the present design shown in Fig. 19. There are 90 2-in.-dia pins and 90 links for each shell, all of 300,000 psi steel.

The fiberglas yoke thickness is 3.17 in. and the stresses are: bearing - 40,000 psi, shear - 20,000 psi, and inter-pin tensile - 30,000 psi. These values are based on UTC's present joint technology for this type of construction, and can probably be raised 20 percent, possibly 30 percent, after a suitable development program aimed at optimizing this joint design.

The clevis joint design, although heavier, is probably the more feasible of the two based on present technology because of the reasons given in the first paragraph. Weights of the case with the clevis joint are given in Table XIX.

Polar Fittings

Polar fittings are made from 7075-T6 aluminum, designed at an ultimate stress of 60,000 psi, to allow a generous safety factor for possible heating or radiation degradation effects. The polar fittings are designed so that the inner and outer fittings index on each other to locate the outer dome concentric to the inner dome. The inner polar fitting has ports for the passage of the hydrogen coolant from between the shells. The outer polar fitting has thru-holes so that it can be held in place by the bolts which hold on the nozzle or aft closure.

Materials and Fabrication Techniques

The glass filaments considered in this design study are Owens Corning S-901 G size filaments. These have been shown by UTC and many other case winders to be the highest strength and most consistent quality filaments available.

The resin system used for this study is Union Carbide ERL 2256 epoxy resin,

or other similar low-viscosity type with metaphenylenediamine or similar aromatic polyamine hardener. This system has been shown by UTC to produce the strongest filament-wound vessels in sizes from 2 in. to 14 ft in diameter.

The inner vessel would be wound using standard winding techniques using a helical pattern and wet winding (glass rovings impregnated with resin as they are wound onto the case). The aft dome would be wound integral with the forward part of the case to be cut off after cure. Joint buildup reinforcement would be added in the joint area and wound in between the helical windings. In the case of a seven-nozzle configuration, reinforcements for the nozzles would also be added between the helical layers. These reinforcements, of special orientation, are pre-wound on a different mandrel and kept refrigerated until use.

After the completion of winding, the case would be B-staged and given an initial cure at approximately 200 F. Then it would be overcoated with plaster and swept to the proper contour for winding of the outer shell. The outer shell would then be wound over the plaster overcoating, B-staged as above, and then the whole mass cured fully. In the bolted flange version, the case would then be cut open at the flange interface, the shells separated from each other, and then drilled and back spotfaced for the bolt holes. In the clevis joint version also, the pin holes would probably be drilled after the case was cut apart.

<center>Problem Areas</center>

Conical Case

Filament winding of conical cases always poses problems because of the changing winding angle from the large to the small end. The angle increases down the cone, forcing the small dome to usually be wound with too high a winding angle. This error can be neutralized by altering the dome contours, but can impose restrictions on diameter ratios, diameter-to-length ratios, allowable wall stress, etc. Cases of this type are proven entirely by burst tests, and may turn out heavier (or lighter) than anticipated.

In addition, it is very difficult to use hoop windings on conical walls; UTC has wound cases up to 15° half angle, but only by semi-staging the resin until very tacky, then quickly winding one hoop layer. When done properly, the windings can be made to stick but, if not, then the case has to be redesigned with a lower cone angle. The present design (with 15° and 16° half angles) is based on the possibility of winding on this cone angle; however, the forward end diameter would probably have to be increased to allow a lower cone angle.

Joint

The present joint (both designs) is at the limit of known technology, and, while based on actual strengths realized in tests, may not be feasible in the size

<center>39</center>

contemplated. Thick sections are not always stronger in relation to their thickness and may have to be operated at lower stresses than anticipated. As noted in a preceding section, many of the joint problems could be alleviated by using three or more rather than two pressure shells.

In the present design, the necessary hoops may be impossible to wind in the joint area because of the high slopes on the buildups; in that case, high-angle helicals would be used in the buildup areas which would raise the weight slightly.

Thermal

The liner, fiberglas, and joint bolts might be cooled to 36 R during the pause phases. While this has been shown to actually increase the performance of the fiberglas, it would embrittle the bolts and liner, possibly to the point of failure if full operating pressure is reached before these materials can heat up. Sharp thermal gradients during startup may create thermal stresses until thermal equilibrium is reached.

Radiation Effects

Gamma ray and particulate radiation, especially that above 1/2-1 MEV energy, are potentially dangerous to a fiberglas laminate. The epoxy matrix, being an organic compound, can be attacked and degraded in several ways by both gamma rays and neutrons.

Neutrons, especially above 1-5 MEV energy, displace whole atoms or groups of atoms from the molecule, creating broken molecules which combine in different ways, or are permanently terminated depending on other conditions. If small groups of atoms are broken off, these can be liberated as a gas, creating gas bubble problems in addition to destroying the chain structure of the polymer. Neutrons can, in some cases, also produce secondary radiations, such as beta or alpha particles, etc., which then can produce secondary radiation damage.

Gamma rays primarily produce chain sissions (ionizing) which produces free radicals which can recombine with other such radicals, or terminate if H atoms or ions are present. This changes the molecular weight and type of the polymer, therefore completely changing its properties. If primarily recombination of the free radicals occurs, then the polymer will gradually increase in strength and modulus and decrease in elongation, creating a brittle material. As the process continues, the polymer would start breaking into sub-units (degradation) and strength and elongation would decrease sharply. These effects would all be reduced noticeably in the fiberglas laminate, since the glass acts as a filler which seems to reduce the radiation damage effects.

Various sources have reported damage threshold levels from 30 to 1000 Mrad (megarads: 1 Mrad = 100 ergs/gm-sec absorbed) of gamma or fast neutron radiation.

The general consensus seems to be, however, that about 600 Mrad of gamma rays or neutrons above 50 MEV will begin to degrade epoxies, and 1000 Mrad should degrade fiberglas laminates.

It is possible also that these intense radiations will damage the glass filaments, especially when they are under stress. Absorption of radiation is proportional to density, and the glass filaments would thus be expected to absorb the greater portion of the radiation entering the laminate. Although glass is not crystalline in nature, it is held together by polar, or association bond-type, attraction between its atoms, and it is possible that a sufficient number of atom "dislocations," or dissociations or free electrons, could degrade the strength of the glass.

If the combined gamma and neutron flux absorbed in the fiberglas is 180 Btu/sec-ft^3 with an attenuation factor of $1/e$ every 0.55 ft, approximately 0.47 times 180 Btu/sec-ft^3 will be absorbed in 5 in. of wall thickness. This corresponds to 84 Btu/sec-ft^3, or 89×10^{10} erg/sec-ft^3, or 15.8×10^7 erg/gm-sec, or 1.58 Mrad/sec absorbed in the wall. In a 1000 sec run, this means 1580 Mrad of radiation is absorbed, probably 1/3-1/2 of which is potentially damaging radiation. If these are the correct figures, then there is a definite radiation effect to be considered in designing this shell of fiberglas.

<center>Design Analysis</center>

Glass Stress

In a case of this size and operating pressure, there are many factors which affect the usable strength of the glass filaments. An individual fiber has a strength of over 650,000 psi; in strand form about 500,000 psi; and in a small optimum pressure vessel, about 400,000 psi is realizable (400,000 psi is termed "idealized" glass stress in Fig. 20). A few organizations have empirically defined the allowable glass stress as a function of various parameters, such as case diameter, wall thickness, winding angle, polar opening differences, etc. In this study, we will use some design factors tabulated in Ref. 32.

UTC has assumed an average composite filament strength of 400,000 psi which has been multiplied by the following reduction factors:

	Helical Factor	Hoop Factor
Case diameter (120 in.)	K = 0.85	0.90
Wall thickness/diameter ($\frac{2}{120}$ = 0.016)	K = 0.73	0.75
Polar opening/diameter ($\frac{18}{120}$ = 0.15)	K = 1.01	---

Helical ultimate glass stress: 400,000 x 0.85 x 0.73 x 1.01 = 251,000 psi
Hoop ultimate glass stress: 400,000 x 0.90 x 0.75 = 270,000 psi

<center>41</center>

If resin content is assumed to be 24 percent bw, the resin bulk factor, K, is 1.68, and the composite density is 0.0705 lb/in.^{3}.

Dome Design

Aft inside dome: (see Fig. 22, Explanation of Filament Winding Terms).

$$R_V = 7.3 \quad R_E = 7.9; \quad \alpha = \sin^{-1} \frac{R_E}{R_a} = \sin^{-1} \frac{7.9}{60.5} = 7.5^{\circ}$$

Aft inside dome: $t_{G_\alpha} = \dfrac{PR}{2\sigma_{G_\alpha} \cos^2 \alpha} = \dfrac{3675 \times 60}{2 \times 251{,}000 \times 0.9825} = 0.447$ in.

$$t_\alpha = K \, t_{G_\alpha} = 0.447 \times 1.68 = 0.750 \text{ in.}$$

Aft outside dome: $\alpha = \sin^{-1} \dfrac{7.9}{66.5} = 6.8^{\circ}$

$$t_{G_\alpha} = \frac{3675 \times 65.6}{2 \cdot x \ 251{,}000 \times 0.986} = 0.487 \text{ in.}$$

$$t_\alpha = 0.487 \times 1.68 = 0.818 \text{ in.}$$

The dome contours will be calculated for the above winding angles and wall thickness and modified to include the joint buildups.

Fwd inside dome: $\alpha = \sin^{-1} \dfrac{7.9}{60.5} \times \dfrac{60.5}{44.4} = 10.2^{\circ}$ at dome-cone equator

$$t_{G_\alpha} = 0.447 \times \frac{60}{44.4} = 0.604 \text{ in.}; \quad t_\alpha = 0.604 \times 1.68 = 1.015 \text{ in.}$$

Fwd outside dome: $\alpha = \sin^{-1} \dfrac{7.9}{66.5} \times \dfrac{66.5}{47.4} = 9.6^{\circ}$

$$t_{G_\alpha} = 0.487 \times \frac{66.6}{47.4} = 0.684 \text{ in.}; \quad t_\alpha = 0.684 \times 1.68 = 1.148 \text{ in.}$$

The contours of the fwd domes will have to be compromised to account for the actual winding angle and the optimum angle required by the forward polar opening size. The theoretical angles based on R_E are:

Inside shell: $\alpha = \sin^{-1} \dfrac{4.3}{45.4} = 5.4^{\circ}$ \qquad outside shell: $\alpha = \sin^{-1} \dfrac{4.3}{48.4} = 5.1^{\circ}$

Thus the basic contour of the inside shell will be a 6° contour adjusted near the polar fitting for the smaller R_E, and near the equator to match a 10° contour and 15° conical wall. The outside contour will be a 6° contour adjusted similarly near the pole, and near the equator for a 9° contour and the 16° conical wall.

Conical Wall

At the aft tangent line:

Inside shell: $\alpha = 7.5^\circ$, $t_{G_\alpha} = 0.447$ in., $t_\alpha = 0.750$

$$t_{G_\theta} = \frac{PR}{T_{G_\theta}} \left(1 - \frac{\tan^2\alpha}{2}\right) = \frac{3675 \times 60}{270,000} \left(1 - \frac{0.132^2}{2}\right) = 0.809 \text{ in.}$$

$$t_\theta = K\, t_{G_\theta} = 1.68 \times 0.809 = 1.358 \text{ in.}$$

Outside shell: $\alpha = 6.8^\circ$, $t_{G_\alpha} = 0.487$ in., $t_\alpha = 0.818$ in.

$$t_{G_\theta} = \frac{3675 \times 65.6}{270,000} \left(1 - \frac{0.1192^2}{2}\right) = 0.887 \text{ in.}$$

$$t_\theta = 1.68 \times 0.887 = 1.490 \text{ in.}$$

At the forward "tangent line":

Inside shell: $\alpha = 10.2^\circ$, $t_{G_\alpha} = 0.604$ in., $t_\alpha = 1.015$ in.

$$t_{G_\theta} = \frac{PR}{\sigma_{G_\theta}} \left(1 - \frac{\tan^2\alpha}{2}\right) = \frac{3675 \times 44.4}{270,000} \left(1 - \frac{0.180^2}{2}\right) = 0.596 \text{ in.}$$

$$t_\theta = K t_{G_\theta} = 1.68 \times 0.596 = 1.001 \text{ in.}$$

Outside shell: $\alpha = 9.6^\circ$, $t_{G_\alpha} = 0.684$ in., $t_\alpha = 1.148$ in.

$$t_{G_\theta} = \frac{3675 \times 47.4}{270,000} \left(1 - \frac{0.1691}{2}\right) = 0.636 \text{ in.}$$

$$t_\theta = 1.68 \times 0.636 = 1.068 \text{ in.}$$

Bolted Flange Joint

Assume 1.125 in. bolts in a double row with 2.2 in. spot face dia and 2.0 in.

space between spot faces; spacing = 2.2 + 2.0 = 4.2 in.

$$\text{Joint load, } n = \frac{PR}{2} \approx \frac{3675 \times 64}{2} = 117{,}500 \text{ lb/in.}$$

$$\text{load/bolt} = \frac{117{,}500 \times 4.2}{2} = 247{,}000 \text{ lb}$$

$$\text{bolt } \sigma_t = \frac{F}{A} \approx \frac{F}{\pi/4 \ D^2} = \frac{247{,}000}{\pi/4 \times 1.053^2} = 284{,}000 \text{ psi}$$

Fiberglas buildup stresses:

$$\text{Bearing: } \sigma_B = \frac{F}{\pi/4 \ (D_o^2 - D_i^2)} = \frac{247{,}000}{\pi/4 \ (2.2^2 - 1.125^2)} = 54{,}200 \text{ psi}$$

$$\text{Bolt shear-out: } \sigma_S = \frac{F}{\pi D_o t} = \frac{247{,}000}{2.2 \times 2.0} = 17{,}850 \text{ psi}$$

$$\text{Inter bolt tensile: } \sigma_t \approx \frac{F/2 \text{ bolts}}{\text{buildup } t \times \text{spacing-spot face areas} + \text{shear area} \times \frac{\sigma_{su}}{\sigma_{tu}}}$$

$$\approx \frac{494{,}000}{4.5 \times 4.2 - 2\pi/4 \ 2.2^2 + 4.2 \times 6 \times \frac{4500}{36{,}000}}$$

$$= 34{,}200 \text{ psi}$$

Interlaminar shear, assuming 5 helical layers: (n = 5)

$$\sigma_{ILS} \approx \frac{\sigma_s}{2 \times n/2} = \frac{17850}{5} = 3560 \text{ psi}$$

Alternate Clevis Joint

Assume the following fiberglas yoke ultimate stresses:

$$\text{Bearing } \sigma_{BU} = 40{,}000 \text{ psi}$$

$$\text{Inter-bolt tensile } \sigma_{tu} = 30{,}000 \text{ psi}$$

$$\text{Bolt shear-out } \sigma_{su} = 20{,}000 \text{ psi}$$

Use 90 pins, 2.0 in. dia

$$t_J = \frac{P\pi R^2}{\sigma_{tu}(2\pi\overline{R} - nd)} = \frac{3675 \times 60^2}{30,000(2\pi 62 - 180)} = 6.60 \text{ in. (2 yokes)}$$
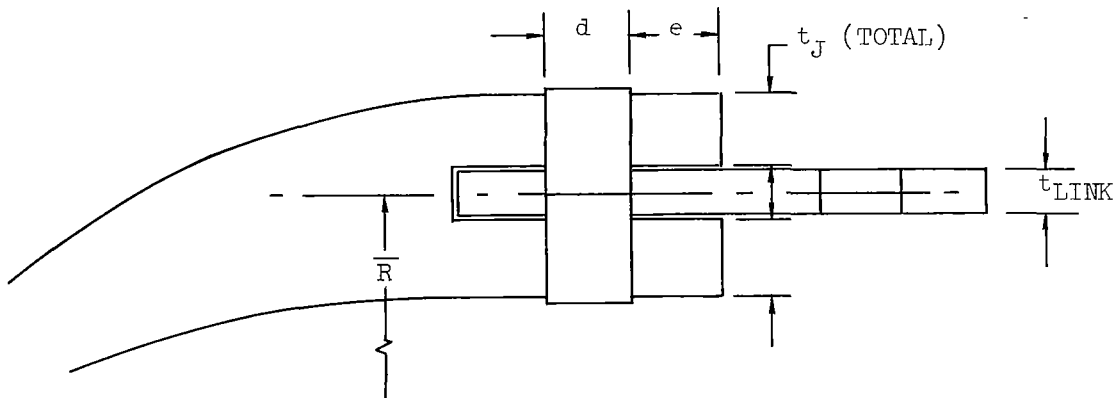
$$e = \frac{d}{2}\frac{\sigma_B - 1}{\sigma_{SU}} = \frac{2}{2}\frac{40,000 - 1}{20,000} = 1.00 \text{ in. (use 2.0 in.)}$$

Pin shear: $\sigma_s = \dfrac{F}{\pi/4 d^2 \times 2} = \dfrac{117,500 \times 2\ 63}{90 \times \pi/4\ 2^2 \times 2} = 82,300 \text{ psi}$

$$t_{link} = \frac{F/link}{\sigma_{tu} \times w} = \frac{518,000}{300,000 \times 2.4} = 0.72 \text{ in.}$$

link shear: $\sigma_s = \dfrac{F}{2\ t\ e} = \dfrac{518,000}{2 \times 0.72 \times 2.7} = 133,000 \text{ psi} \quad (\sigma_{su} \approx 180,000 \text{ psi})$

link bearing: $\sigma_B = \dfrac{F}{t\ d} = \dfrac{518,000}{0.72 \times 2} = 359,000 \text{ psi} \quad (\sigma_{BU} \approx 460,000 \text{ psi})$

Polar Fittings

Design can be quickly approximated by finding the axial load/inch at R_v, assuming this concentrated half way up the flange from R_v, and solving for $t = \sqrt{\dfrac{6M}{tu}}$, considering a section of the flange 1 in. in width.

Aft polar fitting: $R_v = 7.3$; $R_c = 9.68$; Mat'l = 7075 - T6 aluminum

$$\sigma_{tu} = 60,000$$

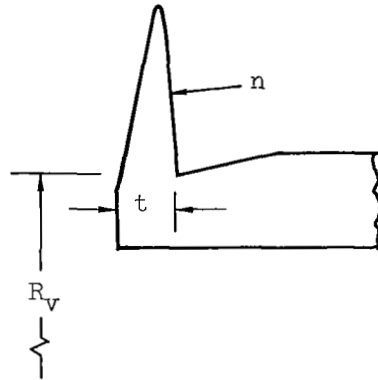$$n = \frac{PR_v}{2} = \frac{3675 \times 7.3}{2} = 13{,}500 \text{ lb/in.}$$

$$t = \sqrt{\frac{6M}{\sigma_{tu}}} = \sqrt{\frac{6 \times 13{,}500 \times 1.19}{60{,}000}} = \sqrt{1.606} = 1.267 \text{ in.}$$

Fwd polar fitting: $R_v = 4.0$, $R_c = 5.63$

$$n = \frac{3675 \times 4.0}{2} = 7350 \text{ lb/in.}$$

$$t = \sqrt{\frac{6 \times 7350 \times 0.82}{60{,}000}} = \sqrt{0.603} = 0.777 \text{ in.}$$

46

APPENDIX B

ANALYSIS OF RADIANT ENERGY EMITTED FROM PROPELLANT
STREAM OF NUCLEAR LIGHT BULB

A simplified analysis has been made to determine the approximate magnitude of the energy which is emitted from the propellant stream of a nuclear light bulb and which is absorbed in the surrounding opaque walls (i.e., all surrounding walls except the transparent walls). This analysis does not consider energy which is emitted from the fuel and which passes through the seeded propellant region. It is assumed in the analysis that the propellant duct length in the flow direction is large relative to its width so that the energy incident on any section of the wall is determined by the temperature of the propellant gases adjacent to the wall. It is also assumed that the temperature across each axial station is constant. The total energy absorbed by the opaque walls surrounding the propellant stream is given by the following equation:

$$Q_{W_R} = \int_0^{A_W} (1-\bar{R}) \, \epsilon_P \, \sigma \, T^4 \, d \, A_W \tag{1}$$

In this expression, ϵ_P is the emissivity of the propellant gases and is approximately equal to unity if there is sufficient seed material in the propellant gases to absorb a large fraction of the energy emitted from the fuel-containment region. In the following analysis, ϵ_P is assumed independent of axial position. The reflectivity of the wall averaged over the incident energy spectrum, $\bar{R}$, is also assumed to be independent of axial position. The surface area of the opaque wall is assumed to be proportional to axial distance. Therefore, Eq. (1) becomes

$$Q_{W_R} = (1-\bar{R}) \, \epsilon_P \, A_W \, \sigma T_e^4 \int_0^1 (T/T_e)^4 \, d \, Z/L \tag{2}$$

The temperature integral parameter, Y, is defined as follows:

$$Y = \int_0^{Z/L} (T/T_e)^4 \, d \, Z/L \tag{3}$$

The value of Y at $Z/L = 1.0$ is denoted as Y_e. Therefore, Eq. (2) becomes

$$Q_{W_R} = (1-\bar{R}) \, \epsilon_P \, A_W \, \sigma T_e^4 \, Y_e \tag{4}$$

It is assumed in the following analysis that the enthalpy of the propellant stream varies linearly with axial distance. Such an assumption is valid if the heat deposition rate in the propellant stream is independent of axial position and if the energy lost from the propellant stream by convection and reradiation is negligible. It is also assumed that the initial enthalpy is 15 percent of the exit enthalpy, which corresponds to a removal of 15 percent of the energy created in the engine structure by the hydrogen propellant before this propellant is heated by thermal radiation. Typical resulting enthalpy distributions for a pressure of 500 atm are given in Fig. 23. The exit enthalpies noted on this figure were determined using the tables of Ref. 9 for the indicated values of propellant exit temperature. Corresponding values of local temperature are given in Fig. 24 and were also determined using the tables of Ref. 9.

Values of the parameter, Y (see Eq. (3)), determined by graphical integration using the temperatures shown in Fig. 24 are given in Fig. 25. Exit values of this temperature integral parameter, Y_e, are given in Fig. 26 for four different hydrogen pressures as a function of propellant exit temperature. As noted on this figure, Y_e would be equal to 0.235 if the specific heat of hydrogen were constant (i.e., if the temperature varied linearly from $0.15\ T_e$ to T_e along the length of the tube).

The average reflectivity of the opaque wall (see Eq. (4)) is determined by the spectrum of the radiation approaching the wall. This spectrum, in turn, is governed by the propellant temperature and opacity. A median propellant temperature, T_m, has been defined as the temperature at the location where Y is equal to half of Y_e. Values of this median temperature determined from information such as that given in Figs. 24 and 25 are plotted in Fig. 27. It can be seen from Fig. 27 that the median temperature defined in this manner is approximately equal to 85 percent of the propellant exit temperature.

The average reflectivity of the opaque wall is determined by the wall material employed. The average reflectivities of tungsten and aluminum are shown in Fig. 28 as a function of the black-body radiating temperature of the incident energy spectrum T_{BB}. The information in Fig. 28 was obtained from Fig. 29 of Ref. 6. The product of Y_e and the average wall absorptivity (equal to $1-\bar{R}$) is plotted in Fig. 29. The average reflectivities used in calculating Fig. 29 were determined from Fig. 28 using the median temperatures from Fig. 27.

It is now of interest to determine the ratio of the radiant energy absorbed by the opaque wall to the energy content of the propellant stream. The total energy which is emitted from the fuel-containment region and absorbed by the propellant stream is given by the following equation:

$$Q_F = \epsilon_F\ A_6\ \sigma T^{*4} \tag{5}$$

48

In this expression, the effective fuel emissivity, ϵ_F, is less than unity because of reflections from the surfaces of the transparent wall. Dividing Eq. (4) by Eq. (5) yields

$$\frac{Q_{W_R}}{Q_F} = (1-\bar{R})\, Y_e\, \frac{\epsilon_P}{\epsilon_F}\, \frac{A_W}{A_6}\left(\frac{T_e}{T^*}\right)^4 \tag{6}$$

The preceeding equation has been evaluated using representative numbers from preceeding analyses and is plotted in Fig. 30. The parameter $(1-\bar{R})Y_e$ was determined from Fig. 29. The emissivities ϵ_P and ϵ_F were assumed to be equal to 1.0 and 0.85, respectively. The area of the outer portion of the propellant duct wall and the struts connecting this outer propellant duct wall, A_W, is $2.05A_6$ for the engine in Fig. 4.

Information similar to that presented in Fig. 30 is given in Fig. 31 as a function of wall reflectivity for a radiating temperature, T^*, of 15,000 R, the standard value for the reference engine discussed in preceding sections. The other parameters employed in evaluating Fig. 31 are the same as those in Fig. 30. It is obviously desirable to maintain as high a wall reflectivity as possible in order to minimize the fraction of the propellant stream energy reradiated to the wall.

As noted in a preceding section, it was assumed in the analysis that the propellant temperature was constant across each axial station. However, it should be possible to adjust the seed density distribution so that the propellant temperature is constant except in the regions near the surrounding walls. The propellant region near the transparent wall would be left unseeded in order to maintain a cold buffer layer next to this wall. The propellant near the opaque surrounding walls would be highly seeded in order to intercept the energy reradiated from the propellant region before it intercepts the peripheral wall. Such a propellant seed distribution theoretically would reduce the ratio of the energy deposited in the wall to that deposited in the propellant from that shown in Figs. 30 and 31.

49

TABLE I

HEAT DEPOSITION RATES IN VARIOUS REGIONS WITHIN NUCLEAR LIGHT BULB ENGINE AT DESIGN POINT

Region	Mechanism of Heating	Heat Deposition Rate Btu/sec	Coolant Circuit Used to Remove Energy Deposited
Pressure Vessel	Neutron & Gamma	0.40×10^5	Secondary
Tie Rods	Neutron & Gamma and Conduction	0.04×10^5	"
Flow Divider	" " " " "	0.189×10^5	"
Cavity Liner	Thermal Radiation & Convection	0.508×10^5	"
Transparent Structure	" " " "	0.812×10^5	"
Fuel Recycle System	Removal of Heat from Fuel	0.88×10^5	"
Beryllium Oxide	Neutron & Gamma	1.601×10^5	Primary
Graphite	" " "	2.14×10^5	"
	TOTAL	6.57×10^5	

TABLE II

TEMPERATURE AND PRESSURE LEVELS IN PRIMARY HYDROGEN

PROPELLANT CIRCUIT OF NUCLEAR LIGHT BULB ENGINE

Hydrogen Propellant Flow = 42.3 lb/sec

NOTE: Station Numbers Refer to Locations Shown in Fig. 8

Station	Location	Temperature Deg R	Pressure atm	Enthalpy Btu/lb
1	Pump inlet	36	1.0	120
2	Heat exchanger inlet	90	707.6	550
3	Heat exchanger outlet	2000	707.5	7200
4	Turbine outlet	1845	507.5	6650
5	Beryllium oxide outlet	2285	501.4	10,440
6	Graphite outlet	4050	500.0	15,500

TABLE III

TEMPERATURE AND PRESSURE LEVELS IN CLOSED SECONDARY HYDROGEN CIRCUIT

OF NUCLEAR LIGHT BULB ENGINE

Hydrogen Coolant Circuit Flow = 42.3 lb/sec

NOTE: Station Numbers Refer to Locations Shown in Fig. 8

Station	Location	Temperature Deg R	Pressure atm	Enthalpy Btu/lb
7	Pressure vessel liner inlet	300	515.0	1100
8	Tie rod inlet	570	511.6	2047
9	Flow divider inlet	595	511.3	2142
10	Cavity liner inlet	715	507.1	2590
11	Fuel cycle heat exchanger inlet	1055	507.0	3790
12	Transparent wall inlet	1665	502.0	5830
13	Transparent wall outlet	2160	500.0	7750
14	Heat exchanger outlet	300	499.9	1100
Total Pressure Loss			15.1 atm	

TABLE IV

TRANSPARENT STRUCTURE REGION CONFIGURATION AND OPERATING CONDITIONS

FOR NUCLEAR LIGHT BULB ENGINE

(Coolant Stations 12 to 13 on Fig. 8)

Inside radius of transparent structure, ft	0.802
Length of transparent structure, ft	6.0
Tube inside diameter, in.	0.066
Tube wall thickness, in.	0.005
Tube outside diameter, in.	0.076
Number of tubes in each 120 degree segment of each cavity	948
Total hydrogen secondary coolant flow per cavity, lb/sec	6.04
Total heat deposition in transparent structure per cavity, Btu/sec	11,600
Coolant inlet temperature, deg R	1665
Coolant outlet temperature, deg R	2160
Film temperature difference inside tubes, deg R	120
Temperature difference in wall, deg R	90
Maximum tube surface temperature, deg R	2370
Dynamic pressure in tubes, atm	0.0725
Total pressure loss in tubes, atm	0.71
Reynolds number in tubes	26,600
Feeder and collector pipe average inside diameter, in.	1.0
Average dynamic pressure in feeder and collector pipes, atm	0.28
Pressure loss in feeder pipe, atm	0.625
Pressure loss in collector pipe, atm	0.625
Average Reynolds number in feeder and collector pipes	1.03×10^6
Total pressure loss in transparent structure, atm	1.96

TABLE V

CAVITY LINER CONFIGURATION AND OPERATING CONDITIONS

FOR NUCLEAR LIGHT BULB ENGINE

(Coolant Stations 10 to 11 on Fig. 8)

Inside radius of liner at propellant inlet, ft	0.911
Inside radius of liner at propellant outlet, ft	1.320
Average radius of liner, ft	1.1355
Length of liner tubes, ft	13.5
Average liner tube inside diameter, in.	0.540
Average liner tube outside diameter, in.	0.600
Number of tubes per cavity	72
Thickness of reflective coating on outside walls, in.	0.002
Total secondary hydrogen coolant flow per cavity, lb/sec	6.04
Total heat deposition in liner per cavity, Btu/sec	7260
Coolant inlet temperature, deg R	715
Coolant outlet temperature, deg R	1055
Film temperature difference inside tubes, deg R	280
Temperature difference in beryllium wall, deg R	25
Maximum tube surface temperature adjacent to propellant, deg R	1360
Dynamic pressure in tubes, atm	0.012
Total pressure loss in liner tubes, atm	0.081
Reynolds number in tubes	2.23×10^5

TABLE VI

SOLID MODERATOR COOLING REQUIREMENTS

FOR NUCLEAR LIGHT BULB ENGINE

(Coolant Stations 4 to 6 on Fig. 8)

Item	Beryllium Oxide	Graphite
Total volume, ft^3	52.5	193
Density, lb/ft^3	188.5	100.1
Void fraction	0.05	0.05
Total weight, lb	9440	18,460
Length, ft	6.5	6.0
Cooling passage diameter, in.	0.098	0.098
Number of coolant passages per ft^2	946	946
Coolant passage configuration	Circular passages on triangular pitch	
Coolant passage spacing, in.	0.417	0.417
Coolant inlet temperature, deg R	1845	2785
Coolant outlet temperature, deg R	2785	4050
Temperature difference, coolant to wall, deg R	100	100
Maximum temperature in solid moderator, deg R	3057	4306
Dynamic pressure	0.19	0.0341
Pressure loss, atm	6.1	1.38
Reynolds number	50,500	17,100

TABLE VII

SPECIFICATIONS FOR BERYLLIUM TIE RODS

FOR NUCLEAR LIGHT BULB ENGINE

(Coolant Stations 8 to 9 on Fig. 8)

Inside diameter, in.	1.0
Outside diameter, in.	1.358
Pyrolytic graphite insulation thickness	0.30
Overall diameter, in.	1.958
Number of rods	24
Total flow per rod, lb/sec	1.76
Total heat deposition per rod, Btu/sec	168
Coolant inlet temperature, deg R	570
Coolant outlet temperature, deg R	595
Film temperature difference inside rods, deg R	27
Temperature difference in beryllium wall, deg R	190
Maximum beryllium temperature, deg R	813
Dynamic pressure in rod, atm	0.308
Total pressure loss in rod, atm	0.67
Reynolds number in rod	3.17×10^6

56

TABLE VIII

SOLID MODERATOR FLOW DIVIDER

FOR NUCLEAR LIGHT BULB ENGINE

(Coolant Stations 9 to 10 on Fig. 8)

Beryllium wall thickness, in.	0.048
Clearance between walls, in.	0.070
Pyrolytic graphite insulation thickness, in.	
Beryllium oxide side	0.221
Graphite side	0.288
Total flow in divider region, lb/sec	42.3
Total flow area, in.^{2}	22.5
Total heat deposition rate, Btu/sec	18,900
Coolant inlet temperature, deg R	595
Coolant outlet temperature, deg R	715
Film temperature difference, deg R	110
Temperature difference in beryllium wall, deg R	10
Maximum beryllium temperature, deg R	835
Dynamic pressure, atm	0.206
Total pressure loss, atm	4.13
Reynolds number	3000

TABLE IX

HEAT EXCHANGER SPECIFICATIONS

FOR NUCLEAR LIGHT BULB ENGINE

(Coolant Stations 2 to 3 and 13 to 14 on Fig. 8)

Number of heat exchangers	7
Hydrogen flow rate per unit, lb/sec	6.04
Heat transferred per unit, Btu/sec	3.777×10^4
Tube inside diameter, in.	0.0625
Tube wall thickness, in.	0.01
Tube spacing, in.	0.1145
Number of tubes	6300
Length of tubes, in.	30
Cross sectional area of tube bundle, in.^{2}	31.3
Pressure loss, atm	0.10
Tube wall material	Stainless Steel
Wall material density, lb/ft^3	500
Tube weight (7 heat exchangers), lb	860
Total heat exchanger weight (1.1 x tube weight), lb	950

OPERATING CONDITIONS

	Inlet		Outlet	
	Tube	Shell	Tube	Shell
Temperature, R	90	2160	2000	300
Pressure, atm	707.6	500.1	707.5	500

TABLE X

NUCLEAR LIGHT BULB ENGINE WEIGHT

All Weights in Lb

Region	Beryllium	Beryllium Oxide	Graphite	Pyrolytic Graphite	Tungsten	Steel	Sub-Total
Cavity Liner	475						475
Tie Rods	80			190			270
Flow Divider	145			800			945
Tungsten Liner					500		500
Solid Moderator		9440	17,470				26,910
Heat Exchangers						1900	1900
Turbopump						3000	·3000
Piping & Manifolding	400			100	50	300	850
Pressure Vessel							30,500
Miscellaneous							5000
Sub-Total	1100	9440	17,470	1090	550	5200	70,350

TABLE XI

CONDITIONS IN CAVITY OF REFERENCE OPEN-CYCLE ENGINE DESIGN

Information Obtained from Ref. 11 Unless Otherwise Noted

Cavity diameter, $D = 6.0$ ft

Cavity length, $L = 6.0$ ft

Cavity volume, $X = 169.8$ ft^3

Cavity propellant flow, $W_C = 236$ lb/sec

Total propellant flow, $W_T = 575$ lb/sec

Critical mass, $w_F = 36.2$ lb (see text and Ref. 14)

Average fuel density, $\bar{\rho}_{F_1} = 36.2/169.5 = 0.214$ lb/ft^3

Cavity pressure, $P = 1000$ atm

Temperature at outside edge of fuel-containment region, $T_6 = 102,000$ R

Density at outside edge of fuel-containment region, $\rho_6 = 0.0215$ lb/ft^3

Viscosity at outside edge of fuel-containment region, $\mu_6 = 6.85 \times 10^{-5}$ lb/sec - ft

Time constant parameter evaluated using ρ and μ at Station 6, $(\rho/\mu)_6 r_1^2 = 2820$ sec

Centerline temperature, $T_8 = 136,000$ R

Density of propellant at centerline conditions, $\rho_8 = 0.0158$ lb/ft^2

Viscosity of propellant at centerline conditions, $\mu_8 = 11.9 \times 10^{-5}$ lb/sec - ft

Time constant parameter, evaluated using centerline conditions, $(\rho/\mu)_8 r_1^2 = 1195$ sec

Axial-flow Reynolds number in full-scale engine, $Re_z = 480,000$

Cavity volume flow based on ρ_6, $Y_6 = W_C/\rho_6 = 10,960$ ft^3/sec

Minimum time constant based on ρ_6, $t_{F_{6_{MIN}}} = X/Y_6 = 0.01546$ sec

TABLE XII

DESIGNATION OF VARIOUS OPEN-CYCLE MODERATOR CONFIGURATIONS INVESTIGATED

Engine Configuration	Structural Material in Liner Tubes	Moderator Coolant	Heavy Water Moderator	Remarks
A	Tungsten-184	Helium	Yes	Original design configuration of Ref. 11
B	Beryllium	Helium	Yes	
C	Beryllium	Helium	No	D_2O replaced by additional graphite
D	Beryllium	Hydrogen	Yes	
E	Beryllium	Hydrogen	No	D_2O replaced by additional graphite

TABLE XIII

COMPARISON OF LINER TUBE CONFIGURATIONS

FOR OPEN-CYCLE ENGINE

Engine Configuration (Refer to Table XII)	A	B	C	D	E
Tube Material	W-184	Be	Be	Be	Be
Coolant	He	He	He	H_2	H_2
Tube Inside Diameter, in.	0.165	0.031	0.055	0.031	0.055
Tube Wall Thickness, in.	0.010	0.005	0.005	0.005	0.005
Pyrolitic Graphite Thickness, in.	-	0.048	0.048	0.048	0.048
Niobium Carbide Thickness, in.	-	0.002	0.002	0.002	0.002
Tube Outside Diameter, in.	0.185	0.141	0.165	0.141	0.165
Number of Tubes	6.09×10^4	8.1×10^4	6.28×10^4	8.1×10^4	6.28×10^4
Coolant Flow per Tube, lb/sec	1.945×10^{-2}	1.635×10^{-2}	1.821×10^{-2}	1.635×10^{-2}	1.821×10^{-2}
Coolant Specific Heat, Btu/lb-deg R	1.25	1.25	1.25	3.37	3.37
Inlet Temperature, deg R	903	903	564	903	564
Outlet Temperature, deg R	1175	1175	845	1175	845
Total Pressure Loss, atm	0.1	35	3.5	3.4	0.34
Total Tube Weight, lb	566	1246	1246	1246	1246
Tungsten-184	566	-	-	-	
Beryllium	-	79	79	79	79
Pyrolytic Graphite	-	945	945	945	945
Niobium Carbide	-	222	222	222	222

TABLE XIV

COMPARISON OF MODERATOR CONFIGURATIONS FOR OPEN CYCLE ENGINE WITH AND WITHOUT HEAVY WATER REGION

Engine configuration A,B,D - with heavy water region
Engine configuration C,E - no heavy water region

Engine Configuration	Radial Thickness of Region - in.		Radius at Outside of Region - in.		Volume of Region, Ft^3		Material Volume, Ft^3		Void Fraction		Summation of Volume, Ft^3		Density, lb/ft^3	Weight, lb	
	A,B,D	C,E	A,B,D	C,E	A,B,D	C,E	A,B,D	C,E	A,B,D	C,E	A,B,D	C,E		A,B,D	C,E
Cavity	36.0	36.0	36.0	36.0	170	170	0	0	1.0	1.0	170	170			
Liner Tubes	0.63	0.63	36.63	36.63	9.0	9.0	0.47	0.47	0.95	0.95	179	179	-	Refer to Table XII	
Beryllium Liner	0.30	0.30	36.93	36.93	4.5	4.5	3.9	3.9	0.16	0.16	183.5	183.5		No Change	
Plenum	0.30	0.30	37.23	37.23	4.5	4.5	0	0	1.0	1.0	188.0	188.0			
Beryllium Oxide	3.50	4.00	40.73	41.23	59	66.85	50.5	58.1	0.144	0.144	247	254.4	188.5	9,530	10,980
Plenum	0.10	0.10	40.83	41.33	1.8	2.14	0	0	1.0	1.0	248.8	256.5			
Graphite	8.70	14.15	49.53	55.48	194	373.8	170.2	327.0	0.123	0.123	442.8	620.3	100.1	17,100	32,800
Plenum	0.30	0.30	49.83	55.78	8.0	10.18	0	0	1.0	1.0	450.8	630.5			
Beryllium Wall	0.30	0.30	50.13	56.08	8.2	10.54	8.2	10.54	0	0	459.6	641.0	115.4	950	1,220
Heavy Water	9.95	0	60.08	-	330.3	0	297.3	0	0.103	-	789.6	-	63.0	18,750	0
Beryllium Wall	0.30	0	60.38	-	10.46	0	10.46	0	0	0	800	-	115.4	1,210	0
Heat Exch & Piping	10.0	10.0	70.38	66.08	585	407.36	31.7	22.4	0.945	0.945	1385	1048.4			

Total weight reduction in solid moderators for configurations C & E ≈ 2,540 lb

TABLE XV

COMPARISON OF EXTERNAL PIPING CONFIGURATIONS FOR OPEN-CYCLE ENGINE
WITH HELIUM AND HYDROGEN MODERATOR COOLANT

Engine configuration A,B,C - helium coolant
Engine configuration D,E - hydrogen coolant

Engine Configuration	Inlets		Outlets		Connecting Pipes	
	A,B,C	D,E	A,B,C	D,E	A,B,C	D,E
ID, in.	2	1.45	2.5	1.75	2.25	1.55
OD, in.	2.2	1.575	2.6	1.83	2.45	1.70
Length, ft	10	10	10	10	10	10
Number	44	44	44	44	44	44
Flow Rate, lb/sec	15.1	4.72	15.1	4.72	30.1	9.48
Fluid Density, lb/sec	8.46	3.1	1.37	0.60	2.72	1.15
Dynamic Pressure, atm	0.416	0.403	1.05	0.976	3.21	2.89
Re_D	7.8×10^6	7.8×10^6	1.51×10^6	1.5×10^6	5.77×10^6	5.77×10^6
$(\Delta P/q)$ Friction	0.462	0.516	0.511	0.705	0.435	0.536
$(\Delta P/q)$ Turns	1.5	1.5	1.5	1.5	1.5	1.5
ΔP Total, atm	0.80	0.811	2.11	2.15	6.21	5.89
Inlet Pressure, atm	1002.2	1000.3	990.1	998.0	981.7	996.0
Inlet Temperature, deg R	898	898	4500	4500	2400	2400
Inlet Station*	13	13	20	20	22	22
Volume, ft^3	2.02	1.08	1.62	0.696	2.26	1.17
Material Density, lb/ft^3	115.4	115.4	1204	1204	540	540
Material Weight, lb	233	125	1950	840	1359	702
Insulation OD, in.	2.5	1.875	3.1	2.33	-	-

TABLE XV (Cont'd)

Engine Configuration	Inlets		Outlets		Connecting Pipes	
	A,B,C	D,E	A,B,C	D,E	A,B,C	D,E
Insulation Vol., ft^3	3.36	2.3	5.55	5.01	-	-
Insulation Density, lb/ft^3	124.8	124.8	124.8	124.8	-	-
Insulation Weight, lb	420	288	692	625	-	-
Total Weight, lb	653	413	2642	1465	1359	702

Total weight saving for Configurations D or E = 2075 lb

*Inlet stations refer to Fig. 4 of Ref. 11

TABLE XVI

COMPARISON OF TOTAL WEIGHT OF OPEN-CYCLE ENGINE EXCLUSIVE OF PRESSURE VESSEL
AND TOTAL QUANTITY OF NEUTRON ABSORBING MATERIALS

Engine Configuration	Weight, lb				
	A	B	C	D	E
Moderator & Liner Tubes[1]					
Tungsten-184	1,171	50	50	50	50
Beryllium	2,611	2,760	2,760	2,760	2,760
Beryllium Oxide	9,530	9,530	10,980	9,530	10,980
Graphite	17,100	17,100	32,800	17,100	32,800
Pyrolytic Graphite	1,015	2,050	2,050	2,050	2,050
Heavy Water	18,750	18,750	0	18,750	0
Niobium Carbide	0	222	222	270	300
Piping	10,561	10,561	10,561	8,486	8,486
Heat Exchangers	13,462	13,462	13,162	8,200	7,900
Total	74,200	74,485	72,585	67,196	65,296
Neutron Absorbing Material					
Niobium Carbide					
Weight, lb	0	222	222	270	300
Absorbing Area[2], cm^2	0	390	390	475	529
Tungsten-184					
Weight, lb	1,171	50	50	50	50
Absorbing Area[2], cm^2	2,060	88	88	88	88
Total Absorbing Area, cm^2	2,060	478	478	563	617

(1) Includes all interior piping for moderator coolant and propellant

(2) Based on neutron absorbing area of 3.67×10^{-3} cm^2/gm for NbC and 3.86×10^{-3} cm^2/gm for W-184

TABLE XVII

TOTAL WEIGHT OF OPEN-CYCLE ENGINE CONFIGURATIONS

Item	Configuration (See Tables XII through XVI)				
	A	B	C	D	E
Pressure vessel internal volume, ft^3	1,385	1,385	1,048	1,385	1,048
Pressure vessel weight, lb	96,000	96,000	72,500	96,000	72,500
Total weight of engine components excluding pressure vessel (see Table XVI), lb	74,200	74,485	72,585	67,196	65,296
Total engine weight	170,200	170,485	145,085	163,196	137,796

67

TABLE XVIII

RELATION BETWEEN VARIOUS MEASURES OF FUEL LOSS RATE FOR OPEN CYCLE ENGINE

Information Obtained from Ref. 17 and Table XI

Criteria Governing Fuel loss Rate	Fuel Time Constant, t_F, sec	Ratio of Fuel Time Constant to Minimum Fuel Time Constant, $t_F/t_{F_{6MIN}}$	Dimensionless Time Constant Based on ρ_6 and μ_6, $\tau_{F_{1-6}} = t_F/(\rho/\mu)_6 r_1^2$	Dimensionless Time Constant Based on ρ_8 and μ_8, $\tau_{F_{1-8}} = t_F/(\rho/\mu)_8 r_1^2$	Fuel Flow $W_F = W_F/t_F$ lb/sec	Ratio of Total Propellant Flow to Fuel Flow, W_T/W_F	$\dfrac{\text{(Fuel Cost)}}{\text{(Payload Weight)}}, \dfrac{\$}{lb}$	$\dfrac{\text{(Mission Cost)}}{\text{(Payload Weight)}}, \dfrac{\$}{lb}$
	①	② = $\dfrac{①}{0.01540}$	③ = $\dfrac{①}{2820}$	④ = $\dfrac{①}{1195}$	⑤ = $\dfrac{36.2}{①}$	⑥ = $\dfrac{57.5}{⑤}$	⑦ = $\dfrac{21,500}{⑥}$	⑧ = ⑦ + 225
Fully Mixed Flow Based on ρ.	0.01546	1.0*	0.0000055	0.0000129	2342	0.245	87,754	87,979
Fuel Loss Rate to Provide Same Cost per lb of Payload as with Solid-Core Nuclear Rocket (see text)	0.616	39.8	0.000218	0.000516	58.8	9.76	2201	2426*
Fuel Loss Rate to Provide Cost per lb of Payload Equal to One-Third of that for Solid-Core Nuclear Rocket	2.32	150	0.00822	0.001942	15.6	36.9	583	808*
Dimensionless Time Constant, $\tau_{F_{1-8}} = 0.01$	11.95	773	0.00424	0.01*	3.02	762	113	338
Ratio of Propellant Flow to Fuel Flow, $W_T/W_F = 1000$	63.0	4076	0.02234	0.0528	0.575	1000*	21.5	246

* Input value

TABLE XIX

SUMMARY OF WEIGHTS OF PRESSURE VESSELS

See Appendix A

	OBLATE - OVALOIDAL CASE			SPHERICAL CASE	
	Double Row Bolted Flange Joint		Clevis Joint	Double Row Bolted Flange Joint	
	Single End Openings	7 End Openings	Single End Openings	Single End Openings	7 End Openings
Forward Case Section:					
Pressure walls	11,042 lb	11,042 lb	11,042 lb	8,390 lb	8,390 lb
Joint	1,385	1,385	6,380	2,180	2,180
Aft Case Section:					
Pressure walls	2,983	3,303	2,983	8,390	8,710
Joint	2,483	2,483	6,060	3,910	3,910
Polar Fittings	100	220	100	100	220
Joint Hardware	972	972	5,430	1,492	1,492
Total	18,965 lb	19,405 lb	31,995 lb	24,462 lb	24,902 lb
Approximate case cost exclusive of tooling and development	$300,000	$330,000	$320,000	$350,000	$380,000

FIG. 1

SKETCHES ILLUSTRATING PRINCIPLE OF OPERATION OF NUCLEAR LIGHT BULB ENGINE

a) OVERALL CONFIGURATION

- MODERATOR
- NOZZLES
- PRESSURE SHELL
- SECTION A-A
- A
- A
- REGION FOR PUMPS, HEAT EXCHANGERS, PLUMBING, SEPARATORS, ETC.
- UNIT CAVITY
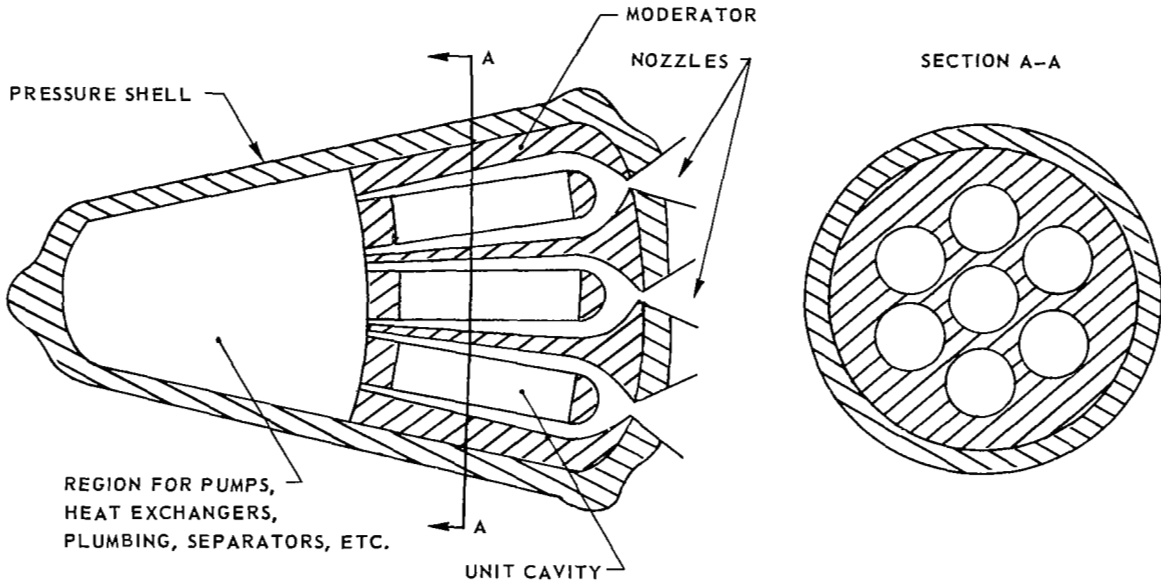
b) CONFIGURATION OF UNIT CAVITY

- MODERATOR
- SEEDED HYDROGEN PROPELLANT
- TRANSPARENT WALL
- SECTION B-B
- REFLECTING WALL
- B
- B
- THERMAL RADIATION
- NEON
- VORTEX REGION
- GASEOUS NUCLEAR FUEL
- NEON INJECTION PORT

70
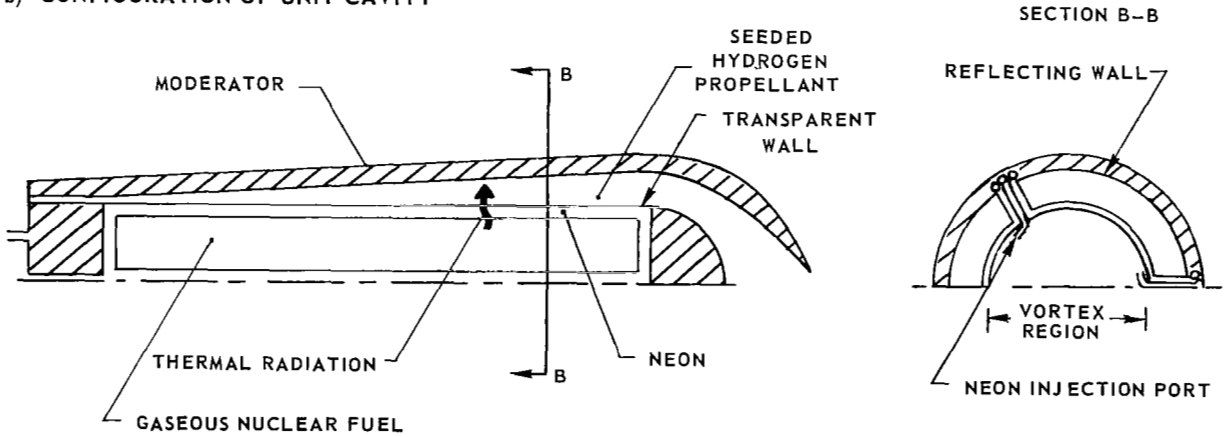
DIMENSIONS OF UNIT CAVITY IN REFERENCE NUCLEAR LIGHT BULB ENGINE

COMPLETE ENGINE COMPOSED OF SEVEN UNIT CAVITIES

ALL DIMENSIONS IN. FT

VOLUME OF UNIT CAVITY = $\frac{\pi}{2}$ $((0.911)^2 + (1.32)^2)$ $(6.0) = 24.2$ FT^3

VOLUME WITHIN UNIT VORTEX = $\pi(0.802)^2 (6.0) = 12.1$ FT^3

FLOW CONDITIONS GIVEN IN FIG. 3

PROPELLANT REGION

0.0931 (AREA = 0.506 FT^2)

MODERATOR REGION

0.502

$\Delta r_1 = 0.016$ (SEE TEXT)

TRANSPARENT WALL (AREA = 3.37 FT^2)

NEON REGION

0.121

1.320

0.911

$r_1 = 0.802$ $r_6 = 0.681$

FUEL REGION

6.0
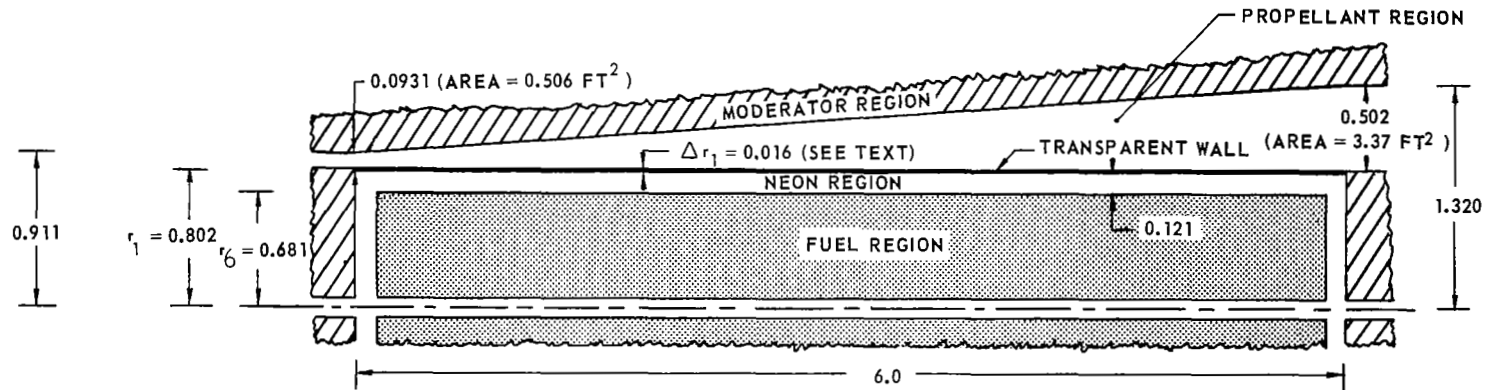
FIG. 2

FLOW CONDITIONS IN UNIT CAVITY OF REFERENCE NUCLEAR LIGHT BULB ENGINE

PRESSURE = 500 ATM

DIMENSIONS GIVEN IN FIG. 2

FLOW RATES THROUGH EACH UNIT
HYDROGEN – 6.04 LB/SEC
NEON – 2.96 LB/SEC
FUEL – 0.19 LB/SEC

NEON CONDITIONS AT EDGE OF FUEL
$T = 15{,}000$ R
$\rho = 0.924$ LB/FT^3
$\mu = 2.6 \times 10^{-4}$ LB/SEC – FT
$V_{z_e} = 1.95$ FT/SEC

HYDROGEN INLET CONDITIONS
$H = 15{,}500$ BTU/LB
$T = 4050$ R
$\rho = 0.336$ LB/FT^3
$V = 35.5$ FT/SEC
$\dfrac{\rho V^2}{2g} = 0.0485$ PSI

NEON CONDITIONS AT PERIPHERY
$T = 2000$ R
$\rho = 6.93$ LB/FT^3
$\mu = 0.575 \times 10^{-4}$ LB/SEC–FT
$V_{z_e} = 0.71$ FT/SEC

HYDROGEN EXIT CONDITIONS
$T = 12{,}000$ R
$H = 1.033 \times 10^5$ BTU/LB
$\rho = 0.0756$ LB/FT^3
$V = 23.7$ FT/SEC
$\dfrac{\rho V^2}{2g} = 0.00458$ LB/IN^2

72
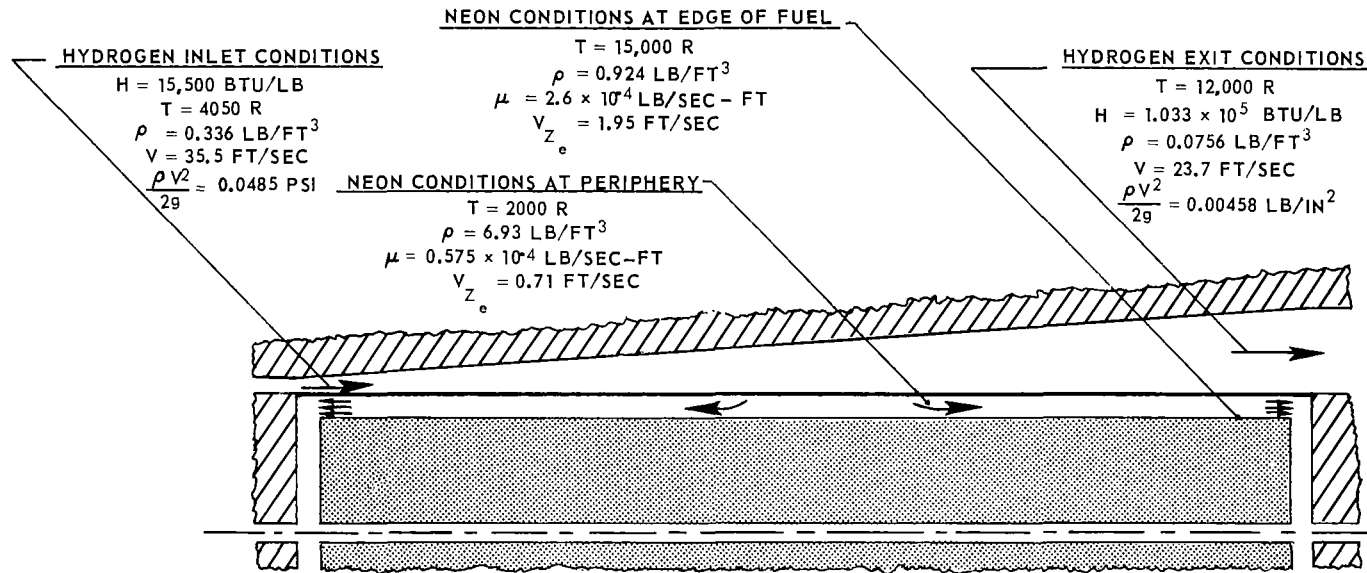
FIG. 3

SIDE VIEW OF REFERENCE NUCLEAR LIGHT BULB ENGINE CINFIGURATION

PRESSURE SHELLS

TRANSPARENT STRUCTURE

TURBOPUMP

MAXIMUM RADIUS = 6.385 FT

TIE ROD

H_2-H_e HEAT EXCHANGER

H_2 – H_2 HEAT EXCHANGERS(7)

FUEL INJECTION PORT

BERYLLIUM OXIDE

GRAPHITE

CAVITY LINER

REAR STRUCTURAL GRID

TOTAL LENGTH = 22.75 FT

73
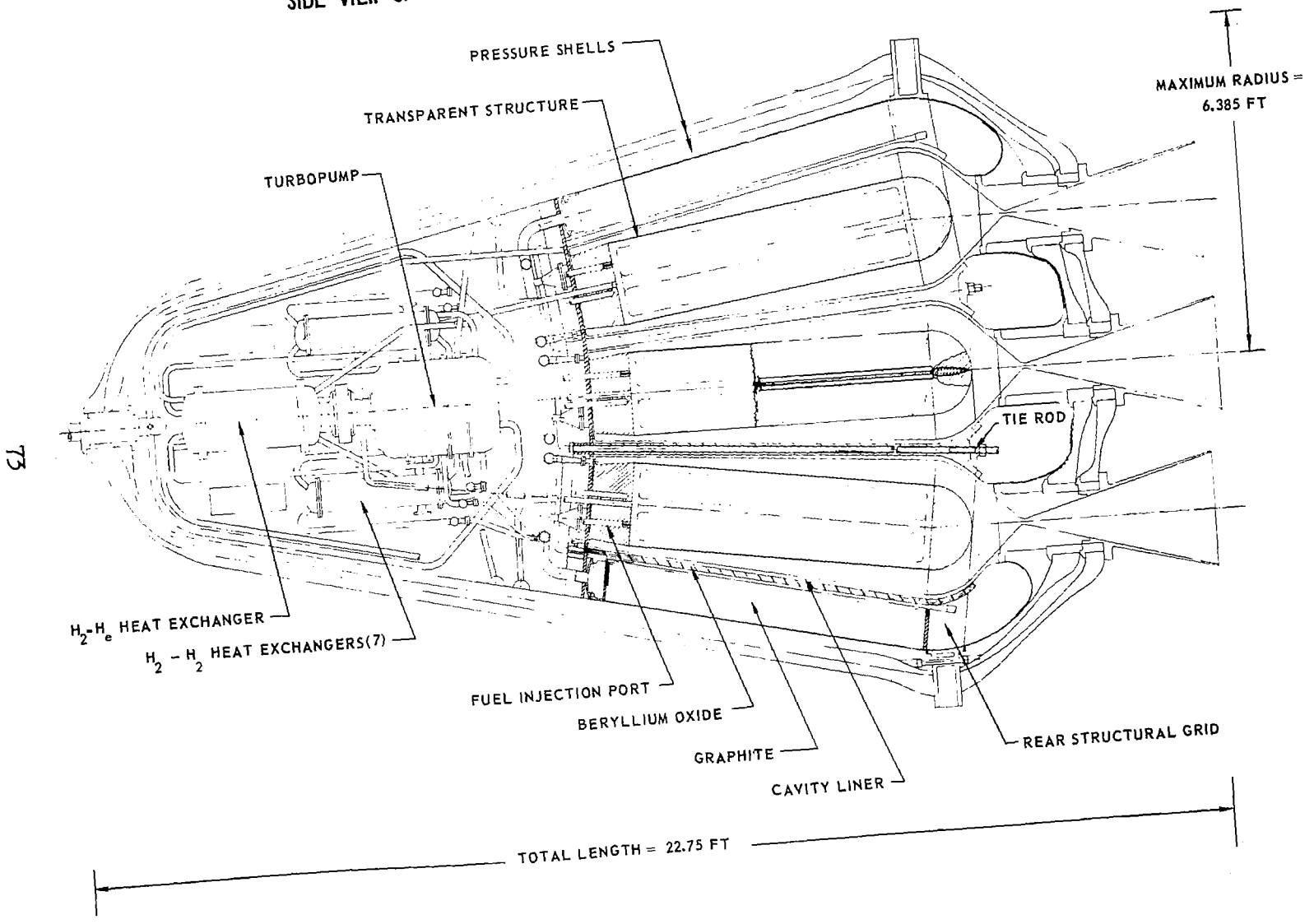
FIG. 4

FRONT SECTION OF REFERENCE NUCLEAR LIGHT BULB ENGINE CONFIGURATION

74

FIG. 5

FIG. 6
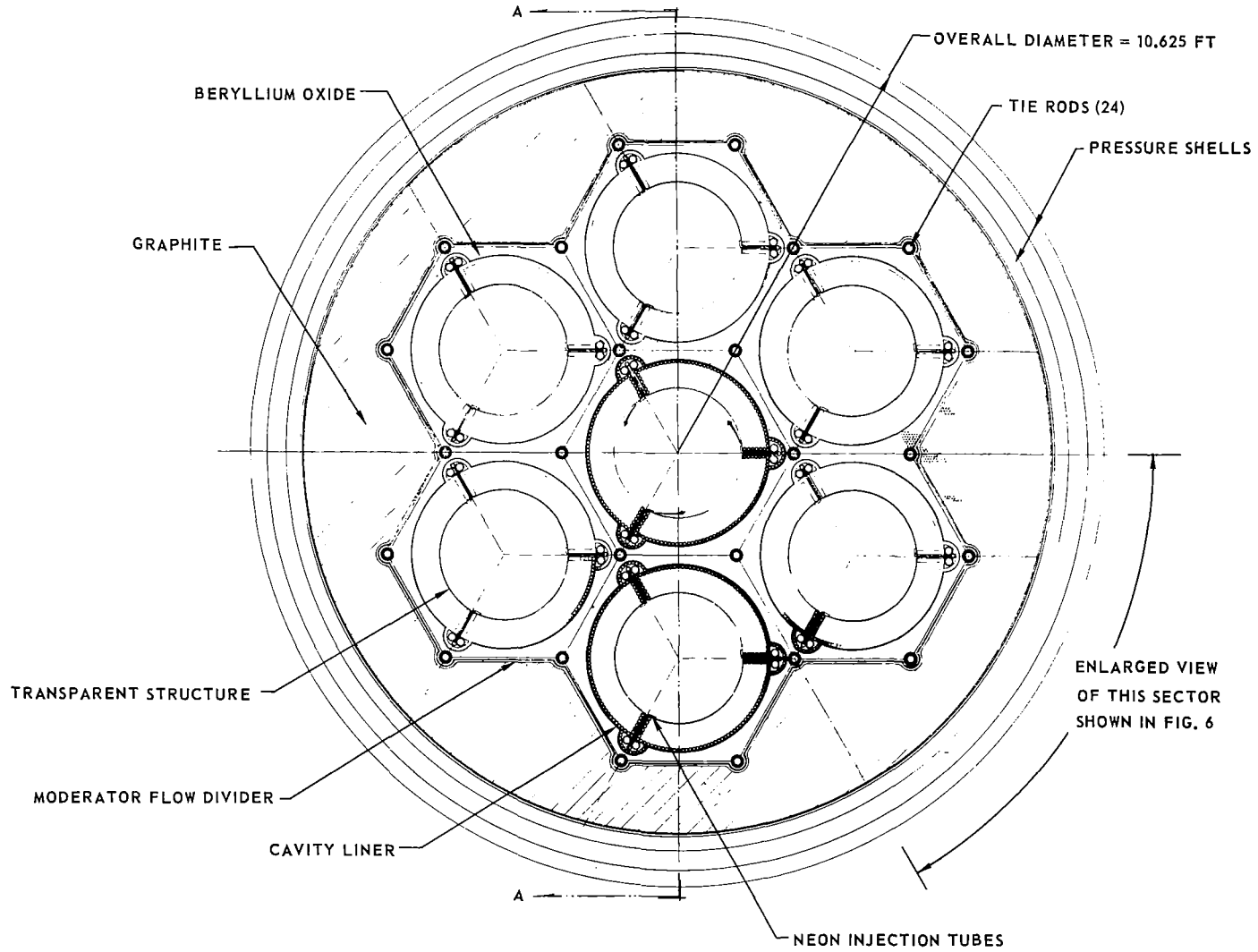
SECTOR OF REFERENCE NUCLEAR LIGHT BULB ENGINE CONFIGURATION

CAVITY LINER

NEON INJECTION TUBES

TRANSPARENT STRUCTURE

FUEL REGION

FLOW DIVIDER

PROPELLANT
REGION

BERYLLIUM OXIDE

GRAPHITE

PRESSURE SHELLS

75
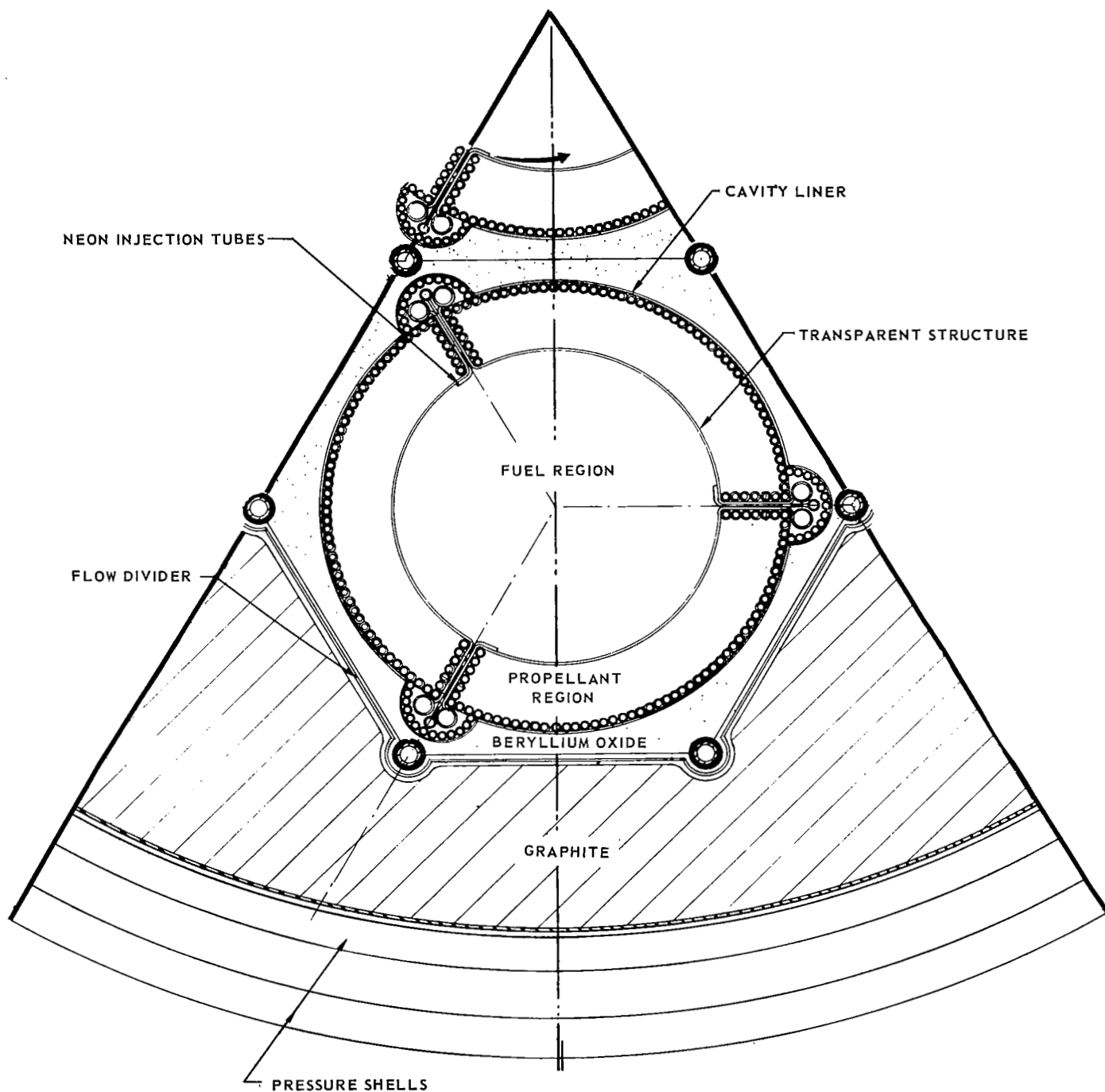
SEGMENT OF TRANSPARENT STRUCTURE AND CAVITY LINER FOR NUCLEAR LIGHT BULB ENGINE

TYPICAL 120°SECTION OF SINGLE CAVITY

NEON INJECTION PIPE

HYDROGEN COOLED
TRANSPARENT STRUCTURE

CAVITY REGION

FEEDER PIPE FOR NEON
INJECTION PIPES

FEEDER PIPE
FOR TRANSPARENT
STRUCTURE COOLANT

COLLECTOR PIPE
FOR TRANSPARENT STRUCTURE
COOLANT

PROPELLANT REGION

BeO REGION

LINER TUBES

76
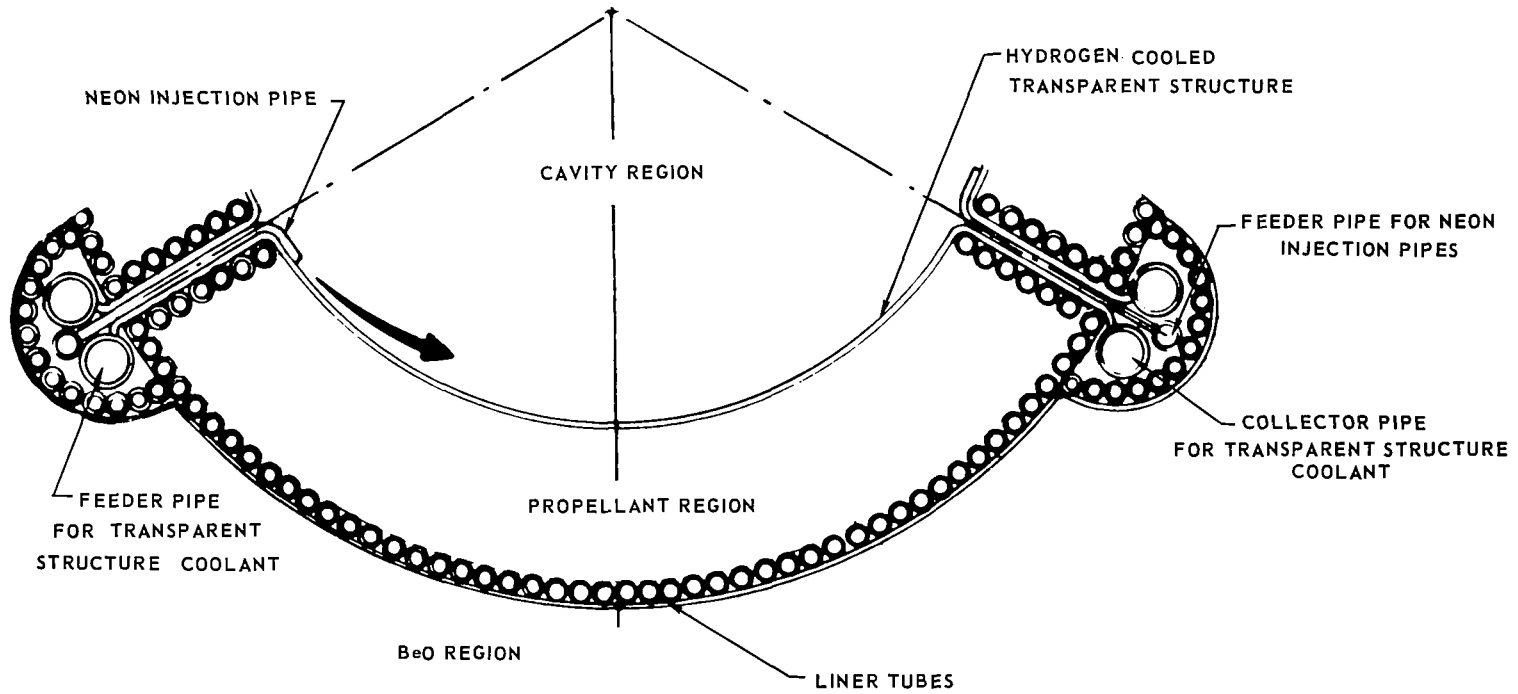
FIG. 7

SCHEMATIC DIAGRAM OF COOLING CIRCUITS FOR NUCLEAR LIGHT BULB ENGINE

P GIVEN IN ATM
T GIVEN IN DEG R
H GIVEN IN BTU/LB
————————— SECONDARY CLOSED CIRCUIT
— — — — — PRIMARY PROPELLANT CIRCUIT
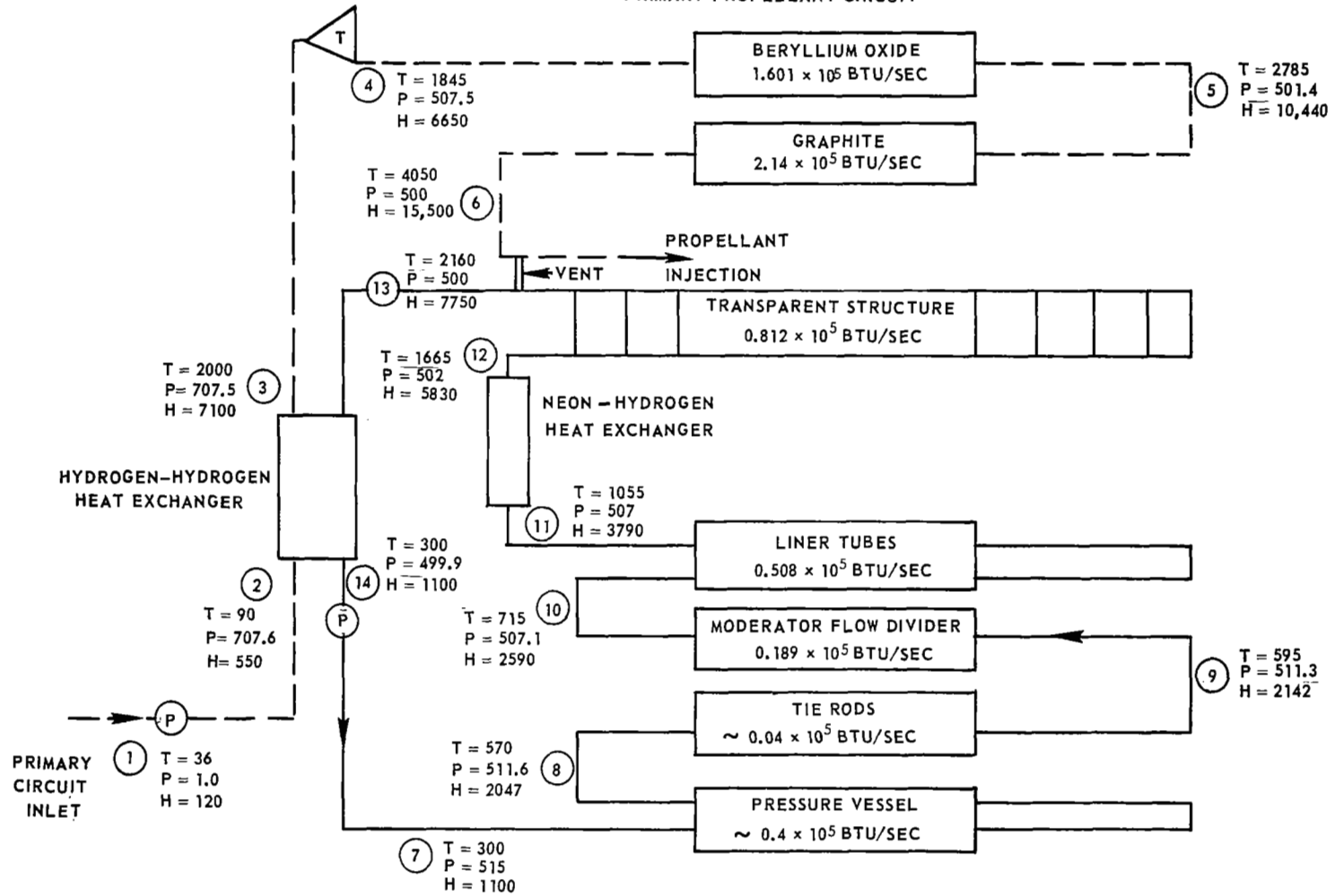
FIG. 8

FIG. 9

NUCLEAR LIGHT BULB ENGINE WEIGHT FLOW DURING STARTUP
FOR FIXED EXHAUST–NOZZLE AREA

NOZZLE THROAT AREA, $A_T = 0.0398$ FT^2

$$W_P = \left(\frac{W}{A}\right)_T A_T$$

$(W/A)_T$ FROM REF. 9

DESIGN WEIGHT FLOW = 42.3 LB/SEC

PROPELLANT-EXIT TEMPERATURE, T_e – DEG R
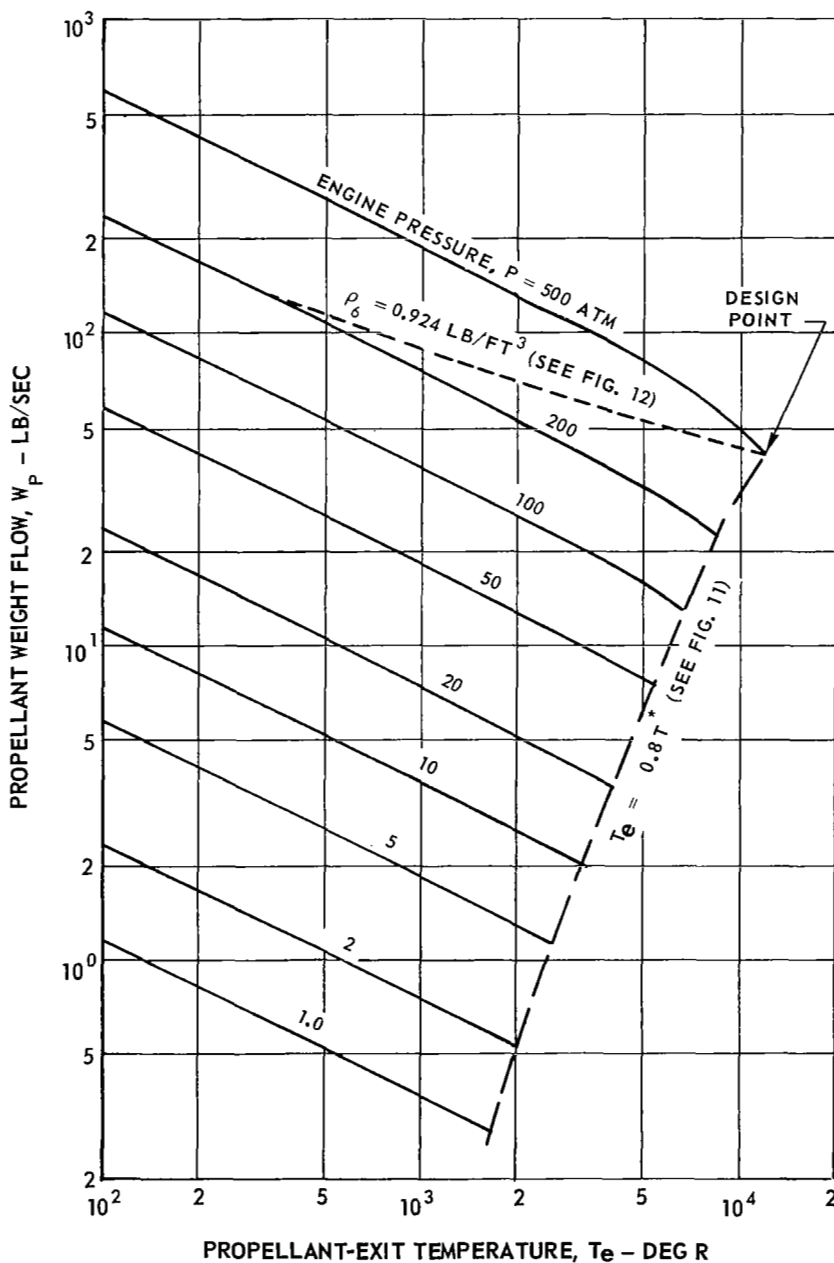
FIG. 10

NUCLEAR LIGHT BULB ENGINE POWER DURING STARTUP FOR FIXED EXHAUST NOZZLE AREA

$$Q = W_P H_e$$

W_P FROM FIG. 9

H_e FROM REF. 9

DESIGN POWER = 4.37×10^6 BTU/SEC
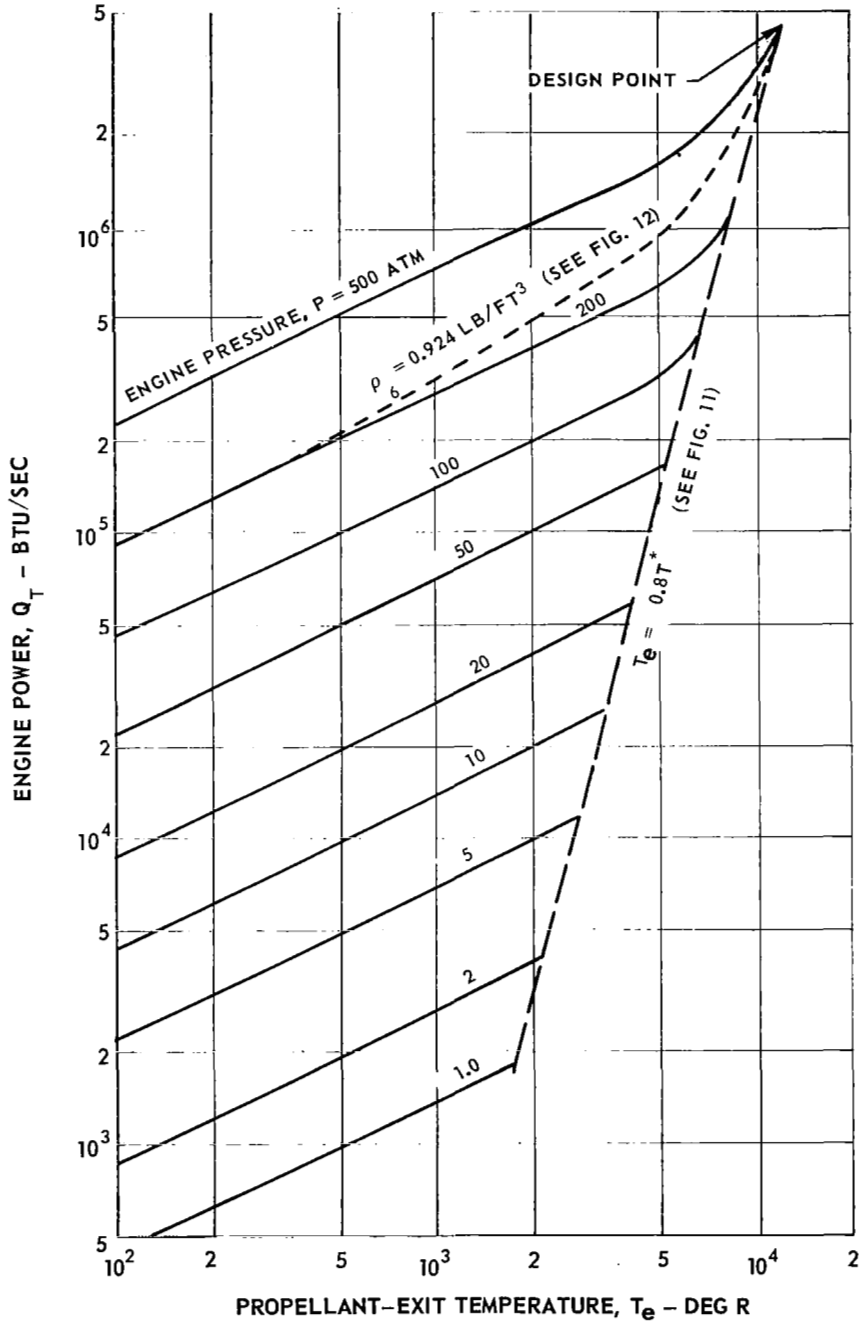
REQUIRED FUEL RADIATING TEMPERATURE DURING ENGINE STARTUP
FOR FIXED EXHAUST NOZZLE AREA FOR NUCLEAR LIGHT BULB ENGINE

DESIGN RADIATING TEMPERATURE = 15,000 R

$$\left(\frac{T^*}{15,000}\right)^4 = \frac{Q_T}{4.37 \times 10^6}$$

Q_T FROM FIG. 10

FIG. 11

FIG. 12
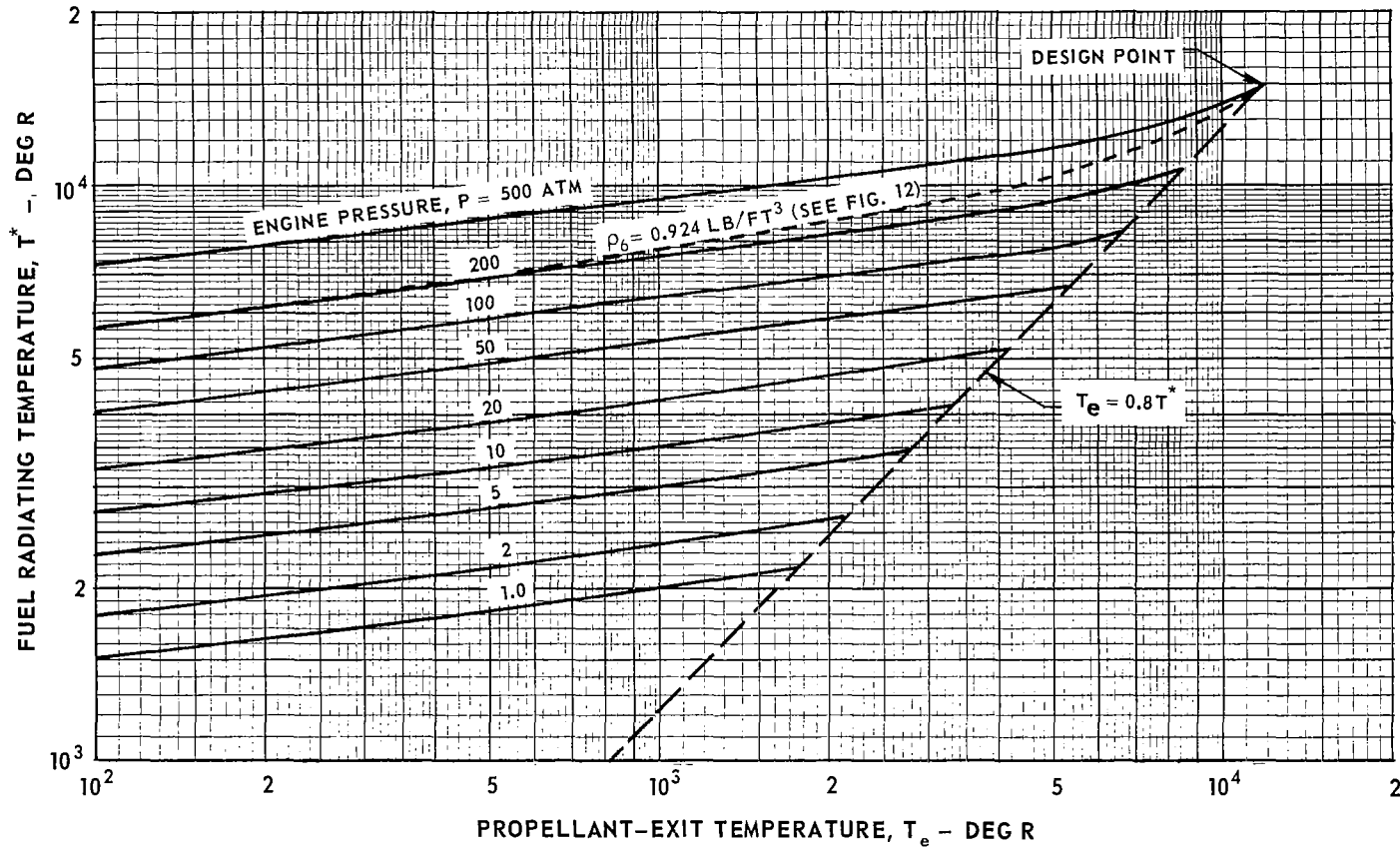
NEON DENSITY AT EDGE OF FUEL DURING NUCLEAR LIGHT BULB ENGINE STARTUP FOR FIXED EXHAUST NOZZLE AREA

NEON DENSITY, ρ_6, AT EDGE OF FUEL AT DESIGN POINT = 0.924 LB/FT^3

$$\rho_6 = (0.924)\left(\frac{P}{500}\right)\left(\frac{15,000}{T^*}\right)$$

P AND $\overset{\bullet}{T}$ FROM FIG. 11

FIG. 13
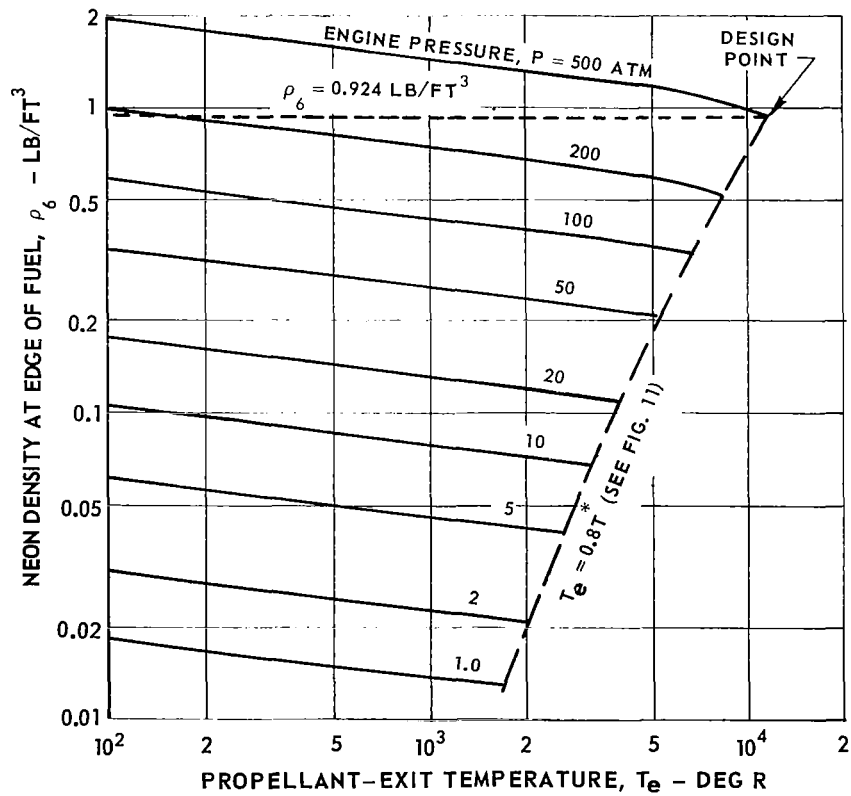
ENGINE PRESSURE AND POWER DURING STARTUP
FOR VARIABLE EXHAUST NOZZLE AREA FOR NUCLEAR LIGHT BULB ENGINE

NOZZLE AREA SCHEDULE SHOWN IN FIG. 14

$$\rho_6 = 0.924 \text{ LB/FT}^3$$
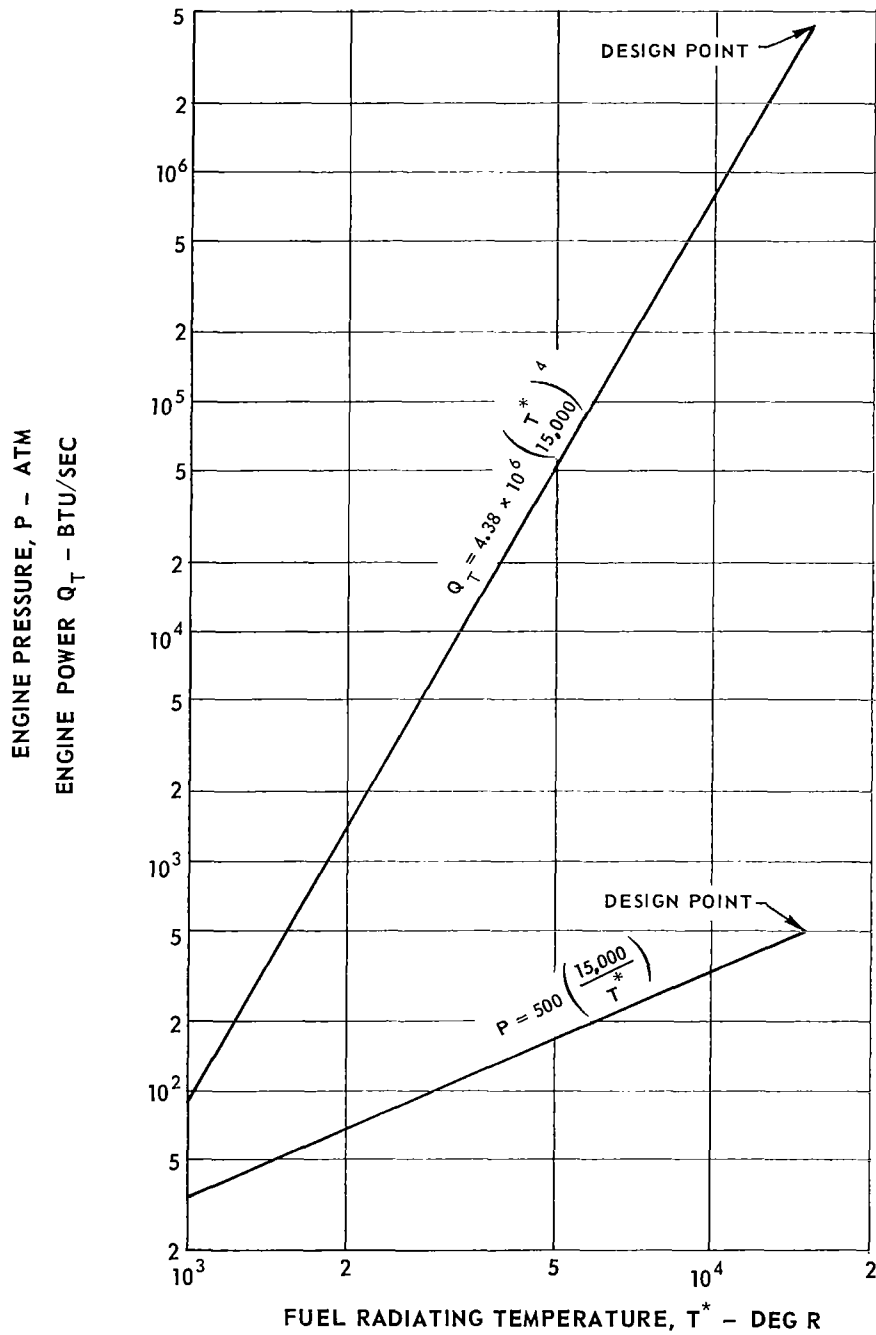
FIG. 14

NUCLEAR LIGHT BULB ENGINE WEIGHT FLOW AND THROAT AREA
DURING STARTUP FOR VARIABLE EXHAUST NOZZLE AREA
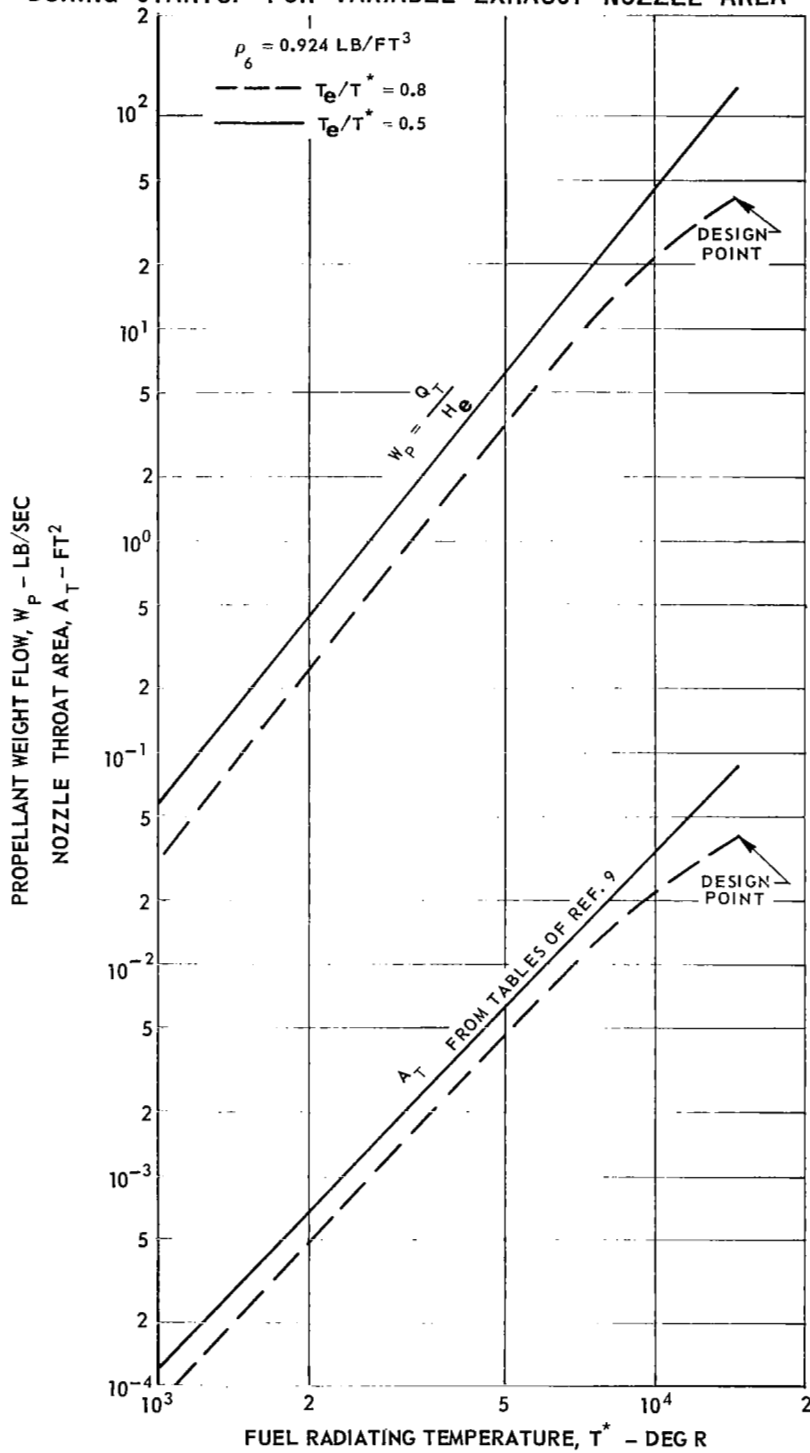
FIG. 15

NUCLEAR LIGHT BULB ENGINE THRUST AND SPECIFIC IMPULSE DURING STARTUP
FOR VARIABLE EXHAUST NOZZLE AREA

84
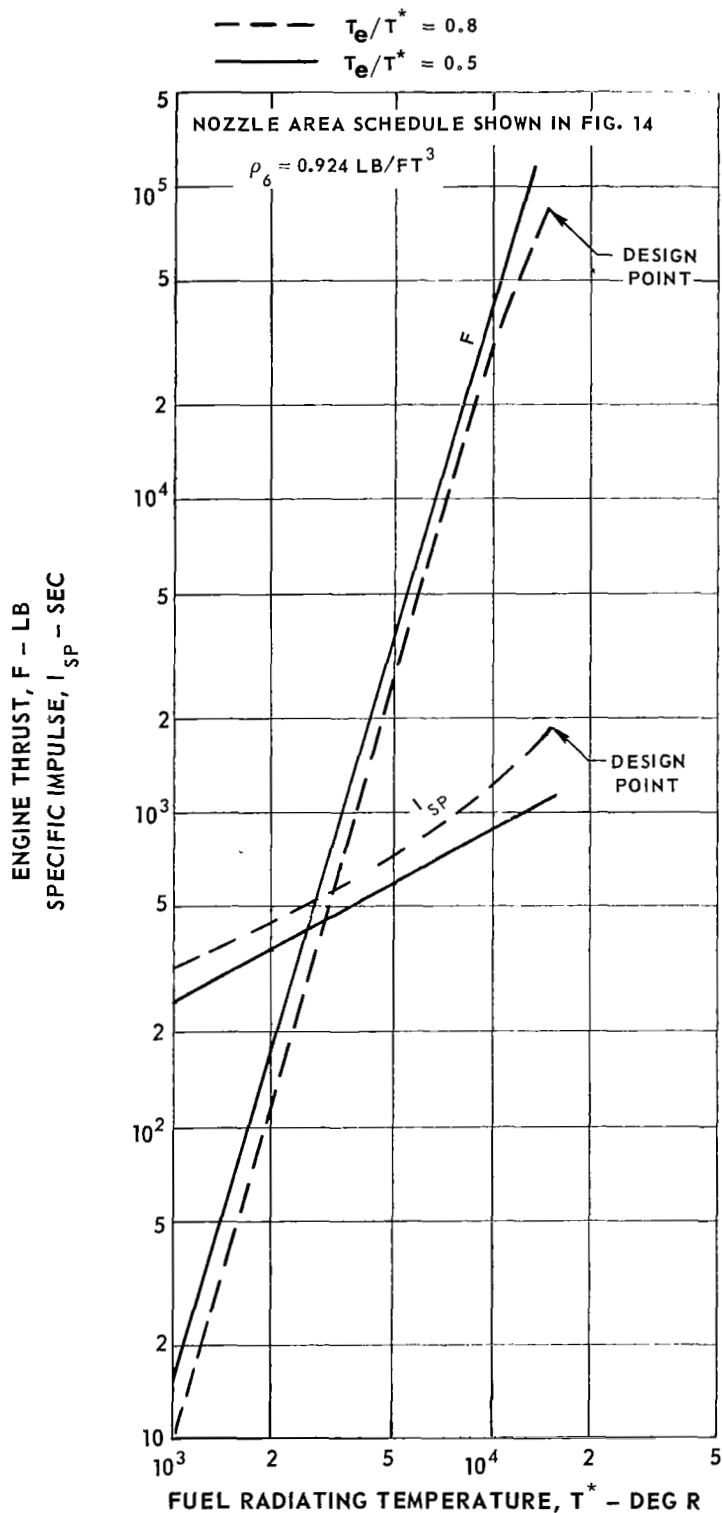
LAYOUT DRAWING OF ENGINE DESIGN CONFIGURATION

SEE FIGS. 3, 6, AND 7 OF REF. 11
FOR DETAILS OF THIS REGION

SPHERICAL PRESSURE VESSEL

A

CAVITY

LINER TUBES

BeO MODERATOR

TURBOPUMPS
4 REQUIRED

GRAPHITE MODERATOR

D_2O MODERATOR

PIPING AND HEAT EXCHANGER REGION

H_2

CYLINDRICAL
PRESSURE VESSEL

BERYLLIUM WALLS

B

B

END VIEW OF NOZZLES

SECTION B – B

85
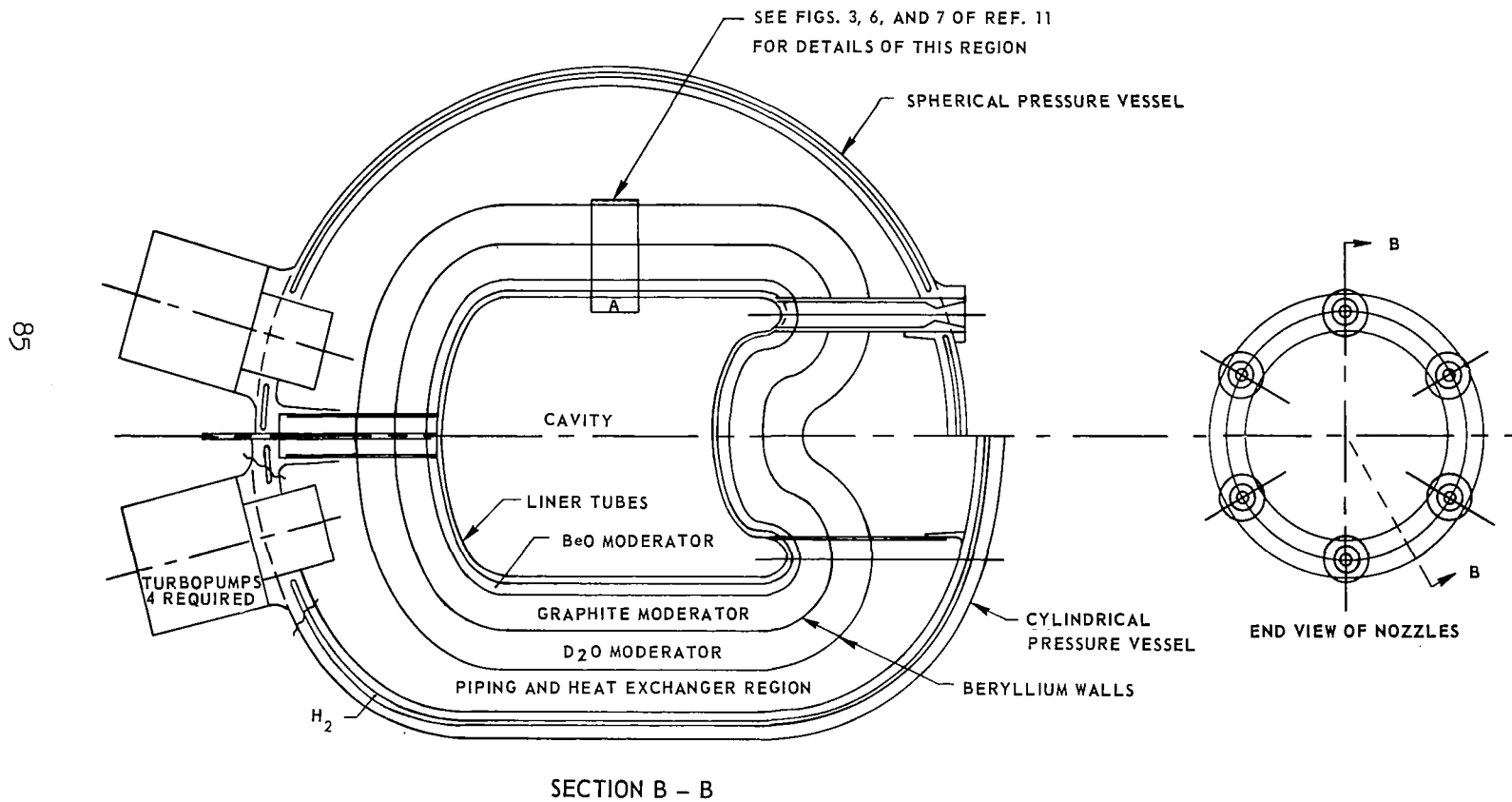
FIG. 16

VARIATION WITH COOLANT HOLE DIAMETER OF NIOBIUM CARBIDE COATING WEIGHT AND TOTAL PRESSURE DROP IN GRAPHITE MODERATOR OF OPEN CYCLE ENGINE

ENGINE CONFIGURATION D (SEE TABLE XII)

AVERAGE VOLUMETRIC HEAT DEPOSITION = 1.092 × 10^4 BTU/SEC-FT^3

NIOBIUM THICKNESS ON SURFACE OF GRAPHITE TO PROTECT GRAPHITE FROM ATTACK = 0.002 IN.

COOLANT TO WALL TEMPERATURE DIFFERENCE = 200 R

SPIRAL COOLING HOLES

MAXIMUM TO WALL TEMPERATURE DIFFERENCE = 100 R

GRAPHITE THICKNESS = 8.7 IN.

COOLANT VOLUME FRACTION = 0.02

FIG. 17

98
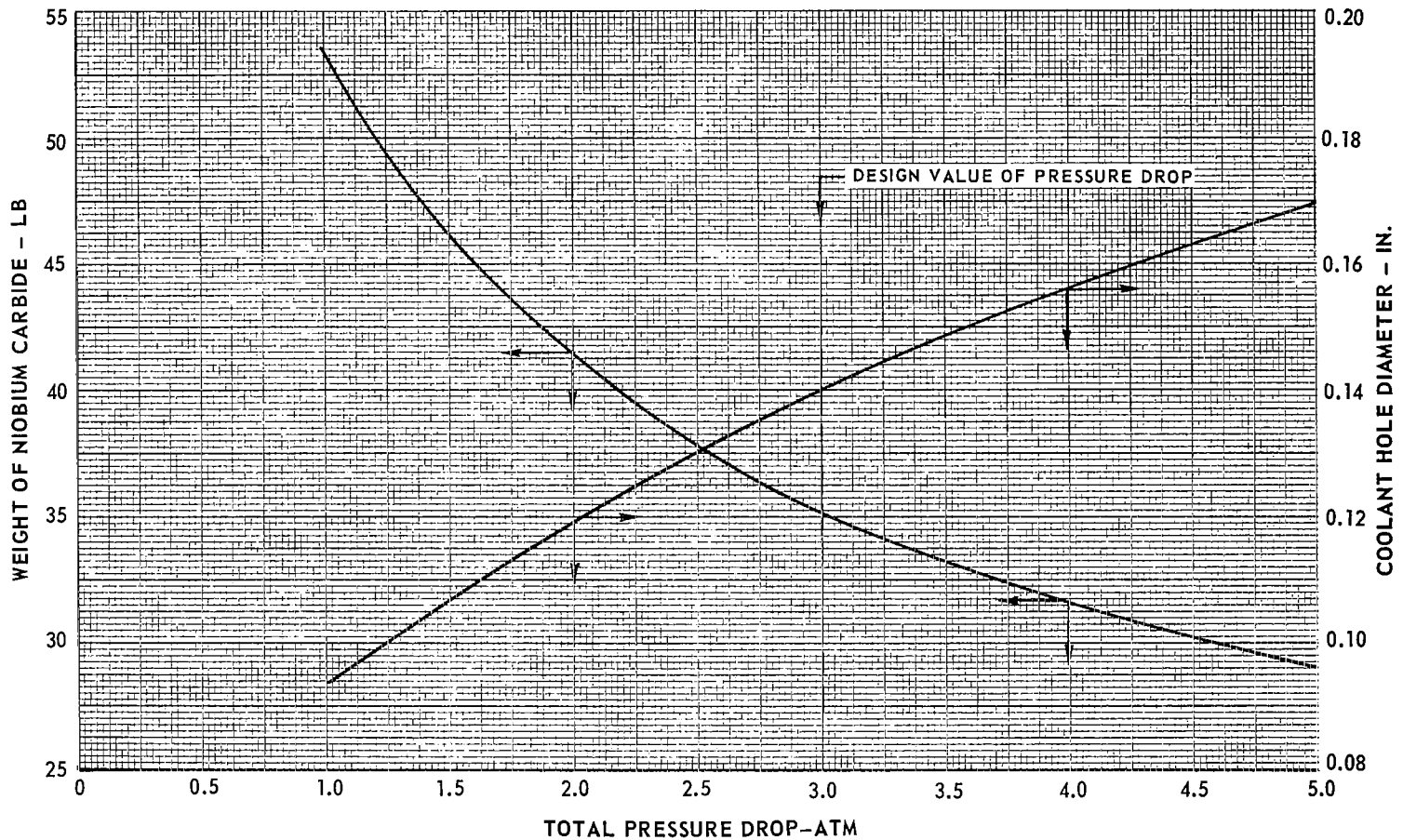
FIG. 18

POSSIBLE PRESSURE SHELL CONFIGURATIONS

SEE APPENDIX A

ALL DIMENSIONS IN FT

87
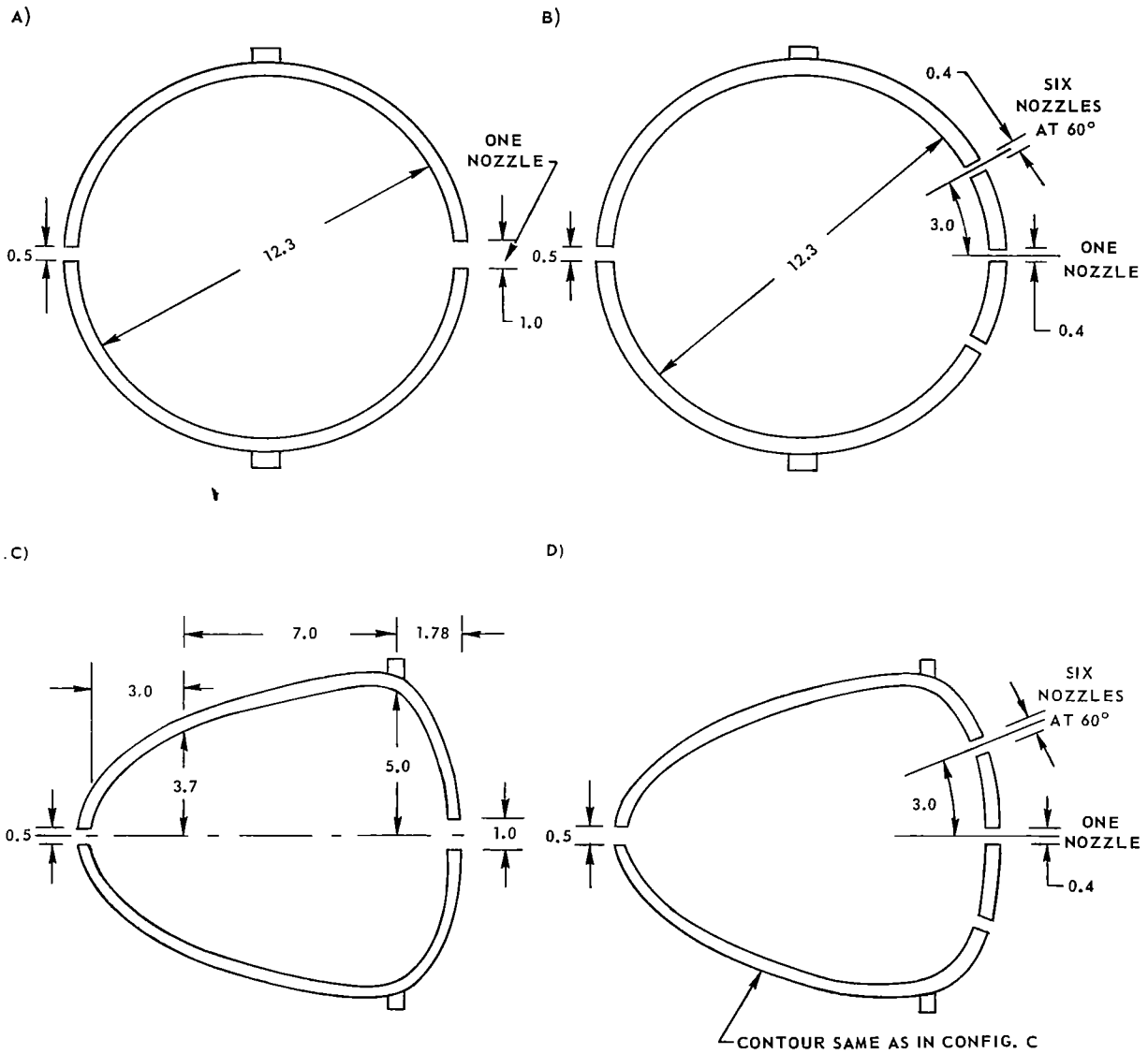
FIBERGLAS PRESSURE VESSEL CONFIGURATION

SEE APPENDIX A

ALL DIMENSIONS IN IN.

BOLT HOLE (1.13 DIA)
(47 BOLTS/ROW)
NUT RECESS (2.2 DIA)
5.6 TYP

2.3
2.1

3.16 TYP
7.05 TYP
PIN (2.0 DIA)
LINK (.72 THICK)
SEAL RING
(TYP)
ALTERNATE CLEVIS JOINT
(90 EACH PINS, LINKS)

2.2
2.0
34.4 R
60.0 R

POLAR FITTINGS
H_2 FLOW PORTS

12.0   15.5   84.0   34.0   12.0

157.5

88

FIG. 19

FIG. 20
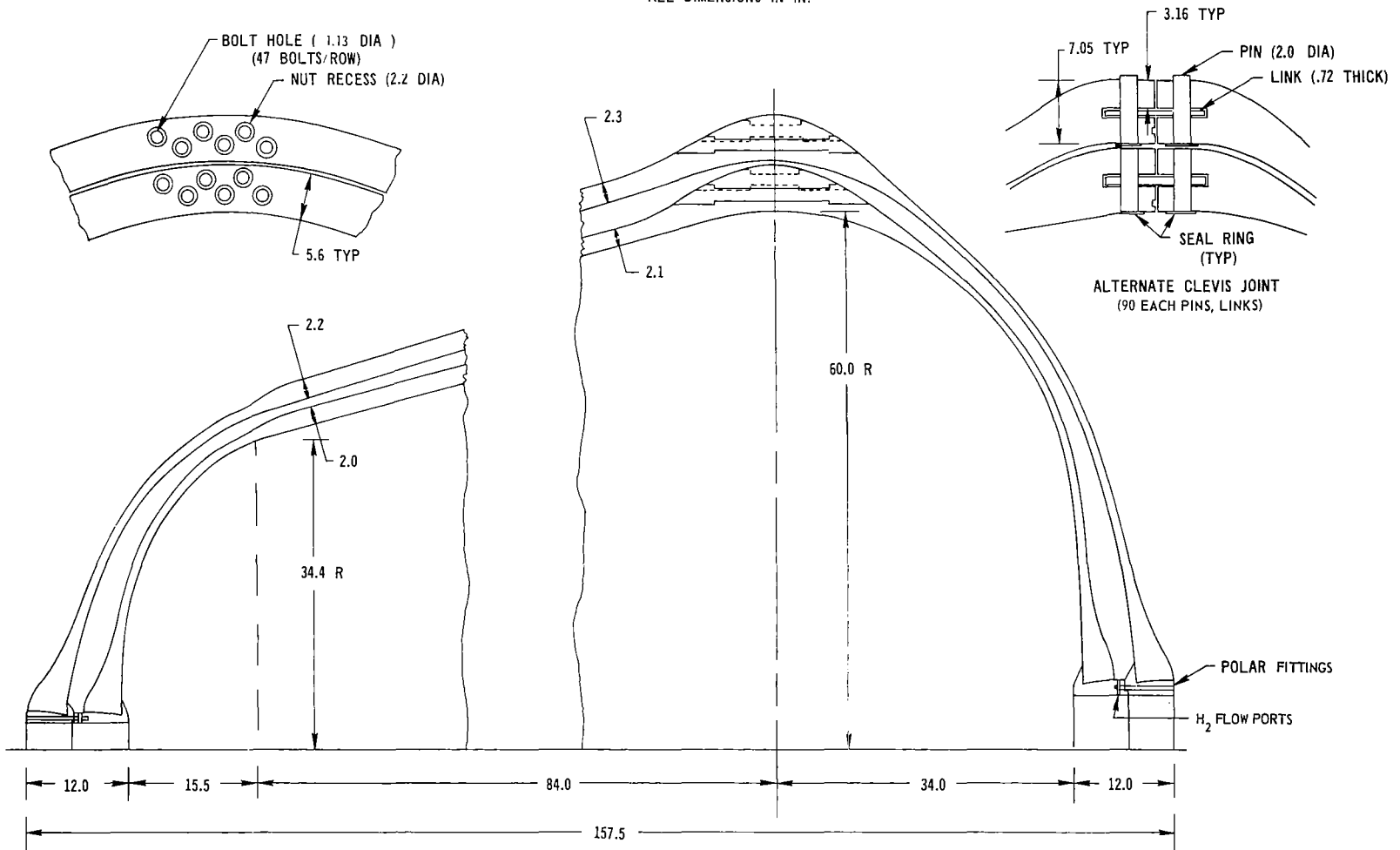
EFFECT OF IDEALIZED GLASS STRESS ON WEIGHT AND COST OF PRESSURE VESSEL

SEE APPENDIX A
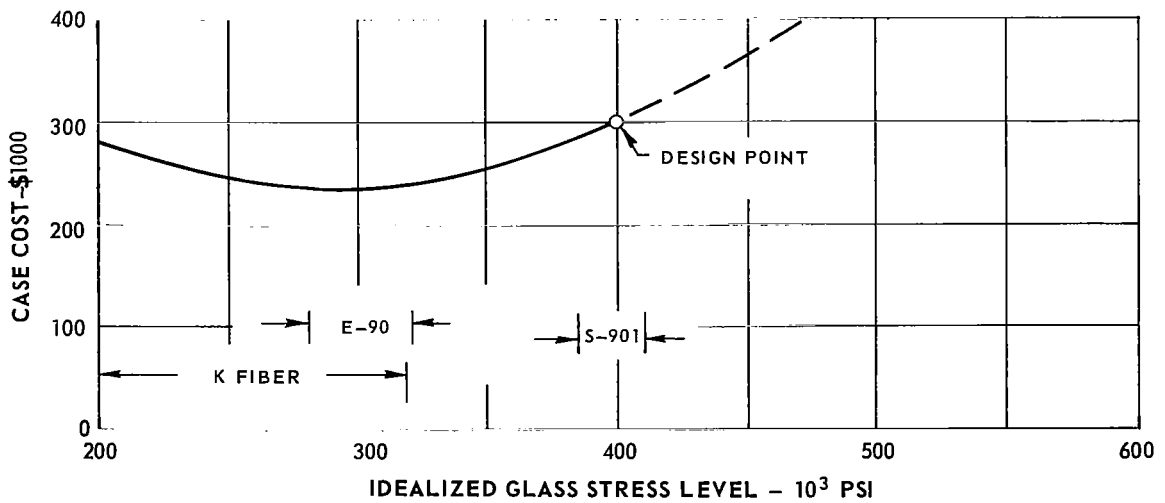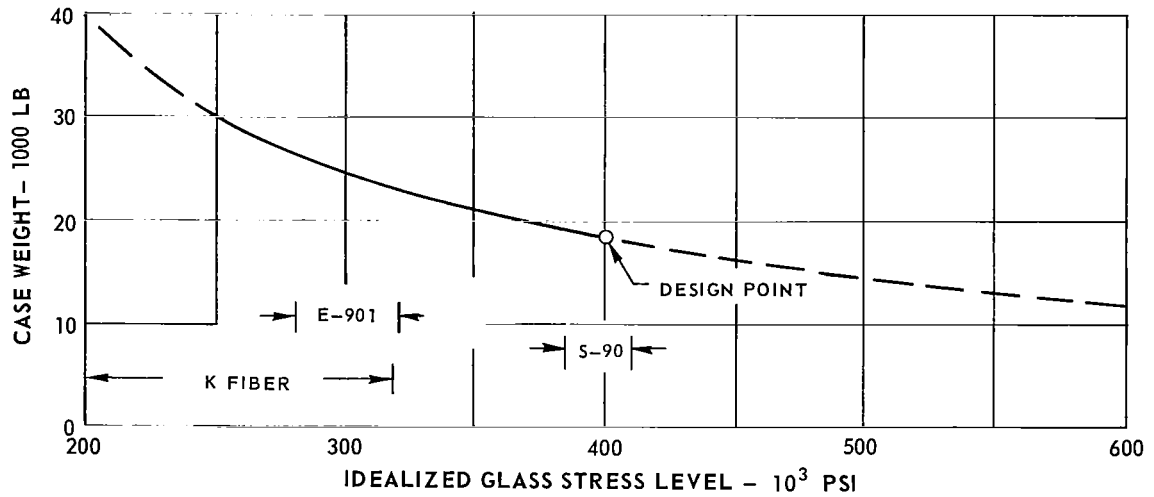
EFFECT OF TEMPERATURE ON STRENGTH OF GLASS FILAMENT – EPOXY RESIN COMPOSITES

SEE APPENDIX A

FIG. 21

FIG. 22
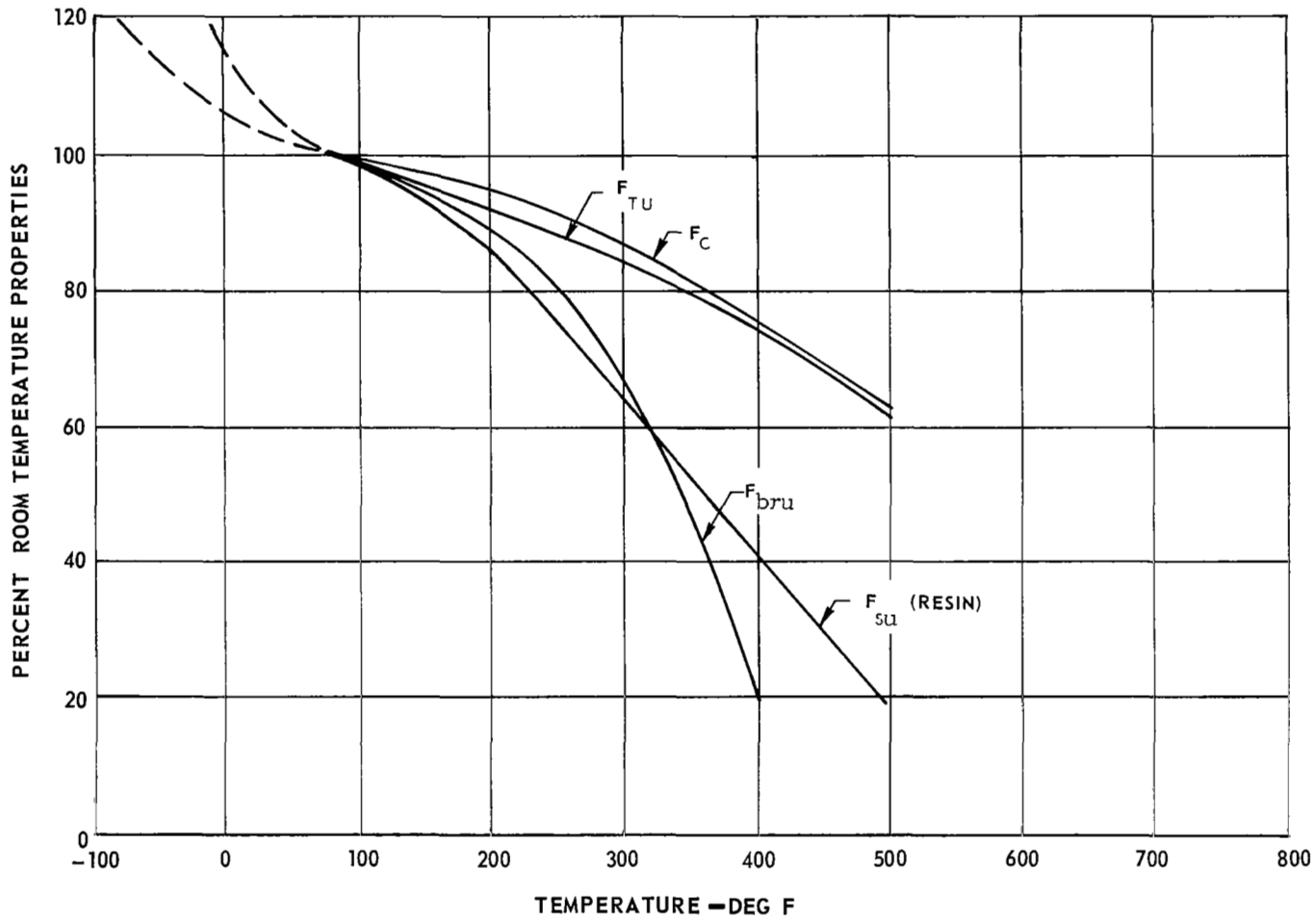
EXPLANATION OF FILAMENT – WINDING TERMS

t_w = TOTAL WALL THICKNESS

t_a = THICKNESS OF HELICAL WINDINGS

t_θ = THICKNESS OF HOOP WINDINGS

a = WINDING ANGLE AT LARGEST RADIUS

R_a = RADIUS TO CENTER OF HELICAL WINDINGS AT TANGENT LINE

R_v = SMALLEST RADIUS AT POLAR OPENING

R_c = LARGEST RADIUS OF FIBERGLAS SUPPORT AT TIP OF POLAR FITTING FLANGE

R_E = RADIUS TO CENTER OF FILAMENT BAND AT POLAR OPENING

K = RESIN BULK FACTOR

σ_w = WALL STRESS IN FIBERGLAS COMPOSITE

σ_G = STRESS IN GLASS FIBERS

t_G = GLASS THICKNESS

SEE APPENDIX A

FIG. 23
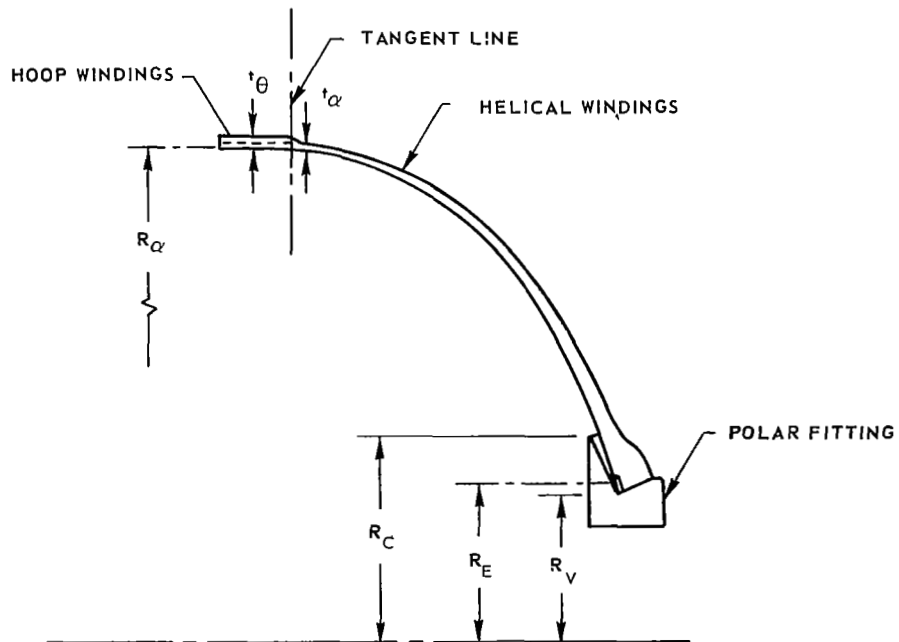
VARIATION OF ENTHALPY WITH AXIAL DISTANCE ASSUMED IN ANALYSIS OF RADIANT ENERGY EMITTED FROM PROPELLANT STREAM OF NUCLEAR LIGHT BULB ENGINE
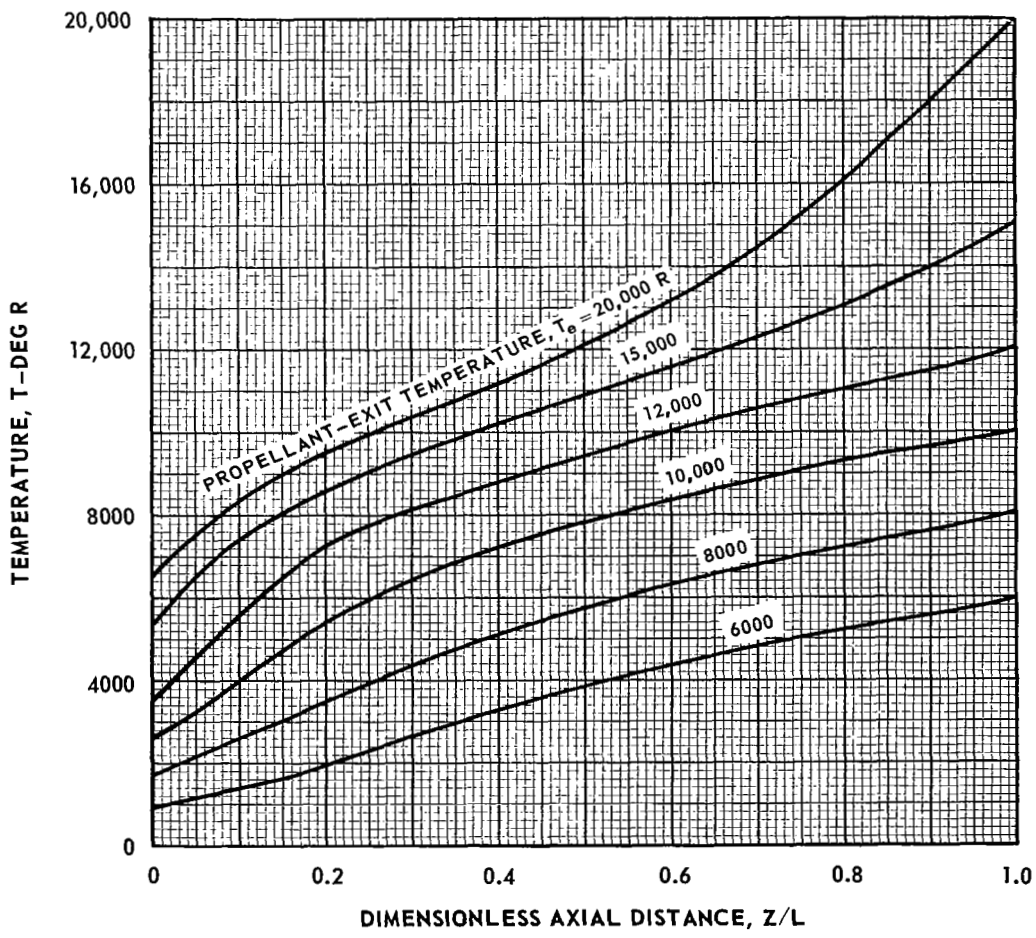
SEE APPENDIX B

P = 500 ATM

ENTHALPY, H–BTU/LB

PROPELLANT-EXIT ENTHALPY, H_e = 186,300 BTU/LB

PROPELLANT-EXIT TEMPERATURE, T_e = 20,000 R; 15,000 R; 145,000 BTU/LB

12,000 R; 103,300 BTU/LB

10,000 R; 66,380 BTU/LB

8,000 R; 39,660 BTU/LB

6,000 R; 24,280 BTU/LB

DIMENSIONLESS AXIAL DISTANCE, Z/L

FIG. 24
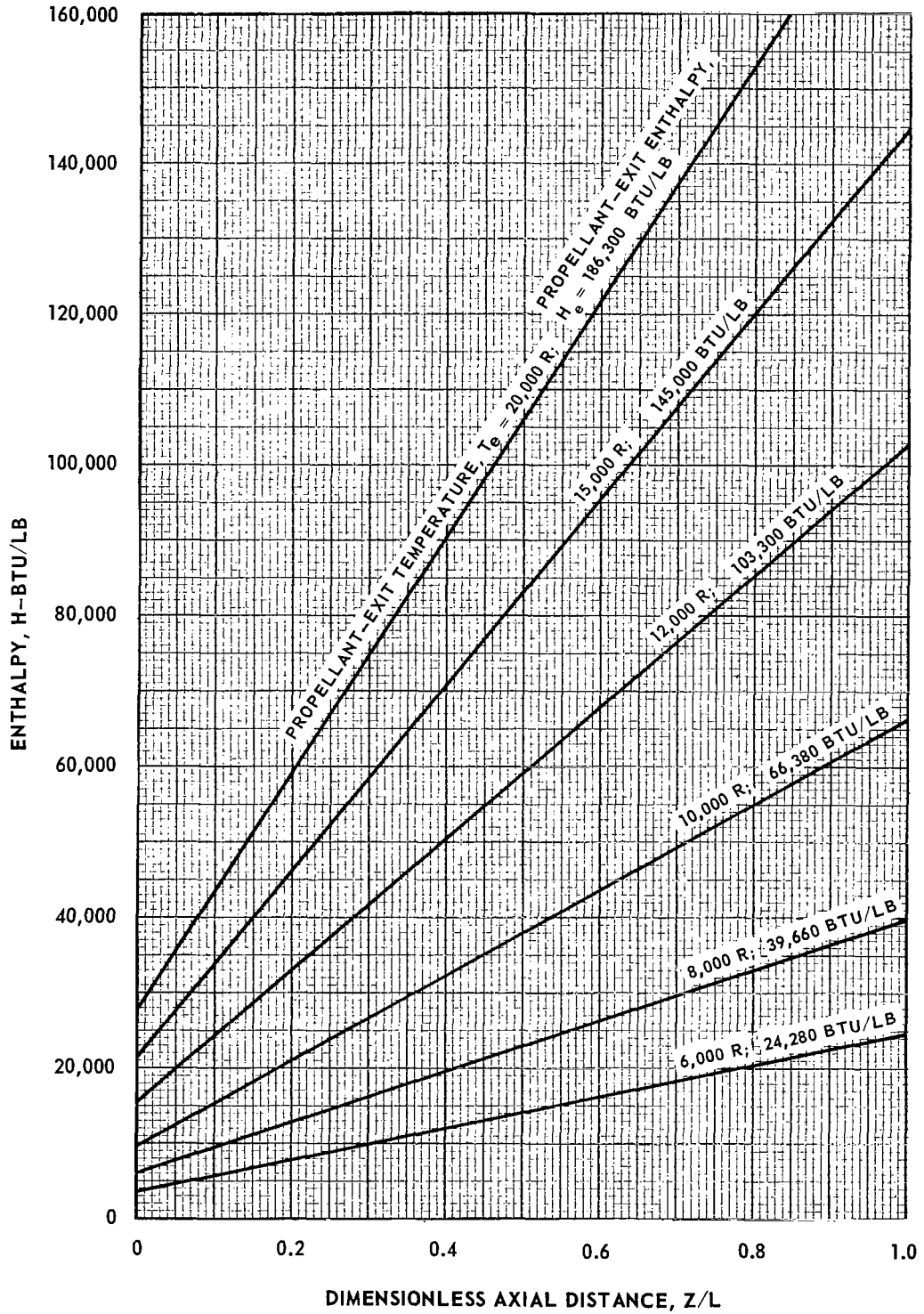
VARIATION OF TEMPERATURE WITH AXIAL DISTANCE EMPLOYED IN ANALYSIS OF RADIANT ENERGY EMITTED FROM PROPELLANT STREAM OF NUCLEAR LIGHT BULB ENGINE

P=500 ATM

TEMPERATURE DISTRIBUTION DETERMINED FROM ENTHALPY
DISTRIBUTION OF FIG. 23 USING TABLES OF REF. 9

SEE APPENDIX B

FIG. 25

VARIATION OF TEMPERATURE INTEGRAL PARAMETER WITH AXIAL DISTANCE DETERMINED FROM ANALYSIS OF ENERGY EMITTED FROM PROPELLANT STREAM OF NUCLEAR LIGHT BULB ENGINE

SEE APPENDIX B

P = 500 ATM

DETERMINED FROM TEMPERATURE DISTRIBUTIONS IN FIG. 24

PROPELLANT-EXIT TEMPERATURE, T_e = 10,000 R, 8000 R, 6000 R

PROPELLANT-EXIT TEMPERATURE, T_e = 12,000 R, 15,000 R, 20,000 R

$$Y = \int_0^{Z/L} (T/T_e)^4 \, dZ/L$$

TEMPERATURE INTEGRAL PARAMETER, Y

DIMENSIONLESS AXIAL DISTANCE, Z/L
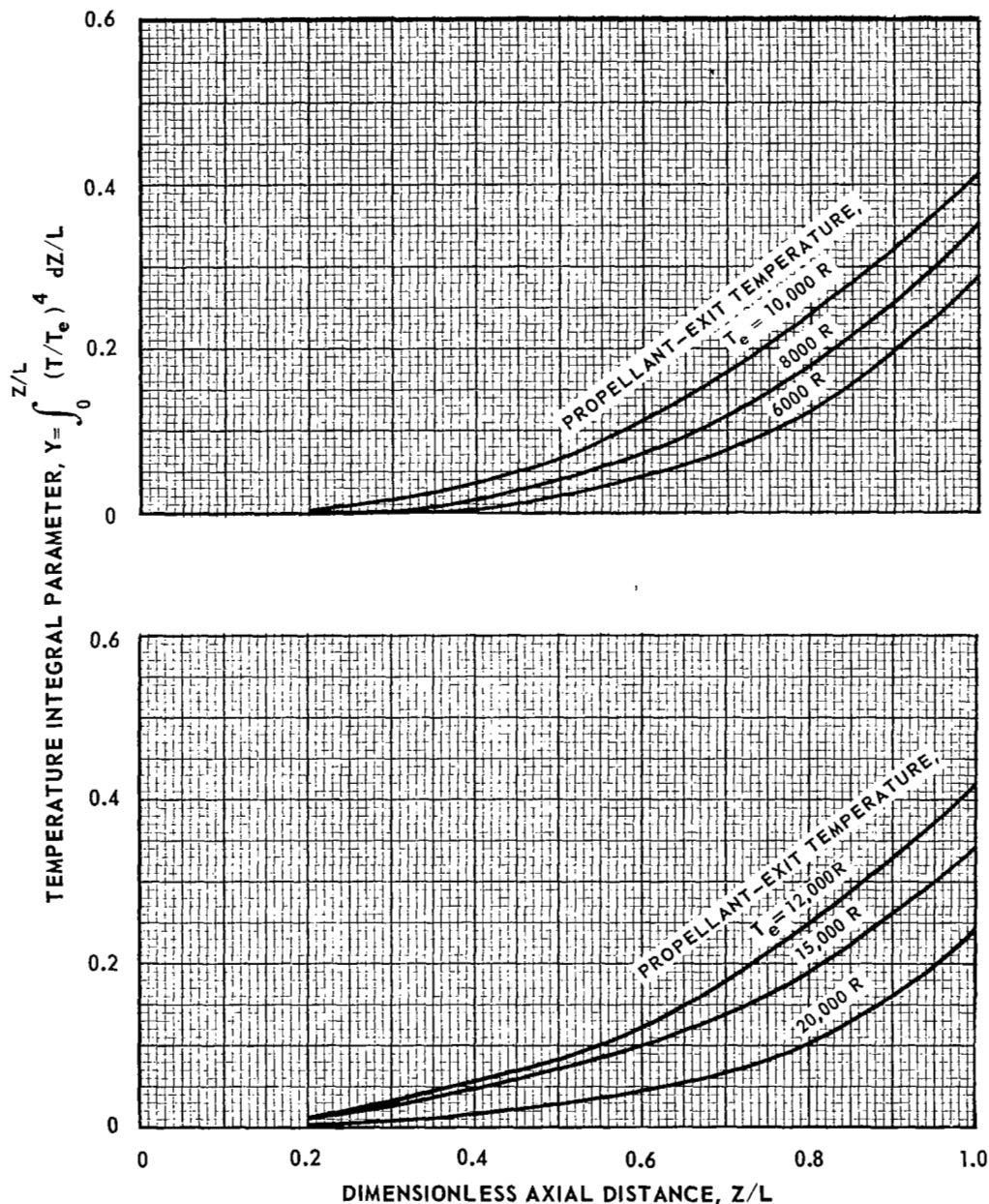
FIG. 26

EFFECT OF EXIT TEMPERATURE ON TEMPERATURE INTEGRAL PARAMETER DETERMINED FROM ANALYSIS OF ENERGY EMITTED FROM PROPELLANT STREAM OF NUCLEAR LIGHT BULB ENGINE
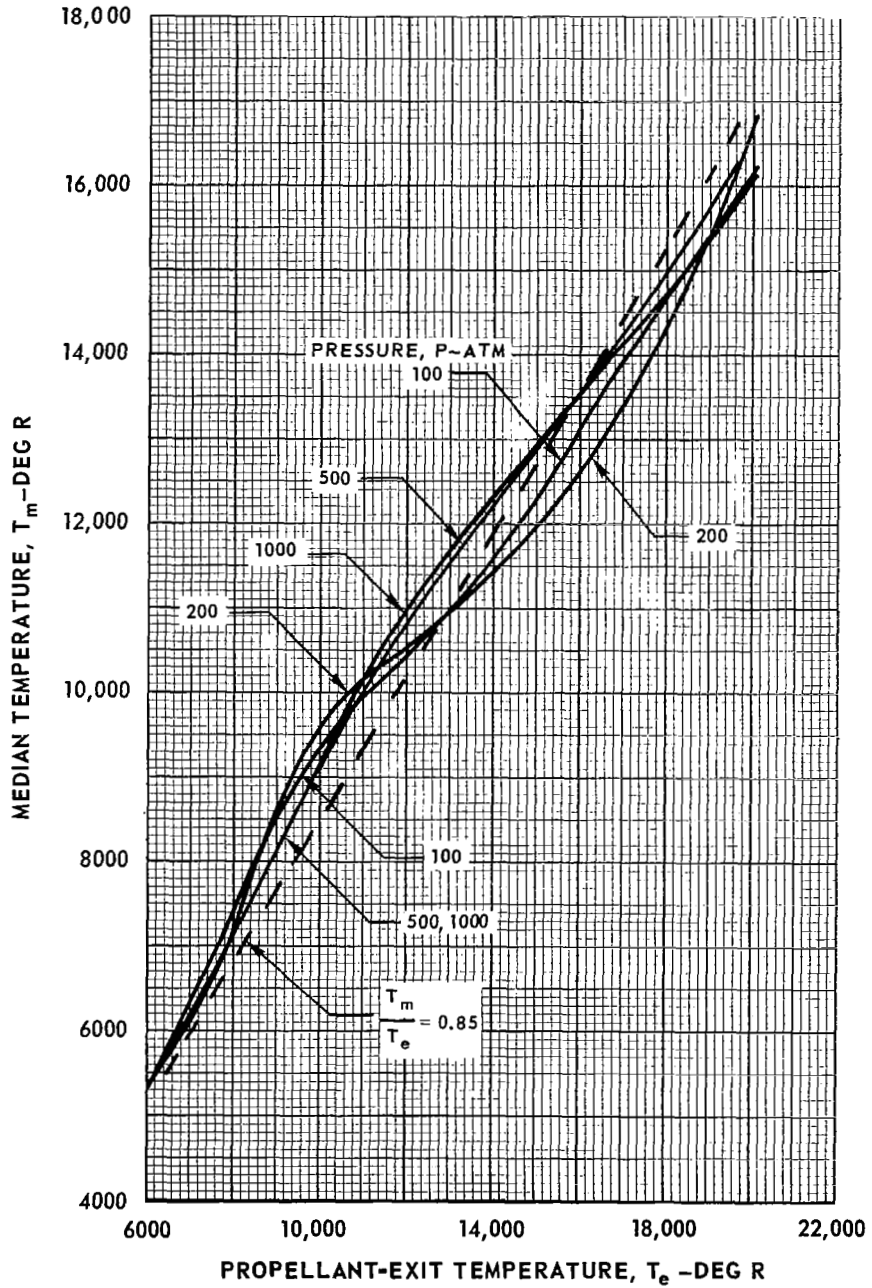
SEE APPENDIX B

FIG. 27
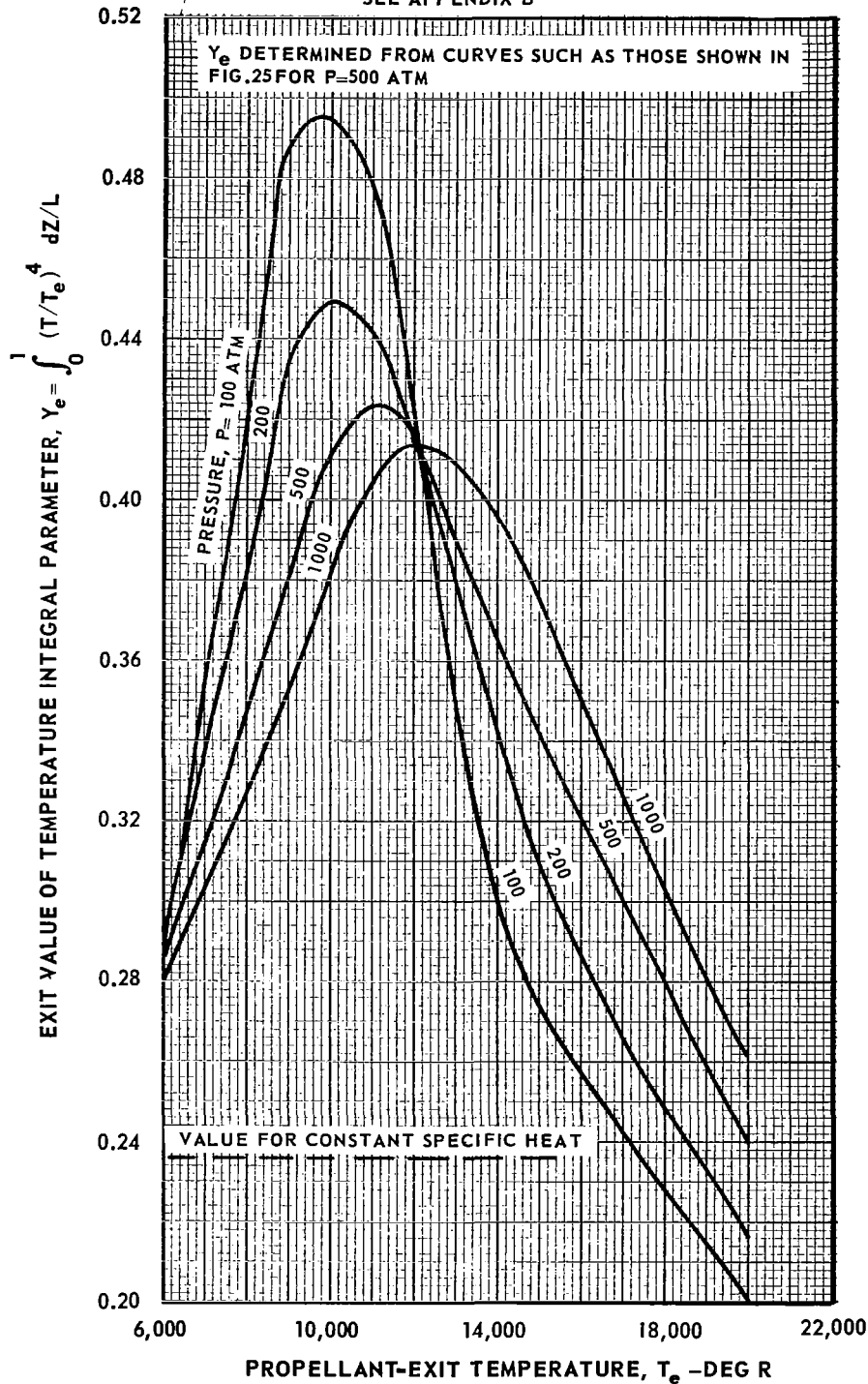
EFFECT OF EXIT TEMPERATURE ON MEDIAN TEMPERATURE DETERMINED FROM ANALYSIS OF ENERGY EMITTED FROM PROPELLANT STREAM OF NUCLEAR LIGHT BULB ENGINE

SEE APPENDIX B

MEDIAN TEMPERATURE, T_m, DEFINED AS TEMPERATURE AT LOCATION WHERE $Y = Y_e/2$

FIG. 28

EFFECT OF INCIDENT ENERGY SPECTRUM ON AVERAGE REFLECTIVITIES OF TUNGSTEN AND ALUMINUM

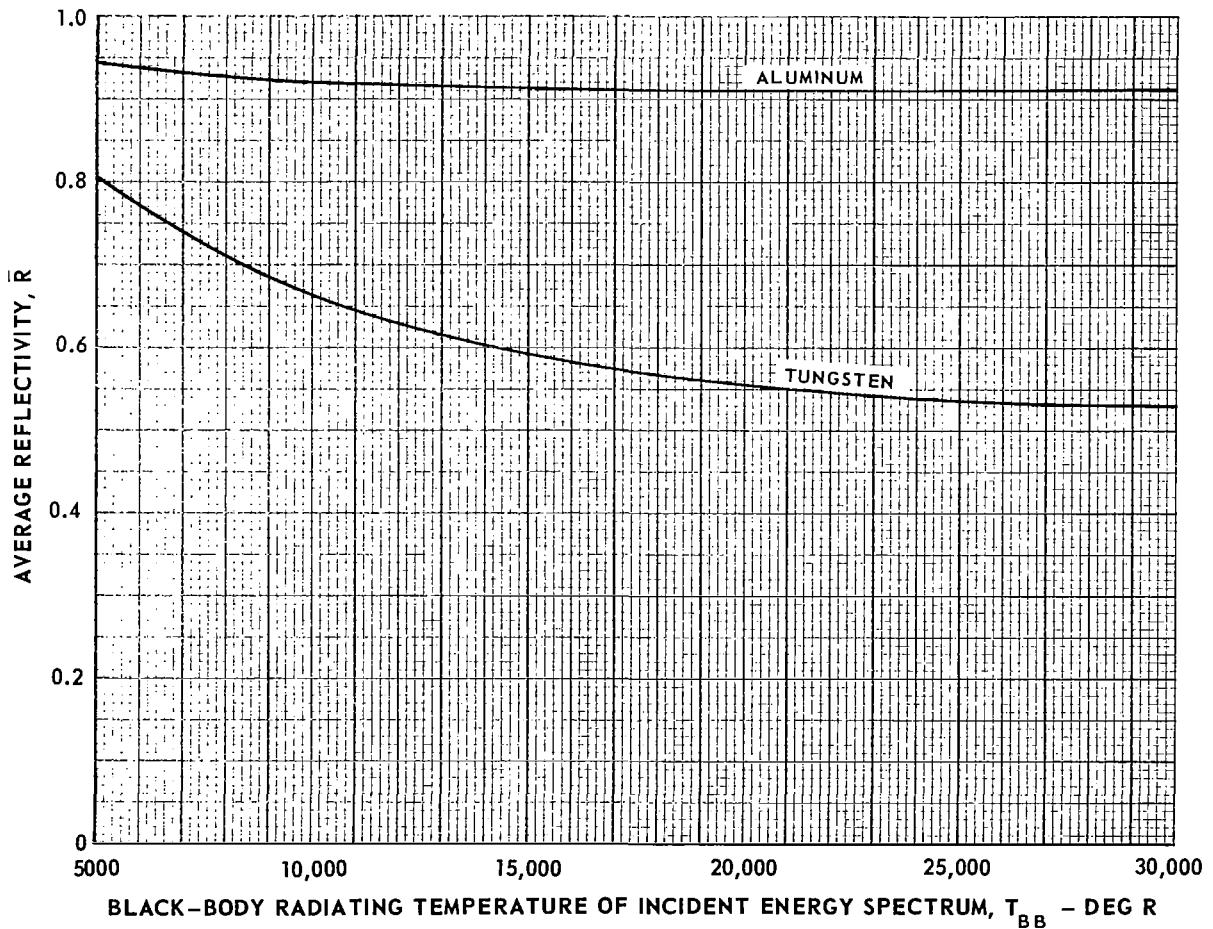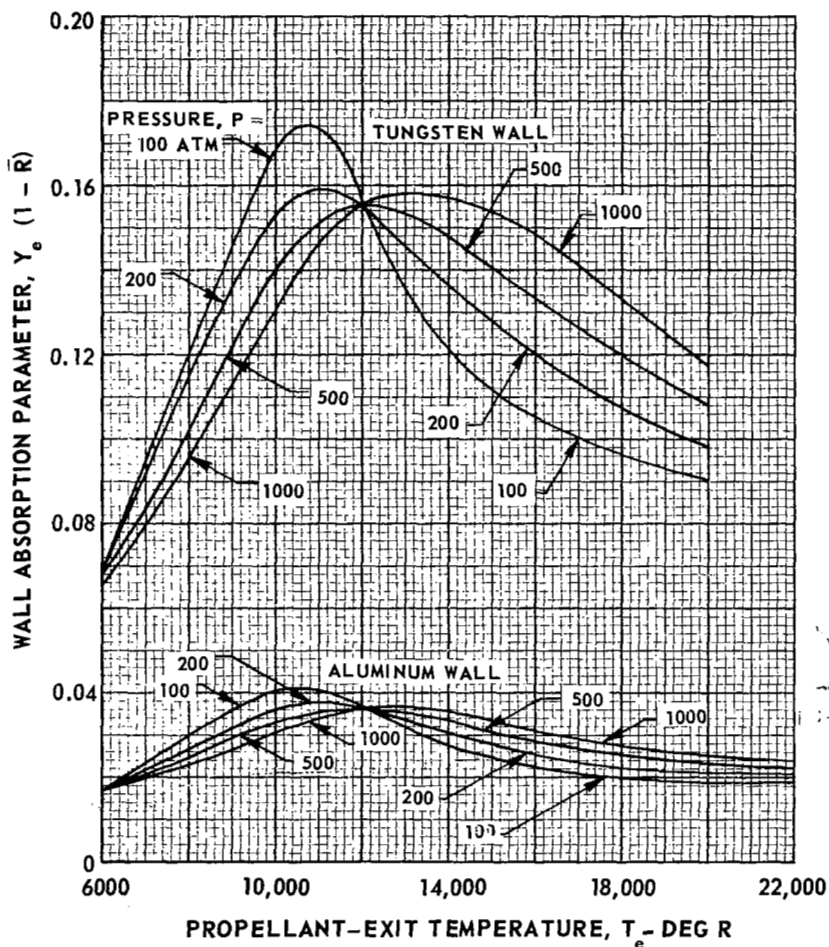CURVES OBTAINED FROM FIG. 29 OF REF. 6

SEE APPENDIX B

FIG. 29

EFFECT OF EXIT TEMPERATURE ON WALL ABSORPTION PARAMETER DETERMINED FROM ANALYSIS OF ENERGY EMITTED FROM PROPELLANT STREAM OF NUCLEAR LIGHT BULB ENGINE

DETERMINED FROM Y_e FROM FIG. 26 AND R FROM FIG. 28 USING T_m FROM FIG. 27
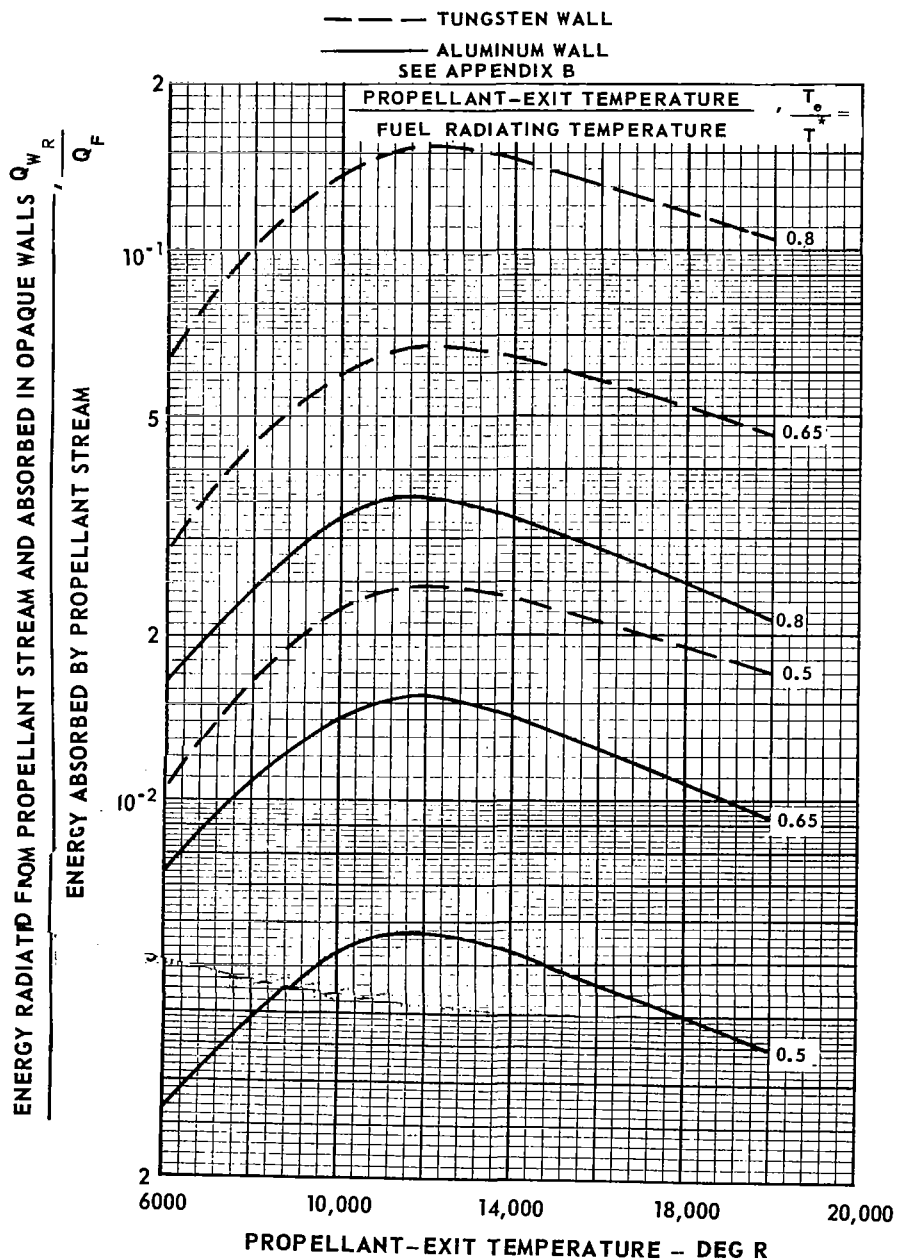
SEE APPENDIX B

FIG. 30

EFFECT OF EXIT TEMPERATURE ON FRACTION OF ENERGY ABSORBED IN WALL DETERMINED FROM ANALYSIS OF ENERGY EMITTED FROM PROPELLANT STREAM OF NUCLEAR LIGHT BULB

$$\frac{Q_{W_R}}{Q_F} = (1 - \bar{R})\ Y_e\ \frac{\epsilon_P}{\epsilon_F}\ \frac{A_W}{A_6}\left(\frac{T_e}{T^*}\right)^4$$

$(1 - \bar{R})\ Y_e$ FROM FIG. 29

$\epsilon_P = 1.0;\ \epsilon_F = 0.85;\ A_W/A_6 = 2.05$

— — — TUNGSTEN WALL

———— ALUMINUM WALL

SEE APPENDIX B

PROPELLANT–EXIT TEMPERATURE

FUEL RADIATING TEMPERATURE , $\frac{T_e}{T^*} =$

0.8

0.65

0.8

0.5

0.65

0.5

ENERGY RADIATED FROM PROPELLANT STREAM AND ABSORBED IN OPAQUE WALLS $\frac{Q_{W_R}}{Q_F}$

ENERGY ABSORBED BY PROPELLANT STREAM

PROPELLANT–EXIT TEMPERATURE – DEG R

99

FIG. 31

EFFECT OF WALL REFLECTIVITY ON FRACTION OF ENERGY ABSORBED IN WALL DETERMINED FROM ANALYSIS OF ENERGY EMITTED FROM PROPELLANT STREAM OF NUCLEAR LIGHT BULB ENGINE
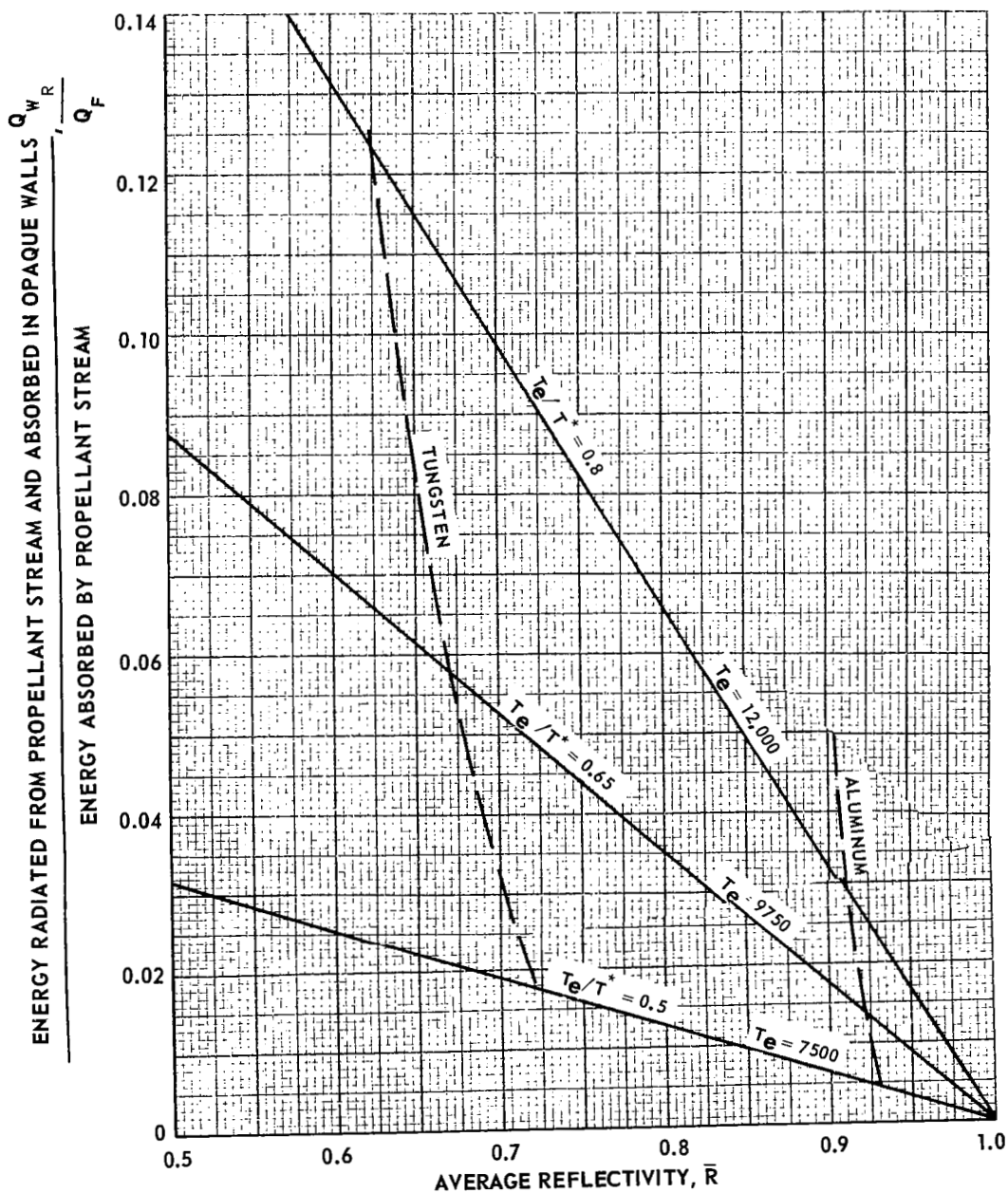
SEE APPENDIX B

$T^* = 15,000\ R$

$$\frac{Q_{W_R}}{Q_F} = (1 - \bar{R})\ Y_e\ \frac{\epsilon_P}{\epsilon_F}\ \frac{A_W}{A_6}\left(\frac{T_e}{T^*}\right)^4$$

Y_e FROM FIG. 26 FOR P= 500 ATM

$\epsilon_P = 1.0;$ $\epsilon_F = 0.85;$ $A_W/A_6 = 2.05$

ENERGY RADIATED FROM PROPELLANT STREAM AND ABSORBED IN OPAQUE WALLS $\frac{Q_{W_R}}{Q_F}$,

ENERGY ABSORBED BY PROPELLANT STREAM

TUNGSTEN

$T_e/T^* = 0.8$

$T_e = 12,000$

ALUMINUM

$T_e/T^* = 0.65$

$T_e = 9750$

$T_e/T^* = 0.5$

$T_e = 7500$

AVERAGE REFLECTIVITY, $\bar{R}$

"*The aeronautical and space activities of the United States shall be conducted so as to contribute . . . to the expansion of human knowledge of phenomena in the atmosphere and space. The Administration shall provide for the widest practicable and appropriate dissemination of information concerning its activities and the results thereof.*"

—NATIONAL AERONAUTICS AND SPACE ACT OF 1958

NASA SCIENTIFIC AND TECHNICAL PUBLICATIONS

TECHNICAL REPORTS: Scientific and technical information considered important, complete, and a lasting contribution to existing knowledge.

TECHNICAL NOTES: Information less broad in scope but nevertheless of importance as a contribution to existing knowledge.

TECHNICAL MEMORANDUMS: Information receiving limited distribution because of preliminary data, security classification, or other reasons.

CONTRACTOR REPORTS: Scientific and technical information generated under a NASA contract or grant and considered an important contribution to existing knowledge.

TECHNICAL TRANSLATIONS: Information published in a foreign language considered to merit NASA distribution in English.

SPECIAL PUBLICATIONS: Information derived from or of value to NASA activities. Publications include conference proceedings, monographs, data compilations, handbooks, sourcebooks, and special bibliographies.

TECHNOLOGY UTILIZATION PUBLICATIONS: Information on technology used by NASA that may be of particular interest in commercial and other non-aerospace applications. Publications include Tech Briefs, Technology Utilization Reports and Notes, and Technology Surveys.

Details on the availability of these publications may be obtained from:

SCIENTIFIC AND TECHNICAL INFORMATION DIVISION

NATIONAL AERONAUTICS AND SPACE ADMINISTRATION

Washington, D.C. 20546